Probabilistic Models for Drug Dissolution

Ana Barat

M.Eng., M.Sc.

A thesis submitted in fulfillment of the

requirements for award of

Doctor of Philosophy (Ph.D.)

to the

Dublin City University

Faculty of Engineering and Computing

School of Computing

Supervisor: Prof. Heather J. Ruskin and Dr. Martin Crane

December, 2006

Declaration

I hereby certify that this material, which I now submit for assessment on the programme of study leading to the award of Doctor of Philosophy is entirely my own work and has not been taken from the work of others save and to the extent that such work has been cited and acknowledged within the text of my work.

Signed: _____

(Ana Barat)

Student ID: 53154452

Date: 11^{th} December 2006

Acknowledgements

I would like to thank my supervisors Prof. Heather Ruskin and Dr. Martin Crane. Many thanks for their supervision and guidance through this research, for encouraging me to submit the work to international conferences and journals and for being so available for discussing problems. I would like to express my gratitude for their time, patience, good humour and good comments, which have made possible for me to get the work to this level.

To my parents, Leonid and Elena, for their encouragement and understanding, for their unconditional love and support, for precious advices and the warmest hospitality.

I also would like to thank people in the postgraduate lab, Puspita, Patricia, Noreen, David, Grainne, George, Tommy, Niall, Ashley, Karl, Noel and Ronan for their optimism, sharing their own experiences and making these three years of postgraduate studies easier and merrier.

Many thanks for the team from the DCU restaurant: Mariana, Cristian, George, Lilia, Petru, Min Nie and Piotr for their support and the fun I had with them during the afternoon for lunch and coffee breaks.

I would like to express my sincere thanks to the people from Jamestown Road Church: the family Millar, the family Shaw, Rachel, Sharon, Femmy, Nadine to name but a few! To my friends from Ireland, France and Moldova who continued to support my taking new challenges.

Finally, to Ubaldo, for his understanding, love and encouragement while I have been away from France.

Thank you all, so much. *Ana Barat, 11/12/2006*

Dedicated to my parents, *Leonid* and *Elena*, whose enthusiasm never stopped motivating me.

Contents

List of Figures

List of Tables

Abstract

The focus of the material presented in this PhD thesis is the development of stochastic Direct and Inverse Monte-Carlo-based models for drug dissolution.

Drug dissolution from different carriers is a complex phenomenon. Limited knowledge is available on some of the underlying constituent processes, which restricts development of mechanistic models. Monte Carlo techniques permit the treatment of certain structures and events in a probabilistic manner. The thesis examines a number of possible ways of using Monte Carlo both (1) to explore modelling for the dissolution of Drug Delivery Systems and (2) to reconstruct general system behaviour during dissolution, using noisy drug delivery data. Further, important investigations on the determination of factors responsible for noise and quantification of noise levels, are reported.

In the first part of the thesis, an investigation of MC-based methods in the field of Drug Delivery is given, with the complexity of drug dissolution and design explored and the contribution of the MC approach reported. The use of Direct MC and Stochastic Cellular Automata models in the simulation of dissolution from pharmaceutical compacts or related phenomena are discussed, together with various features and requirements.

The principal objective here is to extend use of Direct Monte Carlo techniques in simulating drug delivery from compacts of complex composition, taking into consideration special features of the dissolution in an *in vitro* environment. After examining the existing MC models for drug delivery, the need for more sophisticated models is described. Exploratory modelling is proposed in order to address the problems of dissolution related to certain drug carriers with complex internal morphology and difficult-to-predict dissolution profiles. Phenomena such as local interactions of dissolving components, development of wall-roughness at the solid-liquid interface, diffusion through occlusions and pores and moving concentration boundary layers

were examined and directly accounted for in the model. As a result, new models have been developed for: i) matrix soluble drug carriers and ii) bioerodible polymeric micro- and nanospheres for controlled release of proteins. The simulations provide results in acceptable agreement with different drug release profiles obtained during laboratory experiments. The novelty of this work consists in including new features of experimental system complexity in the frame of simple and user-friendly Direct MC models, indicating that the Direct MC technique can be very helpful in exploring design parameters in the field of drug delivery.

The other major axis of the thesis investigates use of Monte Carlo in data reconstruction and noise quantification. The problem posed was whether it is possible to extract detailed dynamic distributional knowledge about a dissolving pharmaceutical system composed from many small entities, when the researcher is provided with insufficient experimental data. A model based on Inverse Monte Carlo simulations was designed to exploit Bayesian principles in retrieving the desired features, such as particle size distribution. Importantly, this work demonstrates that Inverse Monte Carlo methods are capable of reconstructing underlying characteristics of drug carriers involved, even when dissolution profiles available rely on sparse data sets.

The models proposed in this thesis are currently being incorporated in a large-scale project in collaboration between the DCU research team and the Hospital for Special Surgery, New York. The project focuses on developing therapeutic implants with controlled drug release, specifically designed for the regeneration of severely damaged tissues.

Chapter 1

Introduction

1.1 Introduction to Modelling Drug Dissolution

Pharmaceutical Drug Delivery Systems (DDS) are systems which deliver a drug into the body. A DDS consists of one or several bio-active agents (the drug(s)), and one or several excipients, which are substances forming the vehicle or medium for the administration of the active agents. The dissolution profile of the drug molecule can be controlled with a wide range of excipients.

The ultimate aim of a DDS is to undergo dissolution in a biological medium (eg.: gastro-intestinal tract for tablets, biological tissues for implants etc.) and, as released, to undergo absorption. The release of the drug and the ultimate absorption must take place at appropriate rates, in order to ensure the desired effect on the organism. In many drug delivery applications, the release of the excipient (involving diffusion, dissolution, erosion or other mechanisms) determines the release of the bio-active agents. Some modern formulations are very complex, and the relationship between the formulation and process variables and the release profiles are not entirely understood.

From performance considerations, it is important to investigate the effects of factors related to the composition, design and manufacturing process (Göpferich and Langer, 1995), on the phenomenological behaviour of a drug delivery system.

In vitro dissolution testing is very important in terms of designing, developing and testing new formulations, (Siepmann and Peppas, 2001; Crane et al., 2004b), and can be regarded as the first step to modelling the dissolution *in vivo*. The dissolution profile *in vitro* has to satisfy certain criteria established by the pharmacopoeias[1].

Depending on the design and delivery goals of a particular DDS, formulation development and optimisation may require a significant amount of time and effort, as well as financial investment (Sirisuth and Eddington, 2002). The direct benefit of producing accurate models for *in vitro* dissolution is reduction in the laborious drug formulation studies and the minimisation of costs associated with them. This can be achieved by investigating how design parameters such as composition, porosity and device geometry affect the resulting kinetics of drug release (Siepmann and Peppas, 2001) and by selecting only the most interesting candidate parameters to be varied during *in vitro* experimentation (Zygourakis and Markenscoff, 1996). In addition, modelling can lead to the development of better scientific understanding of the behaviour of systems studied.

The following sections briefly discuss problematic aspects associated with the field of drug dissolution, and indicate a number of different modelling approaches taken to provide insights in this active research area.

1.2 Drug Delivery Systems. Examples

In the field of drug development various materials, manufacturing techniques and release mechanisms are used to achieve different drug release profiles. Mass transport mechanisms involved in drug delivery include, but are not limited to: diffusion, dissolution, combined diffusion and dissolution, water-triggered transport (swelling), degradation/erosion, as well as phenomena intrinsic to osmotic, magnetic or electric effects (Siepmann, 2001).

[1] a book published usually under the jurisdiction of government, listing drugs, their formulas, methods for making medicinal preparations, requirements and tests for their strength and purity, and other related information.

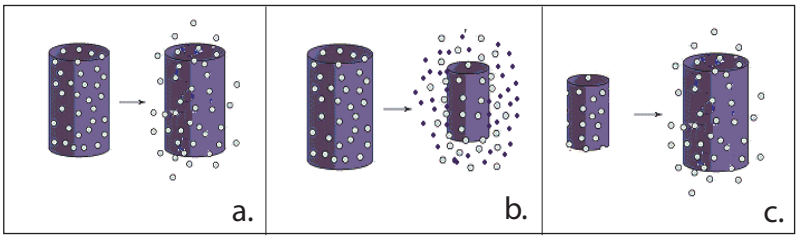

Figure 1.1: Schematic representation of behaviours of different types of DDS, where the excipients are: a) inert matrix. b) bio-erodible. c) swellable.

The simplest DDS are probably soluble *immediate release* systems. These may contain one or more soluble ingredients, with more or less different solubilities, which dissolve relatively quickly. Even in these cases, a combination of elements with dramatically different solubilities generate dissolution profiles, which are not readily predictable. In these drug delivery systems the main release mechanism is diffusion and the release rate of the drug is maintained as desired, by the suppressing or enhancing effect of an excipient.

Over the last decades much research has been carried out on *sustained release* drug delivery systems, (Siepmann and Göpferich, 2001; Ungaro et al., 2004). Sustained release systems are characterised by a very careful use of excipients in order to control, or programme, the *release* of the *active molecule*. This type of DDS is extremely important when the release of an agent is to be delivered in very small quantities over large times, to avoid toxicity related to large amounts of drug. The sustained delivery is also of extreme interest for the areas of medicine involved in prolonged, localised or targeted treatment. For example, sustained drug delivery systems are used, among other applications, in vaccines for delivering antigens, in cancer treatment for delivering the chemotherapeutic agents and in tissue repairing implants for delivering growth factors. Considerable progress has been made in medical sciences, toward the advancement of sustained medical therapies, through the application of various biodegradable or biocompatible polymers. The behaviour of controlled release delivery devices consisting of polymers and other agents can

become very complex.

To illustrate, a water soluble drug, incorporated in a hydrophobic, inert matrix system with channels and pores, (e.g. ethylcellulose, hydrogenated castor oil), is mainly released by diffusion through the polymer into the surrounding medium, Figure 1.1, (a). The release rate of the incorporated drug will depend not only on the particle size and the particle size distribution of the ethylcellulose used, but also on process variables, such as the compaction pressure used in manufacturing the compact (which results in larger or smaller pores in the matrix).

In drug delivery, which is primarily controlled by the erosion of the excipient, Figure 1.1, (b), consisting of bio-erodible polymers, the self-erosion of the matrix is the principal release mechanism (Costa and Lobo, 2001). Device performance depends strongly on the erosion behaviour of the used materials, available in various forms (e.g. different molecular weights). All bio-erodible polymers have characteristic times of erosion. These permit formulation of laws describing the erosion and prediction of monomer or drug release. Descriptions of this kind of DDS are given in Siepmann and Göpferich (2001).

Some of the the most complex examples of drug delivery systems are those controlled by a hydrophilic swellable/erodible excipient, behaving as a reservoir-type controlled-release device, [2] Figure 1.1, (c). The most important characteristic of this kind of system is that, by diffusion of water into the hydrophilic polymeric matrix, the compact swells, radically changing its form and dimensions. The water-soluble incorporated drug molecules, diffuse both within and outside the device, through the disentangled chains of the polymer (Siepmann and Peppas, 2001; Siepmann et al., 2000).

These and other phenomena, such as superposition, synergies or coexistence of these physico-chemical effects, need to be taken into consideration when formulating realistic models.

[2] A DDS with the aim of maintaining a uniform dose over a specified period of time

1.3 The Scope of the thesis

There are four main sections to this thesis:

Chapter 2 opens with an overview of considerations and chronology in modelling DDS. The rest of the chapter reviews and investigates how Monte Carlo (MC) techniques, which have been used in simulating various complex systems throughout the last decades, were initially used in the field of Drug Delivery. This chapter considers what aspects of the complexity of drug dissolution and design can benefit from this particular approach, reporting and examining existing Direct MC and Stochastic Cellular Automata modelling efforts, used to simulate dissolution of pharmaceutical compacts or related phenomena.

Chapter 3 is a methodology chapter. It focuses on elaborating the principles outlined in Chapter 2 and in particular deals with the probabilistic methods for drug dissolution, used in this work.

In Chapter 4, the developments outlined in Chapter 2 are expanded, with focus on new work developed during our research. The problem posed is the *in vitro* dissolution of a binary drug delivery system, consisting of a poorly soluble drug dispersed in a matrix of highly-soluble acid excipient. Modelling challenges related to both the internal morphology of the DDS and the external *in vitro* environment are discussed in this context. A review of the current models, which attempt to describe the behaviour of this DDS, shows how this apparently simple pharmaceutical system is difficult to reduce to empirical or mechanistic modelling. Cellular Automata and MC methods are proposed for analysing this DDS as a complex many-body system, in both qualitative and quantitative terms.

Much of the material presented in Chapters 2 and 4 has been published in the proceedings of the International Conference of Complex Systems, France, 2005 (Barat et al., 2005) and in SIMPAT, Elsevier (Barat et al., 2006a,b). These are included in Appendix 4.

Chapter 5 further explores the complexity involved in DDS behaviour, by in-

vestigating protein dissolution from swellable, insoluble and bio-erodible micro- and nanospheres for sustained delivery, Figure 1.1, (c). This system has been chosen for several reasons: first of all, it's medical application is of utmost importance and secondly, as indicated, it is one of the most complex DDS. The model developed for the more complex system can be reduced, by simplification, to simulate a DDS such as that illustrated in Figure 1.1, (a), or easily upgraded for a DDS such as that in Figure 1.1, (b). As there are many parameters that control the behavior of such systems, a broad sensitivity analysis is performed. The strengths of the model are discussed, together with detailed practical considerations for its use for various types of swellable bioerodible micro- and nanospheres.

Many DDS, including the drug delivery systems studies in Chapter 4, are not used individually, but in groups (or agglomerations), which act like many particle systems, where particles have similar general properties but vary slightly in their physical appearance.

Chapter 6 changes consideration from individual direct study of pharmaceutical compacts to analysing effects of agglomerations of small DDS on the resulting dissolution profiles. Very often, only general data, such as the fraction of dissolved therapeutic agent, are easily obtainable from such systems, whereas dynamical parameters such as size changes and form of the constituent DDS are hard to trace and observed with difficulty, rendering the system akin to a *black box*. Inverse Monte Carlo techniques for elucidating the unknown parameters of a dissolving multiple particle system are proposed and tested in this chapter.

Finally Chapter 7 presents the overall summary and conclusion of the work in the thesis. Recommendations for future developments, upgrades, improvements and studies, arising from the present work, are proposed.

References and Appendices 1-4, containing several implementation details, a glossary of terms, the list of notations used in Chapter 6 and our published papers respectively, are given at the end of the thesis.

Chapter 2

Literature Review of probabilistic models for drug dissolution.

This chapter opens with a general overview on the approaches taken over the last two decades for the problem of modelling drug dissolution. Overall, the conclusion is that modelling the newest drug delivery systems (with complex structure) requires development of new and more adaptable methods in order to achieve a satisfactory resolution. The focus of the present thesis is on exploring and developing *probabilistic methods* for simulating drug dissolution and this provides the context for the remainder of this chapter. A summary of the most relevant examples from literature, for probabilistic simulations used to study drug delivery or related systems, is given here, outlining the main principles of the methods used. A broader description on the MC and other methodologies (CA, multi-agent) is presented in Chapter 3.

2.1 General overview

The introduction section illustrates that the topic of drug release is subject to considerable diversity, so that modelling and simulating the processes involved have

many ramifications. In seeking a better understanding of the phenomena of mass transport, the literature presents a wide range of models - from simple ones: such as the *empirical* and *semi-empirical*, to the more complex: such as those involving *mechanistic* theories.[1] In contrast to mechanistic mathematical models, empirical models quantifying drug release from delivery systems are not so directly based on the exact description of all the real physical processes involved. Empirical models can only describe the resulting, measurable drug release rates (Siepmann and Göpferich, 2001), but do not give a clear insight into the physics of the drug dissolution process.

In order to build a mechanistic model, one has to be aware of both the major processes governing the system and the basic mass transport mechanisms involved in drug release. Such models should be able to provide knowledge about the system's behaviour and are generally powerful with respect to simulating the effect of the device design variables on the resulting drug release kinetics (Siepmann and Göpferich, 2001). Most existing mechanistic models are based on mathematical equations, which describe the mass transport phenomena taking place while the drug is released. A spectrum of mathematical theories, describing drug release from controlled/immediate-release delivery systems, is available (Siepmann, 2001): for reviews see (Siepmann and Peppas, 2001; Siepmann and Göpferich, 2001; Narasimhan, 2001; Costa and Lobo, 2001).

However, most of the present day pharmaceutical compacts typically show much more complex behaviour than those initially modelled by non-linear mathematical equations, and have few simplifying properties which permit the use of non-linear dynamics. For example, a drug delivery system consisting of two or more components which arrange in a matrix structure is not tractable by differential equations because these generally only function well with continuous and homogeneous spatial and temporal conditions. Pores or several components arranged in a matrix fashion imply

[1] A mechanistic model should have as many features of the primary system built into it, as observations and data allow; that is, the model should be consistent with the observed behaviour of the system and be predictive about its future behaviour under the effect of perturbation, (Balant and Gex-Fabry, 2000).

abrupt spatial discontinuity. The whole picture is made even more complex by the presence of one or more moving boundaries, as the components dissolve. In addition, it is seldom a trivial task to identify the most important factors (within formulation components and process parameters), to be addressed in improving the drug release model. In consequence, in the case of multi-component matrix systems or porous systems, the use of mechanistical models based on differential equations involves making simplifications leading to a poor resolution of the system investigated.

In addressing the growing complexity in the drug delivery field, recent research has seen the development of less traditional methods, which consider alternative ways of looking at the drug dissolution. For example stochastic approaches (Chen et al., 1998), such as direct and inverse Monte Carlo (MC) methods and probabilistic Cellular Automata (CA), are based on the idea that the drug release process is often subject to random fluctuations.

Monte Carlo (MC) methods and simulation techniques are algorithms used for solving various kinds of computational problems using random numbers (or rather pseudo-random numbers), in a sampling procedure. Such methods contrast with deterministic algorithms, like molecular dynamics or direct numerical solutions (eg.: Finite Elements, Finite Differences etc.). MC methods are rooted in concepts of statistical randomisation and sampling[2] and were first used to address many-body problems in the middle of the 20th Century.

The term "Monte Carlo" comes from the game of roulette, which exploits random outcomes of final ball position in a spinning wheel. Similarly, Monte Carlo methods randomly select values to create scenarios of a problem. These values are taken from within a fixed range and selected to fit a probability distribution. MC can be considered in either *direct* or *indirect* terms, (Feng, 1997). Monte Carlo methods are useful in cases where other traditional methods, like differential equations and

[2] Sampling experiments are based on the generation of random numbers, followed by various arithmetic and logical steps, which are often highly repetitive, hence highly amenable to handling by computer. In the same way, the power of methods, which contain many variables, has grown with the increase in computer power.

empirical methods fail providing the necessary resolution into the problem, with the limitation that they can get very computationally intensive. Details on MC technologies can be found in Chapter 3.

A Cellular Automataton is a discrete model, consisting of a regular grid of cells, each in one of a finite number of states. The grid can be in any finite number of dimensions. Time is also discrete, and the state of a cell at time t is a function of the states of a finite number of cells (called its neighborhood) at time $t-1$. The advantage of probabilistic CA and direct MC is the possibility of making a simplified, but direct representation of the system studied, which can aid in understanding the importance of a number of microscopic effects in monitoring the model's evolution over time. These methods are of special interest in modelling porous compacts with complex and non-homogeneous inner structure, such as mixtures of constituents with various particle sizes and very different behaviours when exposed to a dissolution medium. Further details on the CA techniques are presented in Chapter 3.

Methods for *optimisation* in drug design based on artificial neural networks and genetic algorithms also exist (e.g. (Sun et al., 2003; Vaithiyalingam and Khan, 2002; Takayama et al., 1999; Chen et al., 1999; Takahara et al., 1997)). When the relationships between drug release profiles and formulation and process factors is not linear and, moreover, is not well understood, artificial neural networks have the advantage of mapping the relationship between variables and responses, such as drug release profiles, through learning or training processes (Sun et al., 2003).

2.2 Review of Direct Monte Carlo techniques applied to dissolution problems

2.2.1 Methods for dissolution of various types solids

Of the many applications of direct MC to different fields of physics, (Landau and Binder, 2000), one is solid dissolution. Both crystalline and amorphous solids are

used in drug manufacture. Crystalline solids are arranged in fixed geometric patterns or lattices, have an orderly arrangement of units and are practically incompressible. Amorphous solids have randomly oriented molecules. They are supercooled liquids where the molecules are arranged in a random manner. Some examples of solid dissolution investigated using direct MC are given below:

Polycrystalline solid

Srinivasan (1997) applied a direct MC method, using a 2D or 3D hexagonal computation grid for the dissolution of a polycrystalline solid in liquid with sink [3]properties. The solid is represented by a labelled circular or spherical region on the grid, placed in the middle of a "liquid" labelled area. Dissolution itself is modelled as a change in energy. The probabilistic process is carried out by selecting a cell at random and allowing it to change to liquid state. If there is a decrease in the total energy associated with the cell, it is allowed to stay in the liquid state, otherwise, it reverts to solid . This model permitted a parametric study of the influence of interface energies on the dissolution of the solid.

Glass

Santra et al. (1998) have investigated glass dissolution in water by treating glass as a random binary system with highly different solubilities. As in the previous example, this model permits for re-crystallisation of the components. For a finite volume of glass exposed to the liquid, the simulation resultes in an initial rapid dissolution, followed by a pseudo equilibrium, with a steady-state of glass porosification continuing at a lower, but constant speed. As we shall see later, porosification is a process which occurs during drug dissolution from some pharmaceutical compacts, as well. In the case of a porous solid dissolving in a liquid, the solid-liquid interface can be viewed as an irregular area of fractal nature, rather than a 1D linear front, where dissolution

[3] The liquid is considered to be infinite. No matter how much solute it accepts, the concentration of the solute in the sink liquid is set to zero.

through pores is different from dissolution at the surface. Cellular Automata and direct MC techniques can directly model these physical situations, demonstrating their advantage in modelling porosification, over differential equation-based methods, which necessarily focus on global effects and common parametrisation, without directly considering the dynamics of the intimate structure of the materials. The MC model above has, for example, permitted a better detailed understanding of the physical processes in glass dissolution.

Calcite

A kinetic Monte Carlo technique which simulates the dissolution and growth of calcite in flowing water is described by Williford et al. (2004). Boundary layer problems are taken into consideration and the diffusion in the fluid is treated by a random walk sub-model. The model is divided into a grid, where each square cell is one calcite lattice unit and represents a site. Each site can be occupied by either a solid phase or by molecules that have been desorbed. Quantitative agreement with measured step velocities was best when the boundary layer parameters were given physically reasonable values, indicating self-consistency of the MC model, (Williford et al., 2004).

2.2.2 Methods for Controlled Release: Applications of Polymers

Controlled release drug delivery involves usually extremely slow release over a long period of time, according to a desired profile. This is achieved, for example, by incorporating the drug into slowly eroding polymers. As mentioned in Chapter 1, the systems formed have quite complex behaviours, which are not trivial for mechanistic modelling.

Controlled release is mostly based on bio-erodible polymers. Depending on the properties of the polymer, the release device can be *surface-eroding* or *bulk-eroding*. In the case of surface-eroding devices, polymer degradation is much faster than water

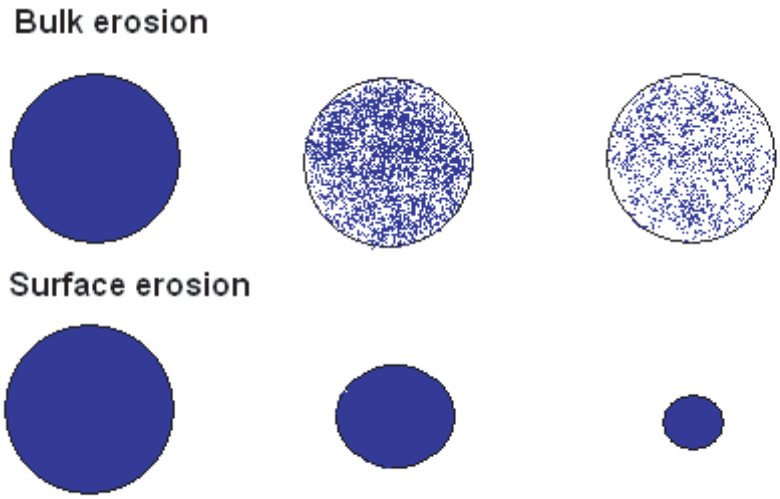

Figure 2.1: Bulk erosion versus surface erosion.

intrusion in the polymer bulk, so that degradation occurs mainly at the outermost polymer layers. This is why erosion affects only the surface and not the inner parts of the matrix, (Siepmann and Göpferich, 2001). Polyanhydrides and polyketals are examples of surface eroding polymers. On the other hand, bulk eroding polymers erode slowly and water uptake by the system is much faster than polymer degradation. In this case, erosion is not restricted to the polymer surface, because the entire system is rapidly hydrated and polymer chains are cleaved throughout the device, (Siepmann and Göpferich, 2001). Good examples of bulk-eroding polymers are poly(lactide) (PLA) and poly(lactide-co-glicolide) (PLGA). The difference between the behaviours of bulk- and surface-eroding polymers is schematised in Figure 2.1. Examples of MC modelling in controlled release are dealt with briefly in the methodology chapter (Chapter 3). In outline, they include[4]:

Bio-erodible polymer matrix (GL)

Göpferich and Langer (1995) (GL) have approached the problem of monomer re-

[4]Each example is accompanied by a mnemonic label to facilitate their presentation

lease from bio-erodible polymer matrices using a Monte Carlo - mechanistic method, where the structural problem is addressed by MC and the dynamics of the dissolution of the components are accounted for both by differential equations and MC. The way the sampling techniques are used to simulate erosion of polymer and porosity dynamics is elaborated in the methodology chapter (Chapter 3). The fit of the GL model to the experimental data of relative monomer release was found to be in good quantitative agreement with the experimental results for a number of cases, and in good qualitative agreement for other cases. Other authors, like Ramtoola and Corrigan (1987); Healy and Corrigan (1992) discussed, without however proving it, the possibility that the pH inside the pores have an influence on the overall release kinetics. The GL model confirmed a previous hypothesis, that the quite unexpected dissolution profiles obtained in the experimental part of the study (Göpferich and Langer, 1995), were due to pH effects inside the pores. From our viewpoint, this work also demonstrate the ability of MC methods to assist in realistic hypothesis formulation and testing when analysing microscopic interactions in the drug dissolution process.

Layered bio-erodible polymer matrix filled with drug (G1)

In (Göpferich, 1997*a*), the author uses a similar model (G1) for a slightly different situation. The problem is to model matrices consisting of several layers of two *different* erodible polymers (polyanhidride and poly(D,L-lactic acid)). Only one of these polymers is loaded with drug. It has to release the drug in two different phases, due to the layers. Figure 2.2 illustrates how the author represents a 3D cylinder in 2D: the grid divides the cross section into individual polymer pixels of the same volume. This is achieved by decreasing the length Δx of the sites from the grid, in the radial direction, proportional to the root of the increasing radius. Extensions of the G1 model to 3D also exist, (Göpferich, 1995). These variants show that MC models are amenable to be upgraded and extended in order to model both variety

and complexity exhibited by the experimental DDS fields.

Bulk-eroding system (G2)

The problem of controlled release devices containing erodible polymers with completely different erosion mechanisms, (surface erosion and bulk erosion), has also been addressed using a MC approach, G2, (Göpferich, 1997*b*). The matrix is composed of several layers of polymers, characterised by different erosion mechanisms,(note that the previous model related only to the same mechanism, and two different erosion rates). The layers are: a surface-eroding core (charged with drug), a bulk-eroding mantle (drug-free) and a surface-eroding crust (drug-loaded).

The following distinctions are made between surface-eroding polymer layers and bulk-eroding layers, in order to simulate their different erosion behaviour:

- A surface-eroding polymer site begins to erode only when it comes into contact with the buffer solution.
- Conversely, all the sites of a bulk-eroding polymer have a chance to begin their erosion, as soon as at least one site, (representing the bulk-eroding polymer), comes into contact with the erosion medium.

This model (G2) gave results in agreement with experiment and illustrated again how MC can be used in modelling problems prevailed by composition of elements and heterogeneity.

In Chapter 5 we address modelling release from PLGA microspheres using MC multi-agent techniques. PLGA is a bulk-eroding polymer used for the manufacturing of nano- and microparticles for controlled release devices with many practical applications.

Generalised model for bio-erodible systems (ZM)

A new type of Cellular Automata method to simulate release from bio-erodible devices, was discussed by Zygourakis and Markenscoff (1996) as a generalised model for surface-eroding DDS, with a view to designing pharmaceutical formulations with optimal release characteristics. The DDS of any shape and the liquid around it was represented as a computational grid, which is designed as a dynamic system with transient behaviour. Microscopic mechanisms of dissolution were defined in terms of local relations between the sites. The ZM model can accept two or three solid components, related to amorphous or crystalline bio-erodible polymers, characterised by different erosion rates. In contrast to the GL model, (Göpferich and Langer, 1995), where the diffusion of monomer, in spite of the heterogeneous environment, is treated by differential equations, this is not the case for the ZM model, and the quantities of matter are treated as discrete. The erosion rates can be made dependent on the micro-environment of the sites concerned.

Possible porosity of the device, with various sizes of the pores is taken into account. The authors discuss methods for time normalisation, together with averaging and normalising the dissolution rates, in order to be able to compare the simulation results with experimental data. The simulation analysis showed how overall release rates are affected by intrinsic dissolution rates, drug loading, porosity and the dispersion of the drug in the bio-erodible matrix. The authors also suggest that a drug design approach, which combines computer simulations and laboratory experimentation, is likely to significantly reduce laboratory experimentation and the associated time and costs.

Swellable systems (LC)

Controlled release devices made of swellable polymer were noted to have the most complex behaviour of all systems considered.

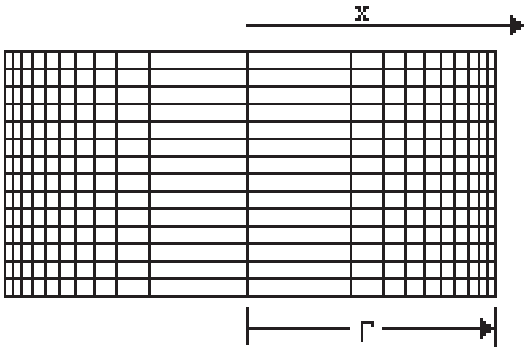

Figure 2.2: Computational grid to simulate a 3D cylinder in 2D

Lee and Chakraborty (2002) studied the diffusion of copolymers[5] through random disordered media at a molecular level, using kinetic Monte Carlo methods (model LC). They investigated possible interactions of the polymeric chain with the fixed obstacles constituting a medium. Study of polymer behaviour is relevant to understanding the behaviour of swellable compacts, (see Section 1.1). In controlled release applications of polymers, a solute is molecularly dispersed in a polymer phase. In the presence of a thermodynamically-compatible solvent, swelling occurs and the polymer begins to release its contents to the surrounding fluid, (Narasimhan, 2001). The kinetics of the drug release process can be decisively affected by the polymer swelling, due to external penetrant uptake, (Grassi et al., 2000). This release process can be controlled either by solute diffusion or by polymer dissolution. In this case the presence of permanent entanglements in the polymers becomes significant, (Narasimhan, 2001).

In the LC model, the polymer is modelled by a chain of spherical beads placed and equilibrated on a 3D lattice partitioned into sites. The lattice sites can be occupied by spherical obstacles. Each MC step consists of an attempt to move chosen beads from the chain. Each movement is accepted or rejected according to the Metropolis criterion, with probability dependent on the quantity $\triangle U$. This quantity represents

[5]A polymer formed when two (or more) different types of monomer are linked in the same polymer chain.

the difference of energy between the old and new chain position. The simulations resulted in a number of interesting effects. For example, the authors found that above a threshold temperature, polymers containing monomers, which are attracted to sites from the medium, are more mobile than those which exhibit repulsive or neutral interactions. The effect is found to be related to the construction of the disordered medium. This study permitted a better understanding of how polymer sequence influences the dynamics of polymers in quenched disordered media.

2.2.3 Monte Carlo in the study of parameter design for drug delivery systems

Often, the semi-empirical Weibull function is chosen to fit different kinds of dissolution data, because it provides the best fit to simulated data. Equation (2.2.1) gives the Weibull function, with a and b - constants. These constants are believed to be connected to the shape of the releasing device, (Antal et al., 1997).

$$\frac{M_t}{M_\infty} = 1 - e^{(-at^b)} \tag{2.2.1}$$

where M_t and M_∞ represent the amounts of drug released at time t and the total amount of drug contained in the DDS, respectively. Recently, Kosmidis et al. (2003a) have used MC methods to model the drug release from various cylindrical and spherical matrices. The authors investigated the physical significance of the parameters of the Weibull function, by performing MC simulations for different precise geometries and fitting the function to the results.

The drug delivery device is simulated by labeling the desired shape on a computational grid. Each site of the grid, belonging to the device, can accommodate certain numbers of particles. Diffusion is defined in terms of the random movement of a particle to a random nearest-neighbour site with equal probability. Further, each decision corresponds to an arbitrary time-unit (Monte-Carlo step), which can be shown to correspond to a real-time unit, (Kosmidis et al., 2003a). Assuming that

the drug inside the device undergoes classical Fickian diffusion, the parameters a and b could be expressed as a function of the total surface of the device S, the total volume of the device V, the diameter of the molecules involved, $\triangle l$, and the mean free time τ[6]. The disadvantage of using this approach of describing dissolution from pharmaceutical devices by the Weibull function, and directly calculating the values of a and b as indicated in Kosmidis et al. (2003a), is that $\triangle l$ and τ usually remain unknown because determining their values is quite difficult.

2.2.4 Monte Carlo in studying fractals and percolation

Fractal dimension provides a suitable concept to describe a complex structure, (e.g.: an internal surface of a porous system, the roughness of a particle or of a surface, an organ of interest (e.g. liver, lungs, a tumor and so on). Percolation theory deals with the statistical formation of clusters, presuming a regular lattice underlying the system, (Caraballo (2004) and refs.), i.e. when, by the random addition of a number of objects, a contiguous path which spans the entire system is created, percolation is said to occur (Landau and Binder, 2000). The percolation threshold is a critical point describing a phase transition, dependent on the nature of the system, hence percolation is related to fractal dimension, (Stauffer and Aharony, 1992). Leuenberger et al. (1987) introduced percolation theory to the field of pharmaceutics to explain the mechanical properties of certain controlled release compacts. These authors were the first to consider a compact as a disordered system consisting of particles distributed at random.

More precisely, a pharmaceutical compact is a heterogeneous binary or multiple system consisting of different components. Monte Carlo simulations can be successfully used to model structures, regarded as the coexistence of clusters of different species (percolating or not, depending on the volume ratios).

In Kosmidis and Argyrakis (2000), the authors also investigated the benefits of

[6] The mean free time reflects the particle's average speed, which is directly connected to the temperature of the system.

the Monte Carlo method, modelling drug release from fractal matrices. They consider the possibility of dissolution when the release device, immersed in gastrointestinal tract fluids, is non-homogeneously penetrated by these fluids. Gastrointestinal fluids are known to create areas or channels of high-diffusivity inside certain pharmaceutical compacts. For this reason the authors assume that the device can be modelled by an "irregular" space rather than a homogeneous Euclidean space. This so-called *fractal space* is represented by a percolation cluster at its critical point, with cyclic boundary conditions. Particles are placed only on the sites of the cluster and they can perform independent random walks on these sites. The Weibull function is again found to be the best semiempirical fit to the simulation results.

A direct MC study of the transit flow though the gastro-intestinal tract by Kalampokis et al. (1999), is based around the design of a heterogeneous tube model, which simulates the villi of the gastro-intestine. The model provided for an empty cylinder with random dendritic-type internal structures, (another example of fractal space). The transit flow is simulated using two diffusion models: the *blind* and *the myopic ant*, respectively. The two diffusion models involve two types of biased random walk, which place different emphasis on the motion toward the output of the tube. The model seems useful to simulate the transit and absorption process of oral dosage forms in the gastro-intestinal tract.

2.3 Conclusions

The results from different Monte Carlo modelling approaches, particularly where these have drawn on extensive computing power, have shown considerable promise for the area of drug design and drug formulation. Further work is clearly needed, especially to counter difficulties in calibration of the MC models to real systems, in order to obtain good quantitative results.

The advantage of MC models in general is that they can address diversity and offer a straightforward means of specifying and describing micro-structural situations

and relationships, thus permitting detailed study of the phenomena occurring at dissolution, including the different types of interactions between the components of a dissolving compact, dissolution through a system of channels and pores, establishment of dissolution boundary layers and so on. In addition, MC models can be easily modified and adapted to mimic a wide range of physical situations corresponding to various drug delivery systems. Finally, the evidence from the literature demonstrates that MC methods offer unexplored potential in the field of DDS. The next chapter focuses in more detail on the probabilistic methods used through this thesis. The two chapters which follow present our developments, using direct MC for two different particular cases of DDS: a soluble system and a bulk-eroding system, while Chapter 6 uses an inverse MC technique to analyse a DDS composed of multiple units.

Chapter 3

Probabilistic methods to model drug delivery

3.1 Introduction

This chapter deals with the methods and technologies used throughout the thesis and developed from outlines given in the literature review (Chapter 2). Monte Carlo (MC) methods, which are the main methodology used in this thesis, are formally discussed together with their variations and their relevance in this study. A comparison of direct versus inverse MC methods is also drawn. At the end of the chapter, an insight on a further more sophisticated MC methodology, Sequential Monte Carlo (SMC), is additionally provided.

3.2 Direct versus Inverse Monte Carlo

In the situation where a near-optimal solution (measured in terms of data fit) to the nonlinear problem is sought, direct MC is an important technique to consider. In the case of Direct Monte Carlo, the outcome of the problem is unknown but the ranges, used to select values for different scenarios for the problem, are assumed based on the previous knowledge (physical, chemical) on the problem, Figure 3.1, (a).

In Inverse Monte Carlo simulation, the random selection process is repeated many times to create multiple scenarios. Each time a value is randomly selected, it forms one possible scenario and solution to the problem. Together, these scenarios give a range of possible solutions, some of which are more probable and some less so. When repeated for many scenarios, the average solution gives an approximate answer to the problem, Figure 3.1, (b). This estimate can be refined by simulating further scenarios.

MC methods are extremely important in computational physics and related applied fields, because phenomena, which are otherwise difficult to quantify, can be treated as distributions of random numbers. Studies including Higdon et al. (2002); Huelsenbeck et al. (2001); Mosegaard and Sambridge (2002); Kosmidis et al. (2003a) and references therein discuss both direct and inverse Monte-Carlo simulations, as well as a broad range of applications. Both direct and indirect MC methods have limitations due to their computational complexity and in order to achieve high order of magnitude or high resolution solutions require specialised high performance computing (HPC) resources, such as bespoke clusters. Given current advances in HPC technology, this disadvantage of MC methods is continuously diminishing in importance.

3.3 Direct Monte Carlo and associated methods

3.3.1 General examples

Direct application concentrates on a straightforward simulation of the original problem. It relies either on the numerical solution defining the system, which can be used to predict the model properties at different stages (Feng, 1997), or simply on the hypothetical behaviour of the entities composing the system. Macroscopic properties of the system as a whole are then obtained at the end as a result of the individual stochastic behaviour of its elements. For example, an ant-hill is a complex biological

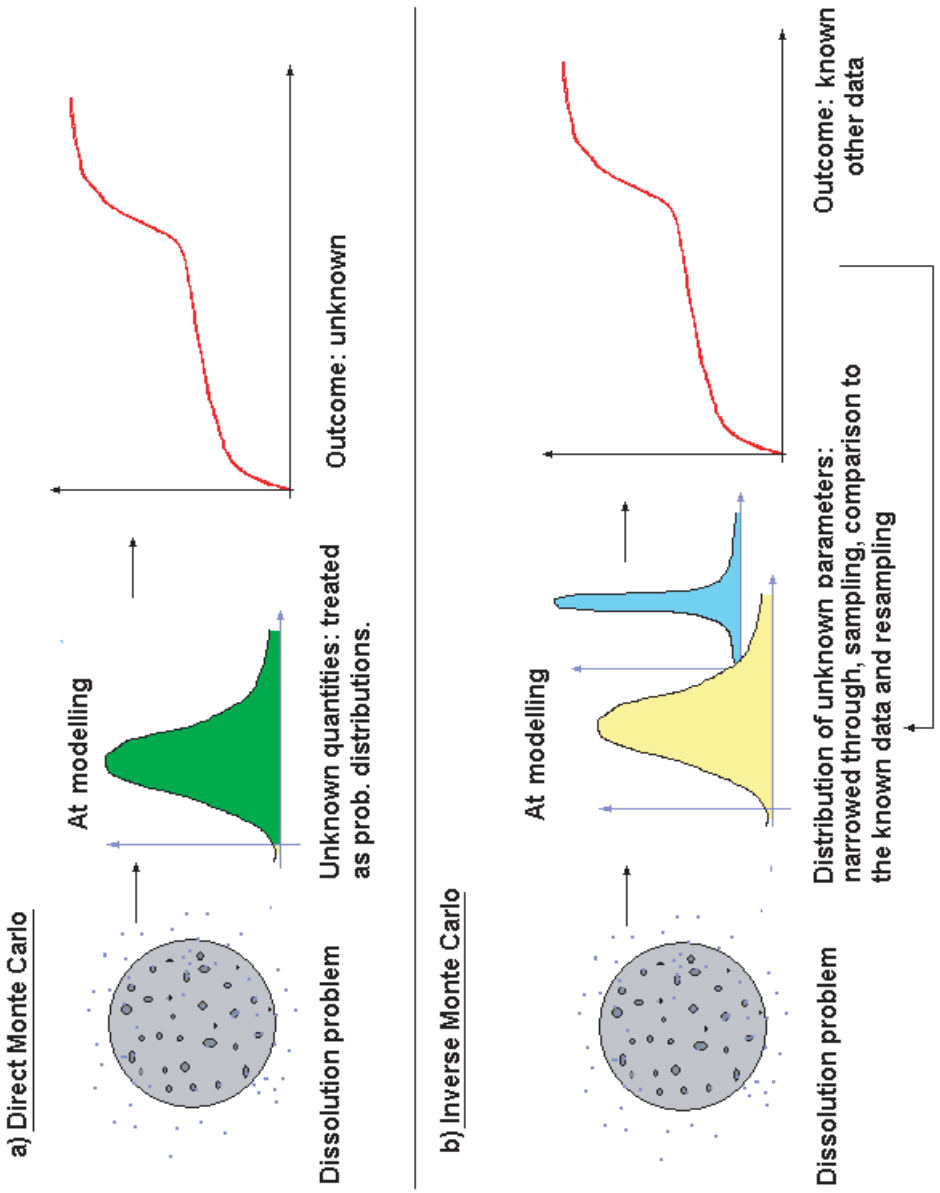

Figure 3.1: Direct versus Inverse Monte Carlo techniques.

system which can be simulated with direct MC techniques. Each ant has its individual characteristics which can be treated in a probabilistic manner. The direction in which the ant will move from its present location is unknown, but may depend on the quantity of food or indicative pheromone left by other ants in the radius of perception of the given ant. The ant is unaware of the ant-hill, which is defined by the emergent behaviour of all ants. The total quantity of food accumulated in the ant-hill is a macroscopic property which may be obtained by applying simple stochastic characteristics for each ant.

Examples of problems, to which direct Monte Carlo techniques have been applied, include the study of systems of interacting atoms, the study of radioactive decay, the simulation of fluid flow from an atomistic perspective (see Landau and Binder (2000)) and the simulation of traffic on roads (Nagel and Schreckenberg (1992) and refs.), etc.

3.3.2 Stochastic Cellular Automata techniques

In modelling systems which exhibit complex behaviour, direct MC sampling methods are often used in the framework of Cellular Automata (CA). CA is an important area in the field of complexity, which links different domains of traditional sciences. One main advantage is that CA focuses on system global phenomena through local simple individual interactions, (Feng, 1997).

Cellular Automata are defined, Chopard and Droz (1998) as an idealisation of a physical system in which space and time are discrete, and the physical quantities take only a finite set of values. This basically reduces to representing the system as a computational grid with specified local relationships, which capture prior knowledge or theories about the microscopic transient behaviour of the real system. An example of this would be the intrinsic dissolution rates of the components belonging to a DDS and dissolution rules, (Zygourakis and Markenscoff (1996) and others. The state of a site of the grid at a given time depends only on its own state at one previous

time-step, and the states of its nearby neighbours at the previous time-step, (Feng, 1997). All cells of the lattice have to be updated synchronously, (Feng, 1997).

Historically, the first CA system was introduced in the 1940s when Ulam and von Neumann developed the idea of using a lattice network for modelling crystal growth (i.e. to model a self-replicating two-dimensional system, (von Neumann, 1966)). Subsequently, Conway's "game of Life", consisting of a CA characterised by very simple rules resulting in very unexpected emergent patterns, was more formally extended, (Wolfram, 2002). In the book "Calculating space", (Zuse, 1970), the author proposed the idea that the physical laws of the universe are discrete by nature and that the entire universe can be imagined as the output of a deterministic computation of a giant cellular automaton. CA techniques have been the subject of extensive work by a number of researchers over the last 20 years. Early potential was realised for statistical physics (Wolfram, 2002), as well as for various fields such as biology, immunology, ecology (Zhang and Liu, 2005; Rohde, 2005; Lichtenegger, 2006) and others.

When considering the transient behaviour of a system, modelled in the framework of Cellular Automata, one or several dynamic features can be treated either as deterministic or as stochastic, with sampling based on direct Monte Carlo techniques. The latter idea is obviously applied when the modeller does not have an exact or complete knowledge about the real system, (which is usually the case).

Allowing evolution through stochastic relations (or rules) specified and statistically averaging over a number of such samples, it is possible to mimic the global, macroscopic behaviour of a system. Predictions can then be made about the system's behaviour as a function of the initial parameters. This permits the investigation of how microscopic behaviour of system components gives rise to important macroscopic features and emergent behaviours.

3.3.3 Stochastic multi-particle and multi-agent techniques

Multi-particle systems are systems composed of many particles, having certain characteristics and interacting between themselves and with their environment according to a number of criteria. When the exact way in which the particles behave is unknown, they can be modelled according to probability distributions. For example, in Chapter 4, when modelling a binary soluble drug delivery systems, the two components - the drug and the excipient - are represented by particles. Technically, the particles themselves are represented by positive numbers, which vary on the sites of a lattice according to probability distributions based on the state and nature of the particles from the neighbouring sites.

The concept of a multi-agent system is more elaborate. The study of multi-agent systems (MAS) focuses on systems in which many intelligent agents interact with each other, (Sycara, 2006). The agents are considered to be independent computational entities, such as objects developed in an object-oriented programming language, software programs or robots. The agents usually have a number of *properties* and perform *actions* in the framework of predefined rules.

The agents are collectively capable of reaching goals that are difficult to achieve by an individual agent or monolithic system. In the case of a DDS with complex inner morphology and complex physics of dissolution, different components of the system, such as different types of macromolecules, can be modelled using agents in the framework of a multi-agent system.

MAS can be claimed to include other than computational systems, (wikipedia, 2006). Biological organisations (like the ant hill from the previous example or species' populations), human organizations, society, life and universe in general can be considered an example of a multi-agent system.

Multi-agent systems can manifest self-organization and complex behaviors even when the individual strategies of all their agents are simple. The agents can function by deterministic or stochastic rules. For example, if a molecule has a number of

directions to move to, the preferred direction can be chosen according to a probability distribution, using direct MC sampling. In this way, in Chapter 5 of this thesis, direct MC techniques are used in the framework of a multi-agent system to model the dissolution from polymeric bulk eroding nano- and microspheres.

3.3.4 Benefits

The benefits of using direct Monte Carlo techniques in drug dissolutions can be the following:

- Provide a better resolution on dissolution problems characterised by different inner porous topologies.
- Treat phenomena or quantities not completely known in terms of distribution densities. Examples of such quantities are the dissolution characteristics of a component when its solubility and diffusivity strongly depends on the environment.
- Direct MC can be used combined with cellular automata, multi-particle and multi-agent techniques to model heterogeneous systems like the DDS.
- Represent the physical system studied as a complex dynamic multi-particle system with a partially stochastic and transient behaviour, in order to observe and predict emergent properties like a particular internal morphology of the system after dissolution has taken place a certain time period or a dissolution profile.

3.3.5 Direct MC for polymer dissolution

In the literature chapter, we have seen that erosion of bioerodible polymers have been approached in model labeled GL by using direct MC techniques, Göpferich and Langer (1995). The MC part involved in treating the dissolution dynamics considers the polymer erosion as a random phenomenon with the hydrolysis of chemical bonds

modelled by a Poisson process. The polymer is represented, (Göpferich and Langer, 1995), by a lattice of sites, containing polymer excipient in a continuous state. A lifetime is assigned to each, where lifetimes of sites are random numbers derived using a first order Erlang distribution:

$$e(t) = \lambda e^{-\lambda t} \tag{3.3.1}$$

where λ is the erosion rate constant and $e(t)$ is the probability that the polymer will erode completely at time t, after its first contact with the water. When the lifetime reaches zero, the polymer is considered to have spontaneously degraded to a crystallised monomer. The process of monomer mass loss can begin. At this point, the mechanistic part of the model is introduced. Mass loss takes place by monomer diffusion inside the matrix, described by a differential equation derived from Fick's first law (Crank, 1975) and relating the spatio-temporal evolution of the concentration of diffusing monomer $C(x,t)$ to the evolution of porosity along the diffusion pathway $\varepsilon(x,t)$ and the effective diffusion coefficient $D_{eff}(C)$. As there is no prior knowledge about the porosity, a probabilistic process is used to calculate the porosity along the diffusion pathway. The function $\varepsilon(x,t)$ represents the element which links the MC part to the mechanistical part. It is built, based on the state of the grid described above, in the following way:

$$\varepsilon(x,t) = \frac{1}{n_y} \sum_{j=1}^{n_y} s(i,j);\ 1 \leq i \leq n_x \tag{3.3.2}$$

$s(i,j)$ takes the value 1 for "eroded" and 0 - for "non-eroded" sites. n_x and n_y are the number of sites in respectively x and y directions. Consequently, on one hand, the concentrations obtained after solving the differential equations are modulated by the overall value of the porosity, but, on the other hand, they are not based on the local effects created by the porous heterogeneous morphology. The authors have

included in the model other differential equations for:

- the velocity of dissolution of the monomer (as a function of the amount of suspended monomer in the solution).
- the pH effects.
- the boundary conditions.

In another model (G1), Göpferich (1997*a*) elaborates the previous direct MC to simulate dissolution of a compact consisting of two different polymers one of which encapsulates small drug molecules. To address this, the author considered two different species of polymer sites (pixels): crystalline (pure polymer) and amorphous (loaded with drug), with individual erosion rate constants λ_c and λ_a respectively. The lifetime t is, on average, higher for crystalline pixels because of their smaller erosion rate λ_c. The release of drug was predicted assuming that, whenever a polymer site erodes, an appropriate amount of hydrophilic drug is spontaneously released directly into the solution.

A similar approach for the dissolution of polymer will be used in Chapter 5 of this thesis to model dissolution of protein from bio-erodoble microspheres.

3.4 Inverse Monte Carlo methods for analysis of inverse problems

3.4.1 Example

Indirect methods are used to solve inversely-posed problems, concentrating on the unknown causes of a phenomenon, the emergent effects of which are observable. Inverse MC methods can be defined as representing the solution of a problem as a parameter of a hypothetical population, and using a random sequence of numbers to construct a sample of the population from which statistical estimates of the parameter can be obtained, (Binder, 1986). For example, we can observe that a number

of species produce the same protein, but that sequences differ in a certain number of amino-acids. Aligning these sequences generates a protein sequence alignment, reflecting the similarities and differences between the species, as an observable effect of the molecular evolution spanning a certain period of time. If the problem is to determine the evolutionary (phylogenetic) relationship between the species, or how the species evolved to produce the observed protein alignment pattern, an inverse Monte Carlo algorithm can be used, (Huelsenbeck et al., 2001). The evolutionary relationship between the species can be graphically represented by a phylogenetic tree. A large population of these trees can be generated using random numbers and each tree compared to the present amino-acid alignment, (giving statistical estimates of the probabilities of the evolution pattern, represented by each phylogenetic tree). Based on the statistical findings, a consensus tree can be built, representing the most likely evolution pattern characterising the set of proteins.

3.4.2 General issues

Inverse Monte Carlo methods have become important in analysis of nonlinear inverse problems where no (or a poor) analytical expression for the forward relation between data and model parameters is available, and where linearization is unsuccessful (Mosegaard and Sambridge, 2002). Indirect methods solve the related problem where the direct mathematical treatment is impossible, using random numbers to generate different states of the related system (Feng, 1997).

The inverse problem is formulated as a search for solutions fitting the data within a certain tolerance, given by data uncertainties. From the point of view of the target of the analysis and the formulation of the problem, inverse MC methods can be divided into two categories: the *sampling* methods and *optimisation* methods. MC sampling is useful when the space of feasible solutions is to be explored, and measures of resolution and uncertainty of solution are needed, (Mosegaard and Sambridge, 2002). The *Bayes theorem* or paradigm is often used in order to calculate

approximate *a posteriori* probabilities for an inverse sampling problem, (Mosegaard and Sambridge, 2002). Indirect MC techniques in a Bayesian formulation are used in Chapter 6 in the context of solving an inverse problem in drug dissolution. Not all inverse MC inversions adopt the Bayesian viewpoint. The review of Mosegaard and Sambridge (2002) gives a number of examples from geophysics where sampling of the parameter space is performed without taking a Bayesian approach. The *Metropolis algorithm* and the *Gibbs sampler* are the most widely used MC samplers for the sampling methods. In this thesis, the *Particle Filtering technique* has been used to solve the dynamical inverse problem posed. This algorithm is described in Chapter 6.

MC optimisation methods are important for searching globally optimal solutions amongst local optima. Simulated annealing (which can be formulated in a Bayesian context) and genetic algorithms (non-Bayesian approach) are examples of inverse MC algorithms for optimisation problems.

The next subsection gives details on the Bayesian formulation.

3.4.3 Bayesian paradigm

The process of refining previous knowledge of the parameters through comparisons with the data is called *empirical updating*. It can be performed on the basis of the classical Bayesian paradigm, which relates probability distributions in the following way:

$$P_{post}(\overrightarrow{\theta}\,|\,\overrightarrow{y}) = \frac{L(\overrightarrow{y}\,|\,\overrightarrow{\theta})P(\overrightarrow{\theta})}{P(\overrightarrow{y})} \tag{3.4.1}$$

where:

- $\overrightarrow{y}$ - a vector containing the available measurements, or the observables.
- $\overrightarrow{\theta}$ represent the unobserved physical quantities of interest, or the state parameters, seeking to give confidence intervals estimates for them.

- $P_{post}(\overrightarrow{\theta}\,|\,\overrightarrow{y})$ is the updated probability of the quantity of interest, $\overrightarrow{\theta}$, given that measured y are observed.
- $L(\overrightarrow{y}\,|\,\overrightarrow{\theta})$ is the likelihood of the model, or the probability of obtaining the data $\overrightarrow{y}$ given the set of parameters $\overrightarrow{\theta}$ and the function $F()$.
- $P(\overrightarrow{\theta})$ is the probability of sampling this particular set of parameters
- $P(\overrightarrow{y})$ is the probability of observing this particular data set.

3.4.4 Sequential Monte Carlo

In Chapter 6 of this thesis, the target is to reconstruct the dynamic behaviour of the powder size distribution of a DDS using sequential observed data: a time series of dissolution points. The Inverse MC technique used is derived from Sequential Monte Carlo (SMC) methods: a set of flexible simulation-based methods for sampling from a *sequence* of probability distributions. These methods were originally introduced in the early 50's by physicists and have become very popular over the past few years in statistics and related fields. For example, they are now extensively used to solve sequential Bayesian inference problems arising in econometrics, advanced signal processing or robotics, (SMC, 2006).

One technique of approaching SMC problems is *particle filtering*. SMC methods approximate the sequence of probability distributions of interest using a large set of random samples, named "particles". These particles are propagated over time using resampling mechanisms. Asymptotically, i.e. as the number of particles goes to infinity, the convergence of these particle approximations towards the sequence of probability distributions can be ensured under very weak assumptions. However, for practical implementations, a finite and sometimes quite restricted number of particles has to be considered. Much research is therefore devoted to the design of efficient sampling strategies in order to sample "particles" in regions of high probability mass.

3.5 Conclusions on the chapter

This chapter presented the methodology related to MC techniques, with the focus on the specific techniques used throughout the thesis. The following chapters discuses how MC methods have been adapted to three different drug dissolution problems.

Chapter 4

Modelling a soluble binary DDS using direct MC techniques

4.1 Introduction

In the area of novel drug delivery systems, *in vitro* dissolution testing is important in designing, developing and testing new pharmaceutical formulations, (Siepmann and Peppas, 2001; Crane et al., 2004b). In order to achieve the appropriate concentrations of the desired drug *in vivo,* (i.e. in the target organs and tissues), during the desired period of time, dissolution profiles *in vitro* need to satisfy certain criteria, generally established by the pharmacopoeias (Sun et al., 2003; Crane et al., 2004b). Thus dissolution *in vitro* can be regarded as the first step toward modelling *in vivo* dissolution and absorption. The dissolution rate is measured, in practice, using one of a number of standard dissolution test methods outlined in international pharmacopoeias, such as the European Pharmacopoeia (EurPh, 2006) and United States Pharmacopoeia (USP, 2006). One commonly used dissolution test apparatus is the Paddle Dissolution Apparatus (see Figure 4.1), known as Apparatus 2, (USP,

2006).

However, there are a number of difficulties related to *in vitro* dissolution testing. Very often, the relationship between the formulation and process parameters of a pharmacological compact, and its required *in vitro* dissolution profile, is not entirely understood, due to the complexity of mass transport at dissolution. Complex mass transport often results in barely trackable effects, like interactions and synergies. For these reasons, experimentation associated with the field of drug design is very costly and time consuming. Thus, modelling drug release can facilitate design of new products, through predictions and selection of key parameters for experimental testing, while helping to gain insight on the phenomena involved in the dissolution process.

Prior to being used to simulate systems such as those involving drug dissolution and delivery, the combination of direct Monte Carlo techniques and Cellular Automata have proved useful in the study of many other kinds of systems exhibiting complex behaviour (Chopard and Droz, 1998; Landau and Binder, 2000). In this part of the thesis we explore the possibilities of MC modelling, for investigating *in vitro* dissolution of a particular class of compacts, used as model drug delivery systems in Healy and Corrigan (1992). The behaviour exhibited by these compacts in reactive media is difficult to predict. Besides this diffusion investigation, our model is designed to capture the particular features of the *in vitro* environment intrinsic to a dissolution paddle apparatus. The following two sections are dedicated to the presentation of the problem and previous solutions proposed. In Sections 3.3 and 3.4 our new MC model is presented and Section 3.5 discusses its validity.

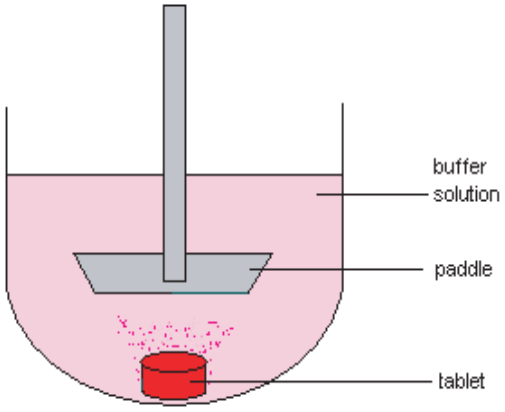

Figure 4.1: Schematic representation of the USP (United States Pharmacopoeia) Paddle Apparatus.

4.2 Multicomponent soluble compacts and the *in vitro* environment

4.2.1 Binary compacts

In the area of dissolution modelling of drug delivery systems, multicomponent soluble systems have not received much attention, despite the fact that solid dosage forms invariably contain multiple soluble components (Ramtoola and Corrigan, 1987). Several theoretical approaches to describing binary systems are due to Ramtoola and Corrigan (1987) and references therein. In the case of non-ionizable [1] binary systems, where the components have different solubilities (C_{s_x} and C_{s_y}) and different diffusion coefficients (D_x and D_y), at the start of the diffusion process, the two components tend to dissolve at rates proportional to their diffusion coefficients. Later on, only one of the components generally remains at the solid-liquid interface. The

[1] can non convert into ions

other component has to dissolve through the porous system formed inside the less soluble component. Only at the critical mixture ratio, defined by:

$$\frac{N_x}{N_y} = \frac{D_x C_{sx}}{D_y C_{sy}} \tag{4.2.1}$$

will there be *no* porous layer formed at the surface and both components will dissolve at a rate equal to that of the pure component. In each case, N_x and N_y are the original amounts of components x and y. In the general case, the dissolution rates of the components are calculated according to Fick's first law (Crank, 1975). When a steady state is reached, the limiting dissolution rate of the component which remains at the surface is given by:

$$G_x = \frac{D_x}{h} C_{sx} \tag{4.2.2}$$

while the dissolution rate of the receding component y is given by:

$$G_y = \frac{D_y C_{sy}}{(h + \frac{\tau}{\varepsilon})(s_1 - s_2)} \tag{4.2.3}$$

where h is the thickness of the diffusion film, τ - the tortuosity with reference to the complexity of the system of channels which forms in 3D, ε - the porosity (often unknown) and $(s_1 - s_2)$ is the thickness of the porous layer formed at the solid-liquid interface. In the case where the components are ionizable the situation is more complex, (Ramtoola and Corrigan, 1987). In experiments on the dissolution of benzoic and salicylic acids in buffered media, the authors found that the dissolution

rates, particularly for benzoic acid at intermediate weight fractions, were lower than theoretical rates and explained these in terms of surface pH effects.

Subsequently, Healy and Corrigan (1992, 1996) conducted experimental and theoretical studies on the dissolution of soluble ibuprofen/acidic excipient compressed mixtures in reactive media, using model compacts. These were obtained by first grinding the two components into powders, mixing the products, and finally compressing them. On dissolving in reactive media, the compacts exhibit complex behaviour, in spite of their binary composition. The authors presented a modified model for dissolution of binary systems of ibuprofen and various acid excipients. The predicted dissolution rates for the excipients tend to be higher than those obtained experimentally in the case of more soluble acids.

4.2.2 Introduction to the *in vitro* dissolution medium

4.2.2.1 Dissolution apparatuses

A specific interest of this thesis is to consider the *in vitro* environment used for dissolution testing, as settings of the dissolution apparatuses are known to affect the process of compact dissolution. In Healy and Corrigan (1992), the *in vitro* environment consisted of a water-jacketed flat-bottomed dissolution apparatus (Healy, 1995), and in Healy and Corrigan (1996), a more standard dissolution apparatus of USP type 2 has been used (see Figure 4.1).

A standard dissolution apparatus consists of a container, filled with the dissolution medium (designed to mimic *in vivo* conditions), with the compact situated at the bottom of the apparatus (see Figure 4.1). The dimensions of the apparatus are such that we can make the assumption that the solvent inside has sink or close-to-sink properties, (i.e. the system behaves as if the tablet dissolves in an infinite solvent).[2]

[2] This means that away from the dissolving compact, the concentration of solute in the solvent can be approximated by zero.

A paddle is used to stir the buffer solution at a constant rate. The stream created produces a velocity boundary layer around the compact. There are two mechanisms of mass transport in the system: diffusion and advection[3], the latter due to the component of the stream velocity oriented along the surface of the compact. This component is responsible for carrying away quantities of matter proportional to it's magnitude. One of the targets of the present work was to build into our Monte Carlo model both mechanisms of transport above.

4.2.2.2 Velocity and concentration boundary layer

The hydrodynamic conditions of the *in vitro* environment are such that the velocity boundary layer at the top of a cylindrical compact is very difficult to describe. Crane et al. (2004a,b) investigated the velocity boundary layer, as well as the concentration boundary layer formed around the curved surface of a cylindrical compact in the USP apparatus, in order to better understand the concentration profiles which form at the solid-liquid interface on dissolution.

In this study, the component of fluid flow parallel to the curved surface of the cylinder, is examined. Far away from the compact, the fluid flows at its maximum velocity: $\vec{U}_0$, but approaching the solid-liquid interface, the velocity decreases to zero at the surface of the solid, where the "non-slip" condition holds. Hence, the term *velocity boundary layer* refers to the small region of space close to the solid immersed into the flowing liquid, where the flow velocity varies from zero to it's maximum $\vec{U}_0$, see Figure 4.2, (a).

As the solid dissolves, a concentration profile is established at the solid-liquid interface. Since the ratio of the diffusivity D to the kinematic viscosity ν of the fluid (i.e. of the buffer solution), is very much less than unity, the concentration boundary layer thickness δ_c is smaller than the velocity boundary layer thickness δ, (Crane et al., 2004a). For the immediate solid-liquid interface, in contrast to the

[3] The term "advection" refers to the transport of material from one region to another.

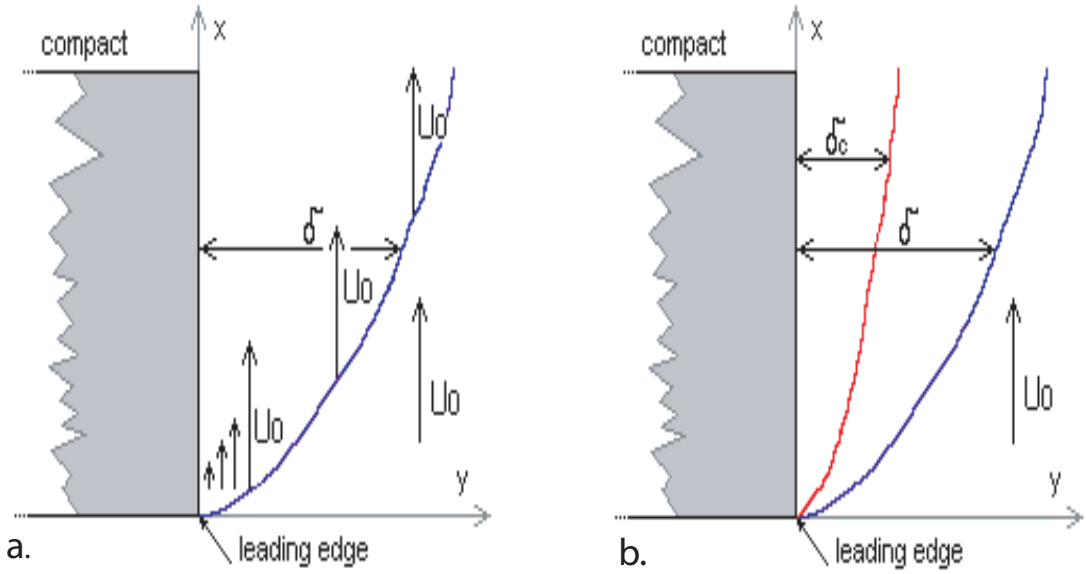

Figure 4.2: a) The velocity boundary layer of a non-dissolving solid immersed in a flowing liquid. b) Velocity and concentration boundary layers for a dissolving solid. The red curve situated closer to the compact surface indicates the points in space where concentration of solute in solvent reaches low, close to zero, values.

velocity profile, the concentration is at saturation, decreasing to zero away from the surface, see Figure 4.2, (b). Thus, by the term *concentration boundary layer*, we mean the region of solution in the solid-liquid interface vicinity, where the concentration of solute in the solvent is greater than zero. The thicknesses of velocity/concentration boundary layers vary with the distance from the leading edge of the compact, Figure 4.2.

4.2.2.3 Mathematics for boundary layers

The velocity boundary layer thickness for a flat plate[4] in an axial flow is given by the solution of the Blasius equation (Prandtl and Tietjens, 1957; Schlichting, 1979):

[4]approximation as, from Crane et al (2004a), the boundary layer thicknesses are very much smaller than the radius of curvature of the cylindrical formulation.

$$\delta = 3.4\sqrt{\frac{x\nu}{U_0}} \tag{4.2.4}$$

where x is the distance from the leading edge of the compact (Figure 4.2) and ν and U_0 are defined as previously.

Equation (4.2.5) gives the relation between δ_c and δ:

$$\frac{\delta}{\delta_c} = S_c^{\frac{1}{3}} \tag{4.2.5}$$

where S_c is the Schmidt number, defined as:

$$S_c = \frac{\nu}{D} \tag{4.2.6}$$

Once the thickness of the concentration boundary layer has been computed, it is possible to compute the value C^* of the maximum concentration at each point (y, x), (Figure 4.2), within the boundary layer. One way to compute the concentration in the boundary layer is to use a Pohlhausen solution, which approximates the variation of concentration by either a polynomial, or, in the case of Crane et al. (Crane et al., 2004b), by a sinusoid:

$$\frac{C^*}{C_{satur}} = 1 - sin\left(\frac{\pi y}{2\delta_c}\right) \tag{4.2.7}$$

Here, C_{satur} is the saturation concentration of a given component, C^* is the concentration at a given point y within the concentration boundary layer.

Figure 4.3: Layered compact versus matrix compact

For the purposes of simplification, the problem of *in vitro* radial dissolution was investigated in Crane et al. (2004a,b) for simple layered binary systems (with 3 to 5 alternate layers, as in Figure 4.3). The investigation in Crane et al. (2004b) used numerical methods in combination with a Pohlhausen profile (Equation (4.2.7)), to model the concentration boundary layer formed around the dissolving cylindrical device in the USP apparatus.

Numerical results, using Finite Element techniques, depicting the concentration profile within the boundary layer during a very short period of time, together with those from a semi-analytical Pohlhausen type approximation to the concentration boundary layer, have shown good agreement with experimental data, (Crane et al., 2004b). These studies have demonstrated that the conditions *in vitro* have an important impact on the way in which a compact dissolves. However, modelling the boundary layer for dissolving *matrix compacts* has never previously been attempted. It seems that matrix compacts exhibit physics which are less tractable by conventional numerical methods.

4.2.3 Experimental setup

We use the data obtained by Healy and Corrigan (1992) for the dissolution of ibuprofen (drug) and a wide range of acid excipients from mixed disks in reactive medium, (phosphate buffer), as reference.

The compacts used in the experimentation were cylinders, obtained by compressing 250 mg of powder, having a composition of drug and excipient on a weight-for-

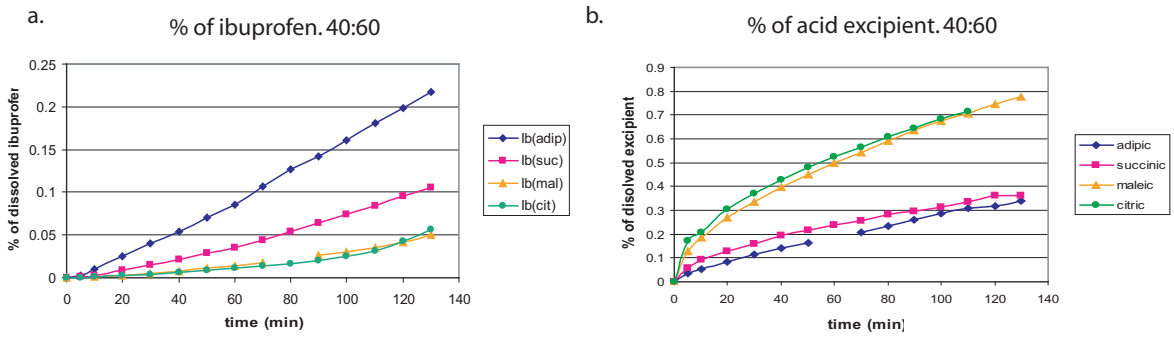

Figure 4.4: Experimental results
a) Dissolution profiles of the acid excipients from 40:60 ibuprofen/acid excipient compressed discs. b) Dissolution profiles of ibuprofen from 40:60 ibuprofen/acid excipient compressed discs. Based on published data, Healy and Corrigan (1992).

weight basis. Previous processing by grinding and sieving the components permits control of particle size of both drug and excipient powders. The drug and the excipient have dramatically different solubilities and slightly different diffusivities, while the acid excipient has an effect on the solubility of ibuprofen at dissolution. The compact dissolves according to the following mechanism: at the dissolution of the acid excipient, the pH of the buffer decreases and this has a suppressing effect on the solubility of the other component (the ibuprofen). The dissolution apparatus consisted of a water-jacketed flat-bottomed 450 ml cylindrical glass vessel. 250 ml medium was used. The medium was stirred with a 3-blade stirrer immersed to a depth of 2.5 cm (Healy, 1995).

As an example, Figure 4.4 represents the dissolution of different cylindrical binary matrix systems: all of them contain ibuprofen (Solubility=6.3 mg/ml, Healy (1995)) and an acid excipient of much higher solubility (see Table 4.1). The left part of Figure 4.4, (a) represents the dissolution profiles for four different acid excipients. Figure 4.4, (b) shows the dissolution profiles for the drug, which is ibuprofen in all cases. It can be observed from Figure 4.4 that the more soluble the excipient, the more it suppresses the solubility, and therefore the release, of ibuprofen.

Type of acid excipient	Solubility, mg/ml
Adipic	44.4
Succinic	120.4
Maleic	694
Citric	883.6

Table 4.1: Solubilities of the acid excipients, from (Healy, 1995).

4.3 Modelling

4.3.1 Main characteristics of the model

In this investigation, we simulated the dissolution of the binary soluble system presented in the previous sections, using a 2D lattice and a Monte Carlo algorithm, as described below. The model specifically takes into consideration both the diffusion and advection mechanisms of dissolution. The algorithm is implemented in C++ and the library OpenGL (OpenGL, 2006) has been used for the visualisation.

We represent the two solid species by particles with different properties. These particles can be moved on the sites of the lattice according to specified rules. In this particular case, we make the assumption that one species dissolves *independently* and is referred to as the *excipient* in the following. Dissolution of the other species, the *drug* in our experimental context, strongly depends on that of the former. The solvent is represented by empty sites. The state $\psi_{(i,j)}$ of a site (i, j) is defined by the quantity and type of the particles with which it is filled, i.e. the concentrations $C_D(i, j)$ and $C_E(i, j)$ of drug and excipient particles, respectively. The state of any site can evolve in time according to a function, which depends on the concentrations at the site itself and those in the local neighbourhood (Figure 4.13). The process of diffusion is simulated merely by the tendency of particles to move to adjacent sites according to specified rules. Figure 4.5 illustrates the possible states in the model and their schematic behaviour. The schemes show the benefits of this kind of model for simulating cases where pores are formed inside a compact by the quick dissolution of one of the components. The second component has to dissolve through

these pores and this process is different from dissolution at the surface.

Our main target is to be able to predict the dissolved quantities of either of the two species, $M_D(t)$ and $M_E(t)$, at each time step.

4.3.2 Initialisation

The spatial configuration of the DDS is generated as follows:

- For each site of the lattice, which has to be occupied by "matter" in solid state, a random number uniformly distributed between 0 and 1 is generated.
- If this number is less than or equal to the proportion of drug, this site is considered as *drug*. It's state is assigned $\psi_{(i,j)}(t) = |D$, and the site is filled with a number n_D of drug particles.
- Otherwise, the site is filled with n_E excipient particles and $\psi_{(i,j)}(t) = |E$.
- In order to simulate the phenomena at the solid-liquid interface, the sites around the solid are assigned the liquid state: *solution*. We distinguish two types of *solution* states: (i) sites which are situated in immediate proximity to the solid-liquid interface and which form the concentration boundary layer with thickness δ_c, (see Section 4.2.2): $\psi_{(i,j)}(t) = |-$, and (ii) those far enough from the dissolving compact and which behave as a sink [5]: $\psi_{(i,j)}(t) = |s$ (see Figure 4.5)
- The sites in the solid which are exposed, through nearest neighbour connectivity, to *solution* sites, are attributed the following states: *leaking drug* and *leaking excipient* ($\psi_{(i,j)}(t) = |+$ and $\psi_{(i,j)}(t) = |x$). From this instant, the

[5] The main difference between the boundary layer solution sites and the sink solution sites is that the first can receive and accommodate diffusing drug and excipient particles, whereas the second have the concentration of the diffusing species set to zero. This artifact comes from the assumption that the concentrations in the stirred liquid are so much smaller then the concentrations in the boundary layer, that these are approximated by zero: $C_{(i,j)} = 0$ when $j = \delta_c$. When, in later stages, particles reach a sink solution site, they will be considered completely dissolved, thus they will be discarded from the system and their quantities - added to $M_D(t)$ and $M_E(t)$.

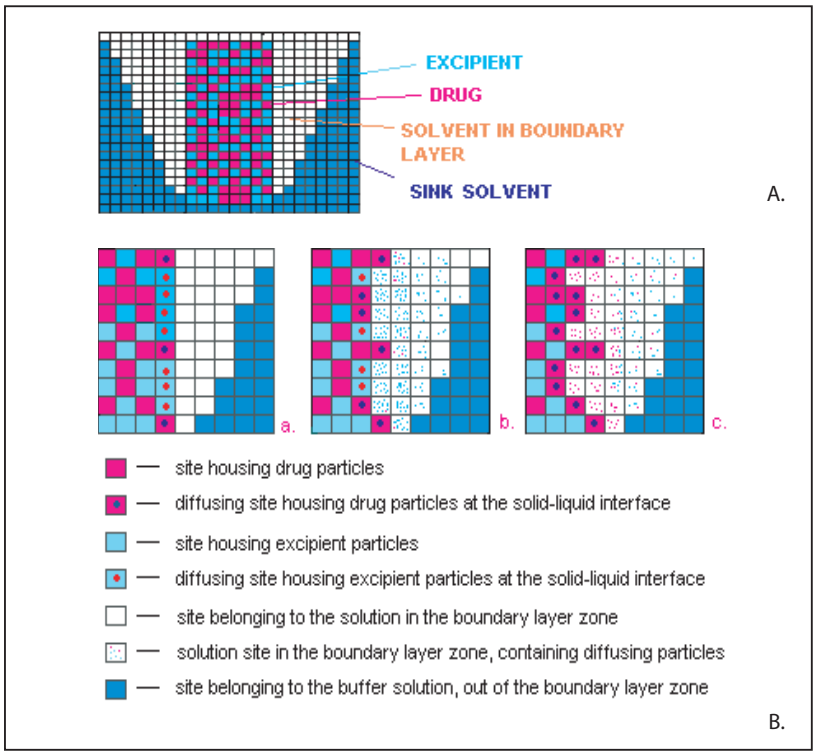

Figure 4.5: 2D model for a dissolving binary system.
a) Schematic representation of 2D model. The real dimensions are not respected in the picture.
b) Simplified model of dissolution of a drug-excipient system. The grid represents a cylindrical tablet in longitudinal cut.

particles from these sites will be allowed to move. The content in particles of leaking sites can only decrease.

4.3.3 Modelling diffusion

Diffusion refers to the process by which particles (molecules or ions) of different species move from higher to lower chemical potential (represented by a change in concentration), as a result of their kinetic energy. In the model we represent the two solid species by particles. Since the components in the compact have highly different solubilities, they are expected to dissolve at different rates. For this reason, we allow for more then one particle to move to an adjacent site. The solubility of

a given species is modelled by allowing not more than a fixed number of particles, $S = C_{MAX}$, on the sites to be considered as filled with solvent. The maximum allowed concentrations in the solvent, $C_{MAX_{Drug}}$ and $C_{MAX_{Excipient}}$, are proportional to the real solubilities. This means that:

$$\frac{C_{MAX_{Drug}}}{C_{MAX_{Excipient}}} = \frac{S_D}{S_E} \tag{4.3.1}$$

In addition, the local solubility of a component depends on the local concentrations (Healy and Corrigan, 1992). Only the sites in the states $\psi_{(i,j)}(t) = |-$, $\psi_{(i,j)}(t) = |+$ and $\psi_{(i,j)}(t) = |x$ can diffuse. If the site (i, j) is in one of the above states, the possibility of diffusion is considered by first looking at the kind of particles about to diffuse: dependent (drug) or independent (excipient) particles.

The decision to permit a batch of particles to diffuse is accepted or rejected by:

- Consulting a gradient-dependent probability, p_E in the case of the excipient (Equation 4.3.2). In the following, (i, j) symbolises the current site and $(i*, j*)$ - the adjacent site to which the possibility of diffusion is considered.

$$p_E = \frac{C_{E(i,j)} - C_{E(i*,j*)}}{C_{E(i,j)}} \tag{4.3.2}$$

- Consulting a probability, dependent on the excipient concentration in the neighbourhood, p_{D_0} ($p_{D_0} = f(\sum C_{E(i*,j*)})$, where $(i*, j*)$ are all the neighbouring sites) and a further, gradient-dependent probability, p_{D_1}(Equation 4.3.3) in the case of the drug particles about to diffuse:

$$p_{D_1} = \frac{C_{D(i,j)} - C_{D(i*,j*)}}{C_{D(i,j)}} \tag{4.3.3}$$

- The diffusion operation itself is performed by calculating the number of particles of excipient, f_E, and those of drug, f_D, which will move to each of the adjacent sites. The number of excipient particles which hop from the site (i, j)

to the site $(i*, j*)$ are given by:

$$f_E = p_E \times X_E \tag{4.3.4}$$

where X_E is a variable, uniformly distributed between one particle and the maximum number of particles allowed on the site $(i*, j*)$. The quantity of the particles on a site is limited by the species solubility C_{MAX}, therefore

$$X_E = \mathcal{U}(1, C_{MAX_E} - C_{(i*,j*)_E})) \tag{4.3.5}$$

- A normal distribution can also be used to calculate X_E.

In order to perform a synchronous updating of the diffusion operation, we compute for all the cells on the lattice the incoming and outgoing quantities, and only then update the actual concentrations and increment the Monte-Carlo time step. After the update, all the particles which diffuse to sites in a state of sink solution $\psi_{(i,j)}(t) = |s$, are considered to be completely dissolved and are discarded from the system. The values of $M_D(t)$ and $M_E(t)$ are incremented respectively by the number of either kind of particles discarded from the system.

4.3.4 Modelling advection

Fine-grained

As mentioned, advection plays an important role in mass transport in the *in vitro* environment of the apparatuses used for dissolution testing. The flow created in these is very complex (Crane et al., 2004a,b; McCarthy et al., 2003). In this model we make the assumption that there is always a free stream component which is oriented parallel to the surface of the compact, exposed to the dissolution medium.

If the simulations consider the size of the site to be much smaller then the thickness of the diffusion boundary layer, the advection operation can be performed us-

ing the Pohlhausen concentration profile (see Section 4.2.2) in a discretized form, adapted for our lattice model: $(C^*_{E(i,j)},\ \psi_{(i,j)}(t) = |-)$. We make the assumption that a velocity/concentration boundary layer is established at the liquid/solid interface. At the surface, the velocity is zero and thus the concentrations of all the diffusing species are at saturation. Therefore, in immediate proximity to the solid surface, there are only diffusion-based phenomena. As we move away from the surface, the velocity increases from zero to it's maximum $\vec{U_0}$ at the edge of the velocity boundary layer. At the same time, the concentration decreases, because the flow is responsible for carrying away quantities of matter proportional to the velocity of the stream.

In order to simulate the advection process, we consider every solution site within the boundary layer and the number of particles of drug and excipient $a_{D(i,j)}$ and $a_{E(i,j)}$ which will be carried away from it by the stream, to symbolise the mass transport property. The quantities $a_{D(i,j)}$ and $a_{E(i,j)}$ are computed so that, after they will have been discarded from the system, a Pohlhausen concentration profile is represented by Equation 4.2.7 in discretized form in the boundary layer region.

After an advection step is performed, there are cells from the boundary layer, in *solution* state, which have the outgoing quantities of particles $a_{D(i,j)}$ and $a_{E(i,j)}$, different from zero. The corresponding update operation consists of a sweep of the lattice which finds and discards these particles from the system, symbolising the mass transport due to advection. These values are added respectively to $M_D(t)$ and $M_E(t)$, while $a_{D(i,j)}$ and $a_{E(i,j)}$ are re-set to zero. As the tablet dissolves, the solid-liquid interface recedes in the space.

Coarse-grained

When the size of a site is of the same order of magnitude as the thickness of the diffusion boundary layer, the advection mass transfer can be performed by *inverse Monte Carlo* simulations. We consider that diffusion *in the pores* and diffusion *at*

the surface of the solid does not occur in the same way. At the surface, larger X_E than in Equation 4.3.5 (see previous section) are allowed to diffuse to adjacent sites. A normal distribution can be used in this case: $X_E = N(\mu, \sigma)$, where μ is the mean and σ - the standard deviation of the distribution. In order to find out μ and σ, it is possible to:

- Sample values for μ and σ : μ_i and σ_i- from, for example, uniform distributions.
- Use these values to perform a simulation and generate a dissolution profile.
- Compare the dissolution profile obtained to the real data.
- Accept μ_i and σ_i if the results of the simulations are satisfactory.
- Reject μ_i and σ_i in case of unsatisfactory results, re-sample other values, μ_{i+1} and σ_{i+1}, and repeat all steps.

4.3.5 Updating

Before beginning any mass transport operation, the following update is performed:

* If $\psi_{(i,j)}(t-1) = |D$ and this site has any *solution* $|-$ in the neighbourhood, then it becomes a leaking drug site:$\psi_{(i,j)}(t) = |+$.

* If $\psi_{(i,j)}(t-1) = |E$ and this site has any *solution* $|-$ in the neighbourhood, then it becomes a leaking excipient site:$\psi_{(i,j)}(t) = |x$.

* If $\psi_{(i,j)}(t-1) = |P$ this site has any *solution* $|-$ in the neighbourhood, then this pore, and all the cluster of pores connected to it becomes *solution.*

If the concentration of a leaking site decreases under the solubility (C_{MAX_D} or C_{MAX_E}), its state is updated to the *solution* state. This implies that the particles at the site are completely dissolved and that the site can begin to receive new particles:

* If $\begin{cases} \psi_{(i,j)}(t-1) = |+ \\ C_{D(i,j)} \leqslant C_{MAX_D} \end{cases}$ then $\psi_{(i,j)}(t) = |-$.

* If $\begin{cases} \psi_{(i,j)}(t-1) = |x \\ C_{E(i,j)} \leqslant C_{MAX_E} \end{cases}$ then $\psi_{(i,j)}(t) = |-$.

After the updating phase, the diffusion can begin.

4.4 Results and discussion

A MC time step, corresponding to time t, sequentially applies the operations of diffusion, advection and updating to all the sites from the lattice. The system is left to evolve during many MC iterations, incrementing the time value after each iteration. Samples of $M_D(t)$ and $M_E(t)$ are taken periodically, in order to plot their profiles at the end of the simulation.

We average simulation results over a number of initial configurations of the device, because the spatial packing of the two components in the compact has some slight effect on the dissolution results. The number of simulation runs needed to obtain an average depends on the dispersion of the results, which is sensitive to the size of the lattice used. In the following, 20 simulations were enough to obtain the average on a lattice of 80×130 sites.

In this section, we analyse the capacity of the model described above to predict correct effects of the design parameters, such as initial drug loading, initial porosity, form of the compact etc., on the dissolution rates. Despite strengths, such as conserving the behaviour encountered in real life (through microscopic content of the rules specified), any computer solution is prone to develop and exhibit its own spurious effects. We must therefore investigate the extent to which purely numerical phenomena may affect the results of the simulations.

4.4.1 The effect of the acid excipient solubility

The suppression effect of the acid excipient is indirectly modelled by defining rules for dramatically decreasing the diffusing probabilities of the drug in the presence of local high concentrations of excipient. We have carried out simulations with

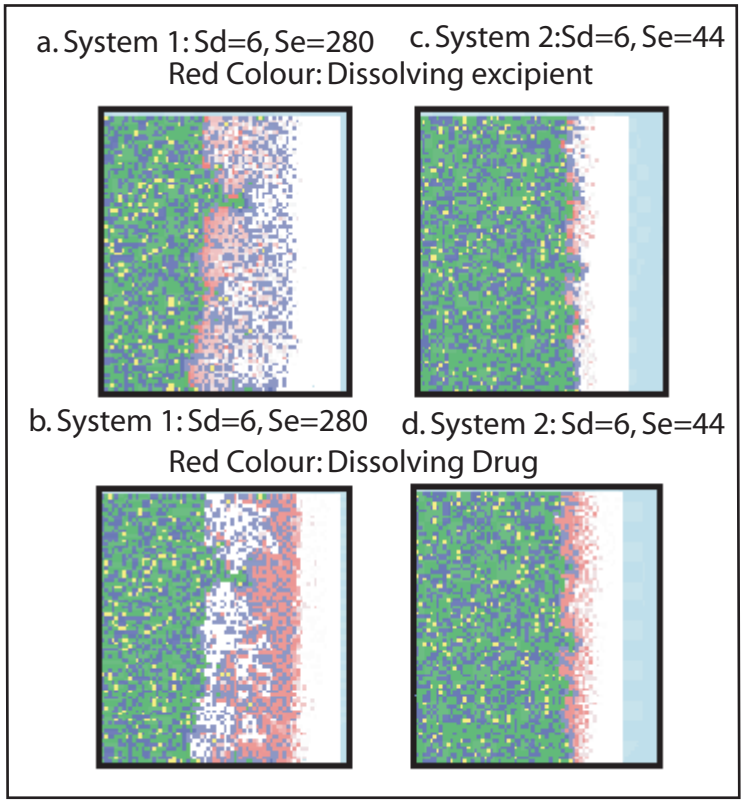

Figure 4.6:
Colour code: green - solid excipient, blue - solid drug, yellow - pores, white - solution in the boundary layer, clear blue - sink solution, shade of red in (a) and (c) - the concentration of excipient in the boundary layer solution, shade of red in (b) and (d) - the concentration of drug in the boundary layer solution.

binary systems where the properties of the dependent species (drug) are retained for all experiments for a range of solubilities S_E of the independent and more soluble species (excipient).

Figure 4.6 compares the behaviour of the system for two different excipients E_1 and E_2, $S_{E1} > S_{E2}$. The properties of the dependent component, the drug, are kept constant during the two simulations and $S_{E1} > S_D$, $S_{E2} > S_D$. All the figures show the state of a 130×80 sites compact after 4000 generations. Figure 4.6, (a) and (c) shows the concentration profiles for, respectively, E_1 and E_2. In both cases irregular dissolution fronts are developed, but the extent of their roughness is obviously a function of the solubility of the excipient. The excipient influences the dissolution

of the dependent species by filling the free space with its particles and consequently decreasing the local solubility of the drug. The higher the solubility of the excipient, the higher the capacity of a solution site to accommodate excipient particles.

For the case of E_1, we note that the excipient has strongly receded from the surface, (Figure 4.6, (a)), and has created a porous layer, through which the poorly-soluble drug dissolves only in the region where the excipient concentrations are very low, (Figure 4.6, (b)). The drug dissolves through the pores created by the dissolution of E_1. For E_2 very different behaviour is exhibited. The porous layer is much thinner than in the previous case and the drug boundary has receded inward to a greater extent. This type of behaviour of binary drug delivery systems has been observed experimentally and described by Ramtoola and Corrigan (1987).

We have plotted the fraction of the dissolved drug and excipient against the time, comparing the dissolution profiles of drug and excipient with those obtained in experiment. The simulated results reproduce well the behaviour observed in the dissolution of real binary compacts, containing ibuprofen and acid excipient (Healy and Corrigan, 1992).

Figure 4.7 shows the drug and the excipient profiles for different solubilities and for two different drug loadings. The porosity of the matrix is kept constant. Each dissolution curve is obtained by averaging the results of a particular number of simulations (20), characterised by the same initial parameters but with different initial configurations of the compact, (the two species are randomly distributed in the compact for each simulation). The plots show that as the solubility of the excipient increases, the dissolution of the drug is suppressed to a progressively greater extent. As in experiment (Healy and Corrigan, 1992), a positive curvature for the drug and a negative curvature for the excipient are obtained.

With highly-soluble excipients, the dissolution of the drug is very slow at first, but when almost all the excipient is dissolved, the drug changes its dissolution rate, as can be seen for some of the profiles in Figure 4.7, (c). In Figure 4.7, (c), the orange

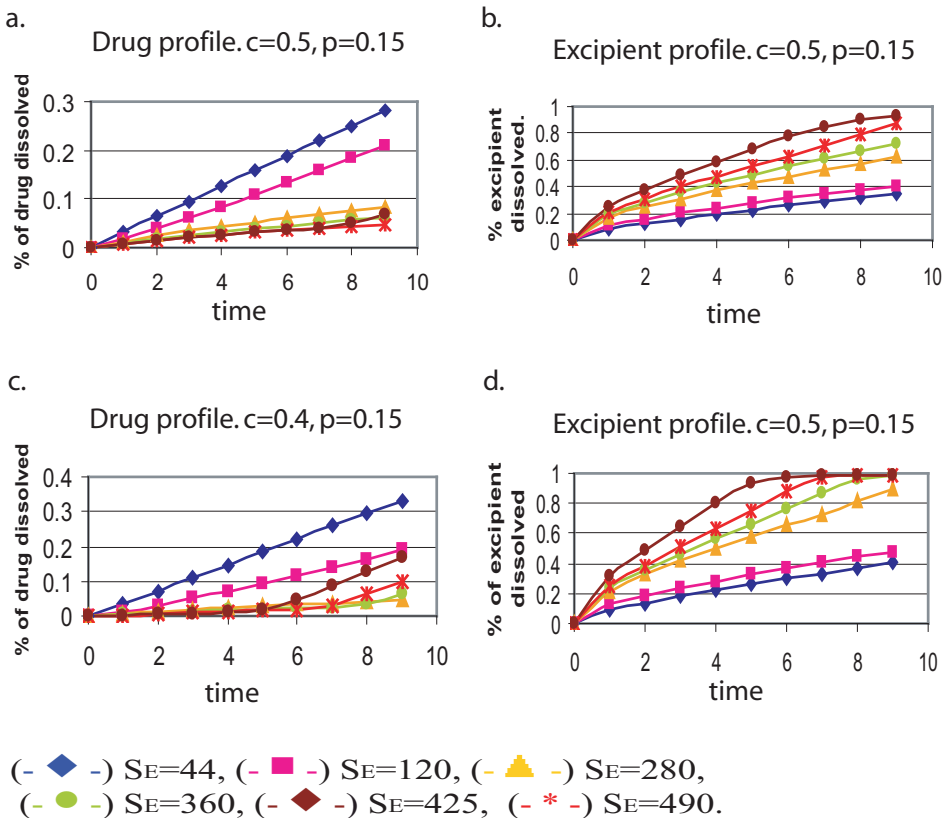

Figure 4.7: The effect of the solubility of the independent species on the dissolution of the dependent species

ibuprofen profile corresponds to the micro-environment represented on Figure 4.6 (c) and the blue profile shows the case of E_2, (Figure 4.6, (d)).

We note that suppression of the advection step from this model leads to simulation results that strongly underestimate the quantities of drug dissolved, hence taking into consideration environment-related features are important. Figure 4.9 shows the way in which the dissolution results are underestimated especially for drug used in a binary system with excipients of a lower solubility. Without the advection operation, it is not possible to obtain profiles for the ibuprofen like those in combination with adipic or succinic acids. In Figure 4.9, (b) the effect is less clear because of the scale of the representation, but the dissolution rates of the drug are still strongly underestimated.

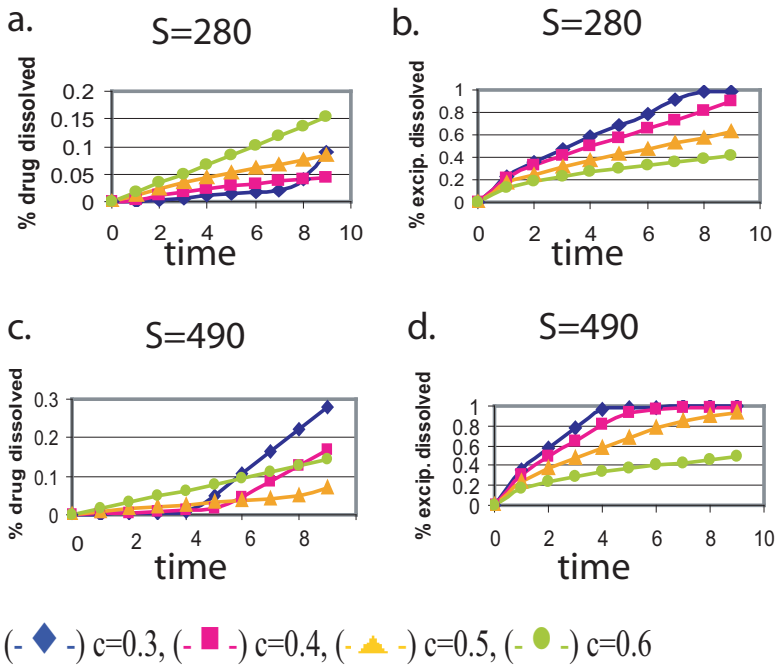

Figure 4.8: Loading effect for excipients with high solubility

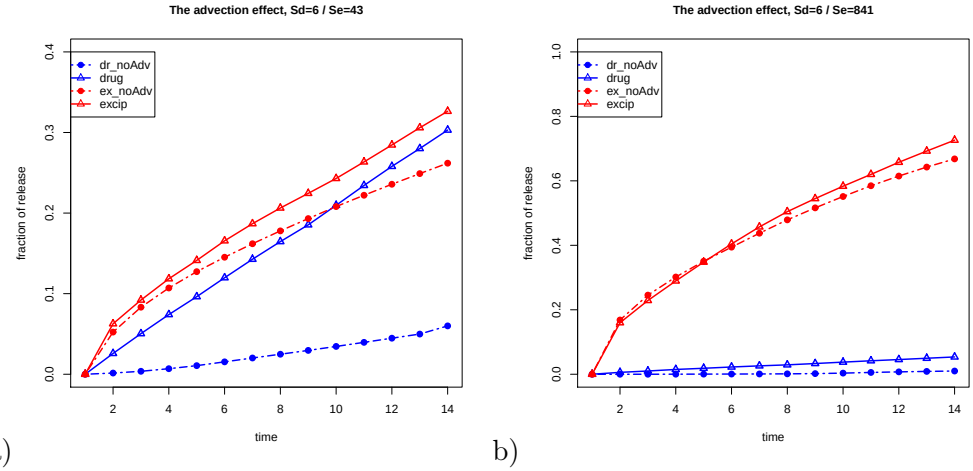

a) b)

Figure 4.9: The effect of the advection operation in the simulation. The pointed curves represent simulations where the advection step has been suppressed. The continuous curves represent simulations where both diffusion and advection have been taken into consideration.

4.4.2 Loading effect

In terms of the effect produced by the drug loading at the initial stages of the simulation, the more drug the matrix contains, the less excipient is present, hence the higher the dissolution rates for the drug. Figure 4.8 confirms this theory and shows more explicitly the effect of the initial loading of drug on the dissolution profile of the components. The same trend is observed in the experimental data: the greater the drug loading, the greater the fraction of the total drug mass released.

However, if we produce simulations with an "excipient" of a lower solubility, such as $S_E = C_{MAX_E} = 44$, the loading effect is directly opposite to the previous case, (Figure 4.10). For 50% drug loading, a smaller fraction of total drug mass is released than in the case of 40% of drug. A matrix with lower initial drug loading contains a higher excipient loading. On dissolution, the excipient creates a certain level of wall roughness, increasing the dissolution area for the drug and thus enhancing dissolution of drug, which is not suppressed by the relatively low excipient concentrations.

After performing quantitative simulations (see Section 4.5), directly comparable to the experimental profiles, this inversion-effect appeared for situations of modelling mixtures of ibuprofen with adipic and succinic acid, respectively, (see Table 4.1), but did not appear in the experimental results. The reason for this appears to be that the model generates values of excipient concentrations which are too low for the case of 50% drug loading. This may be happening because modelling a 3D problem in 2D, as discussed in section 4.5), is overly-simplistic for the mechanisms involved. We have also found, when calibrating quantitative models with experimental data from dissolution of ibuprofen-only compacts, that the method of simulating advection, (as for results in Figure 4.10), is not sophisticated enough to mimic advection from experiment. After introducing a correction for the advection, the inversion-effect disappeared and agreement with the experimental data was obtained.

Among all acids used in experiment, adipic acid is the acid with the lowest

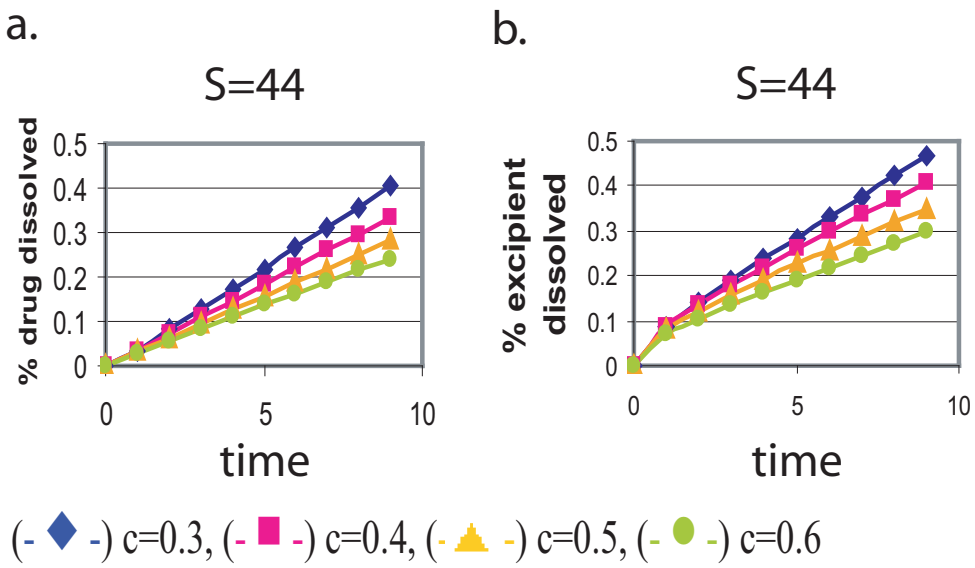

Figure 4.10: Loading effect for excipients with relatively low solubility
a) Dissolution profiles for the drug. b) Dissolution profiles for the excipient.

solubility [6]. The refined quantitative advection-corrected model suggests that the inversion effect reappears and increases for lower values of the excipient's solubility. It is unclear whether this would be confirmed in reality if the corresponding components were available for experimentations.

4.4.3 The effect of initial porosity

Figure 4.11 presents simulation results for different porosities for dissolution of compacts containing very soluble excipients. The porosity value represents the fraction of sites in the compact, which are free of particles. For the excipient, a higher porosity value enhances its dissolution rate. This effect increases in proportion to the excipient solubility, (Figure 4.11, (b) and (d)). In Figure 4.11, (d) the porosity factor causes the dissolution profiles to be highly dispersed. On the other hand, drug dissolution is suppressed more markedly for higher porosity at the start of the disso-

[6] it is the solubilities which are compared instead of the pKa values, because these were very close for the acids used

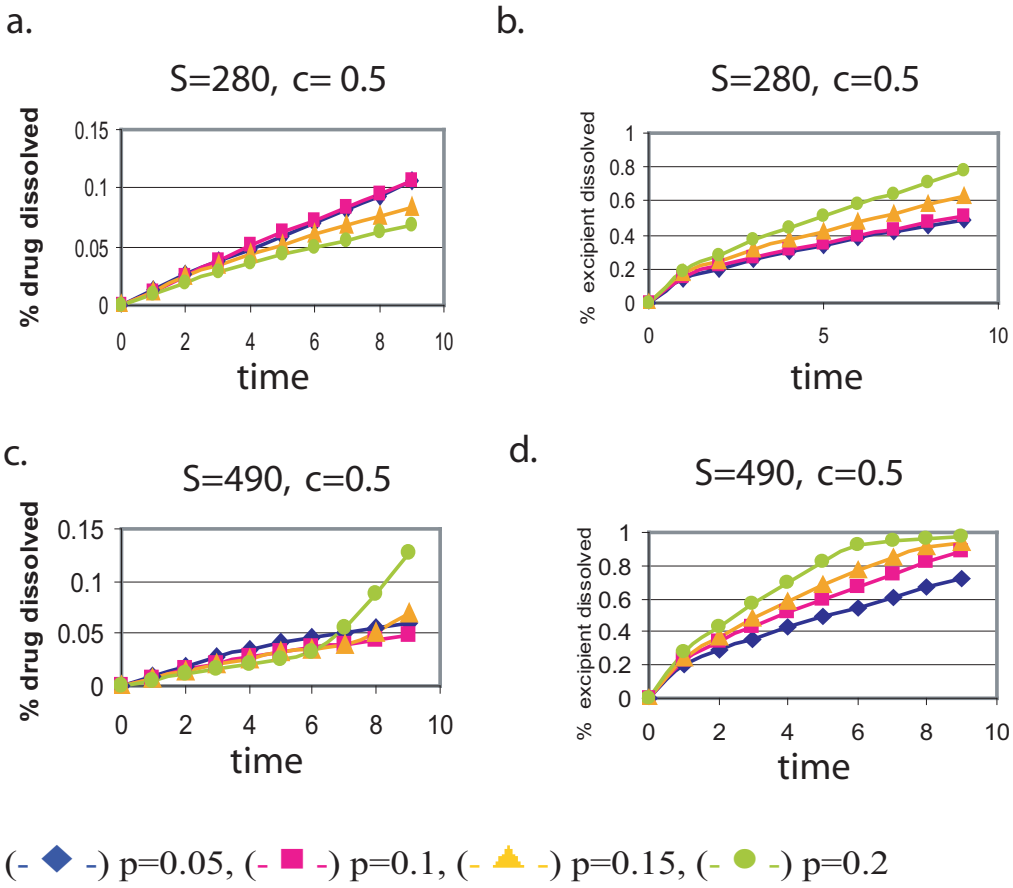

Figure 4.11: Porosity effect for excipients with high solubility

lution phase. This is due to the suppression effect of the excipient, which dissolves quickly at high porosities.

Figure 4.12 shows the effects of the porosity on a system where the excipient is less soluble than in the previous case. Trends for the dissolution profiles of the excipient are similar, but less marked, with less dispersed profiles. However, the effects of the porosity factor for the drug differ from the previous case. Here, the higher the porosity, the higher the dissolution rate of the drug, as it exhibits a more independent behaviour. This means that, for this system, at a given solubility value of the excipient, the excipient's influence on the drug's dissolution is completely cancelled or inverted, marking a *phase transition*. As noted in Subsection 4.4.2,

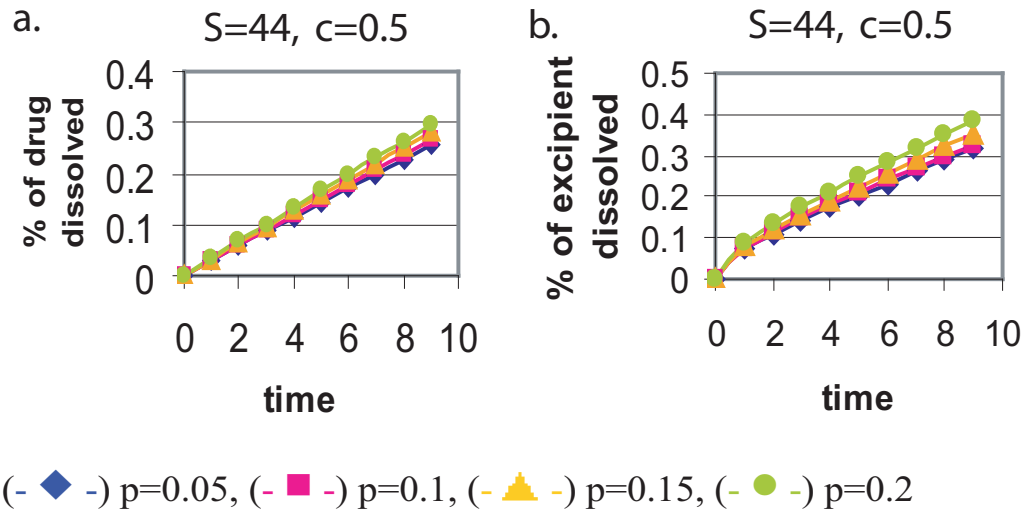

Figure 4.12: Porosity effect for excipients with relatively low solubility. a) Dissolution profiles for the drug from 50:50 drug/excipient matrices. b) Dissolution profiles for the excipient from 50:50 drug/excipient matrices.

potential anomalies due to modelling require experimental verification in regard to whether the effects mentioned are totally model-related, or actually reflect reality.

4.4.4 Neighbourhood effect

We find that different versions of our model may be adapted to simulation of different features of the dissolution problem. Two different types of neighbourhoods were considered, Moore and von Neumann, Figure 4.13, (a). The Moore neighbourhood seems the most appropriate for our problem, because it permits for additional directions of particle movement in the 2D space, compensating for a 2D simulation of 3D reality to some extent. The von Neumann neighbourhood provides good results for compacts containing more than 50% excipient. When the quantity of the excipient in the tablet decreases, however, models using the Von Neumann neighbourhood, although showing correct qualitative results for the drug dissolution, strongly underestimate the quantities of dissolved excipient in the buffer solution, see Figure 4.13, (b). This is an overly-simplistic model-related effect, with under-estimations due to

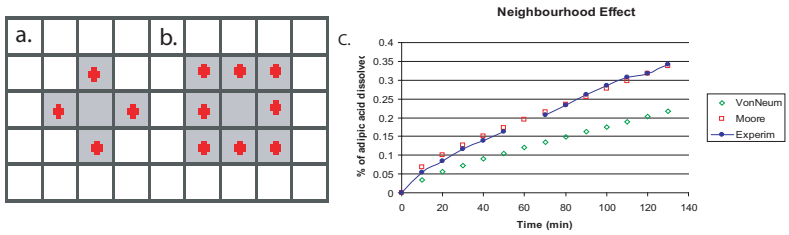

Figure 4.13: a) Von Neumann neighbourhood. b) Moore neighbourhood. c) Dissolution profiles of adipic acid from 40:60 mixed matrices. Continuous curve: experimental (one point misses from this curve bacause this experimental point misses as well). Dots: Simulations.

the fact that the slowly-dissolving drug sites, may, at times, completely block the excipient.

Models based on the Moore neighbourhood, with its eight nearest neighbours, provide simulations with fewer "trapped excipient" effects. The results presented in this Chapter are obtained with the Moore Neighbourhood.

4.5 Quantitative simulations

This section presents work done in order to obtain quantitative results. Mainly, quantifying the models consisted of:

- mapping the experimental binary system into 2D binary lattices, according to the mean size of the powder particles of drug and excipient.
- computation of input parameters, such as number of particles per site, solubilities, the distribution of the number of excipient particles allowed to transfer to adjacent sites, time taken for dissolution, time interval of sampling the quantities of interest, etc according to the physical properties of the two components, i.e. diffusion coefficients, density ratios.
- calibrating the parameters, related to the advection process, by inverse evaluation, (i.e. sampling, comparing to the experimental data, then re-sampling).

- establishing how different acid excipients suppress the dissolution of ibuprofen.

We attributed *an actual size* to the sites from the lattice, equal to the average diameter of the acid excipient powder fragments ($125\mu m$). For the experimental data available, the average diameter of the ibuprofen powder fragments was of orders of magnitude smaller than the excipient average diameter of fragments. For this reason, we assume that the ibuprofen powder simply fills the spaces between the larger excipient fragments. If the ratio of the coarsest to the finest average fragment component diameters was closer to 1, the size of the site could be taken as equal to the diameter of the smallest component, since there is a finite chance that fragments arrange in a less compact way, allowing for the possibility of a larger initial porosity.

As noted, discretisation is achieved by allowing the sites of the lattice to fill with "particles". The diffusivities, densities, and solubilities of the components are used afterwards to calculate the weight of a virtual particle and the loadings of virtual particles per site, in order to set input parameters of the simulations. Given that the experimental results are measured in terms of weight fractions, both drug and excipient particles are chosen to have the same generic weight m_p, (which implies that they have different volumes). For example, to obtain the results presented below (Table 4.2), we have made the choice that a virtual particle weighs 2×10^{-9} g. This is actually $\frac{1}{6}$ of the maximum possible weight (i.e. at saturation) of the less soluble element, the ibuprofen, found in the volume of a site of $d = 125\mu m$. Then, for each component, we compute the number of initial particles per solid site, $C_{MAX_{Solid}}$ and the maximum number of particles per site at saturation, $C_{MAX_{Liquid}}$:

$$C_{MAX_{Solid}} = \frac{V_{site} \times \rho_{component}}{m_p} \tag{4.5.1}$$

$$C_{MAX_{Liquid}} = \frac{V_{site} \times S_{component}}{m_p} \tag{4.5.2}$$

	$C_{MAX_{Solid}}$	$C_{MAX_{Liquid}}$	μ	$\rho\ (mg/cm^3)$	$D\ (cm^2/min)$
ibuprofen	1064	6	1	0.98	$5.155 * 10^{-4}$
adipic acid	933	43	23	1.56	$4.567 * 10^{-4}$
citric acid	1486	841	142	1.118	$4.595 * 10^{-4}$

Table 4.2: Input information for quantitative simulations. $C_{MAX_{Solid}}$ is the number of particles per solid site and $C_{MAX_{Liquid}}$ is the number of particles per liquid site

where V_{site} is the volume of the site and $\rho_{component}$ is the density of the component and $S_{component}$ is the solubility of the component. Then, given the weight fraction $c = \frac{m_{ib}}{m_{ex}}$ in which the two components are mixed, we compute the way the number of sites of drug relates to that of excipient:

$$v = \frac{nb_{ib}}{nb_{ex}} = c \times \frac{\rho_{ex}}{\rho_{ib}} \tag{4.5.3}$$

This equation suggests that for a given formulation characterised by its weight fraction c, the sites will combine in a volume fraction, v. The Table (4.2) summarises some of the input parameters for the quantitative simulations, as well as some physical characteristics of the real systems.

The conversion from Monte Carlo time steps to minutes uses Fick's first law:

$$\frac{dQ}{Adt} = \frac{DC_s}{h} \tag{4.5.4}$$

where dQ is the amount of drug released, h is the thickness of the diffusion boundary layer, D is the diffusion coefficient, C_s - the solubility and A is the total area through which the diffusion takes place, (Costa and Lobo, 2001).

The Monte Carlo time step is taken to be the time needed by a virtual particle of ibuprofen to make it's transition to an adjacent site. We took into consideration the fact that, at the surface of the compact, matter passes into the solvent more quickly due to the advection. More particles of ibuprofen, $n_{surface}$, are allowed to pass into the solution at the surface of the compact in the same interval of time. The experimental profile, obtained from the dissolution of an ibuprofen-only tablet,

was used for the calibration of the distribution of $n_{surface}$.

Figure 4.14 compares the simulated data to some of the available experimental dissolution profiles. The first parts of the Figure, (a) and (b) shows the dissolution of the ibuprofen in mixture with the adipic excipient which has a relatively low solubility, $S_{adipic} = 44.4$ mg/ml. In Figure 4.14, (c) and (d) the excipient used is the citric acid, $S_{citric} = 883.6$ mg/ml.

The good agreement between the simulated and experimental results motivates use of the models to find estimates of other quantities of interest, such as the variation of porosity and thickness of the porous layer, which influence both drug delivery and mechanical properties of a DDS. It is also important understand the dynamical features of these parameters for many other applications, as we shall see later in the thesis. For example, in the cases of therapeutical implants, designers endeavour to find a good compromise between the drug delivery properties of the implant and it's mechanical properties, *as the components dissolve from the compact and form channels and pores.* In illustration, Figure 4.16, (a), (b) shows the temporal dynamics of the porous layer in the case of mixtures of ibuprofen and four different acid excipients. The *thickness of porous layer* is given here *in terms of number of sites*, but can be easily converted to physical units of length as the diameter of a site is known. It can be observed that both curves, i.e. the porosity[7] and thickness of the porous layer have the same shape as the receding acid excipient dissolution profiles (compared to Figure 4.16, (d)).

Limitations

Figure 4.15 shows a typical formulation for which the model is able to predict only the general trend and not good estimates, such as those obtained in Figure 4.14. This happens for the cases where the drug loading is high. Two dimensions are not enough to model such configurations, because for $\geq 50\%$ drug, only a few channels

[7]The porosity is defined as the ratio between the number of sites labelled as pores and the total number of sites currently belonging to the device.

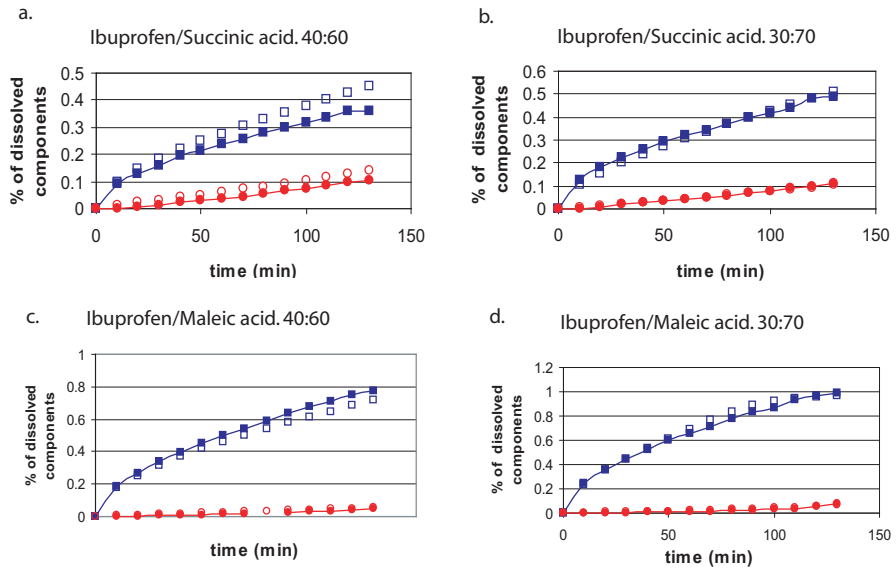

Figure 4.14: Simulated versus experimental dissolution profiles (provided by Healy et al., TCD, Dublin, a. - (Healy and Corrigan, 1992). b,c,d.- unpublished data). Continuous lines with filled dots: Dissolution profiles of ibuprofen and excipient from ibuprofen/acid excipient compressed discs. Empty dots: Quantitative simulated results corresponding to the experimental situations. Circles: ibuprofen. Squares: acid excipient.

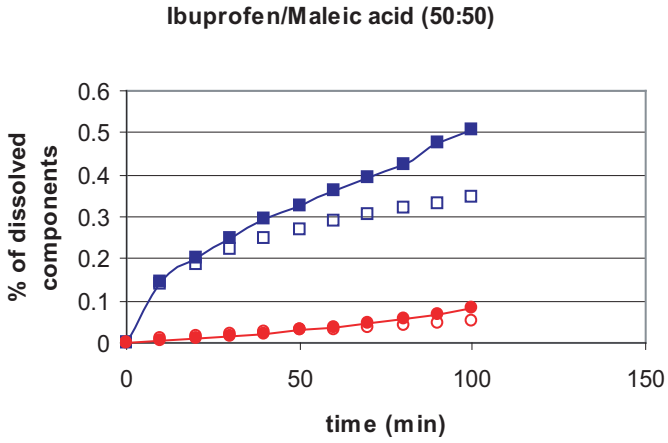

Figure 4.15: Simulated versus experimental (provided by Healy et al., TCD, Dublin). Continuous lines with filled dots: Dissolution profiles of ibuprofen and excipient from ibuprofen/acid excipient compressed discs. Empty dots: Quantitative simulated results corresponding to the experimental situations. Red: ibuprofen. Blue: maleic acid.

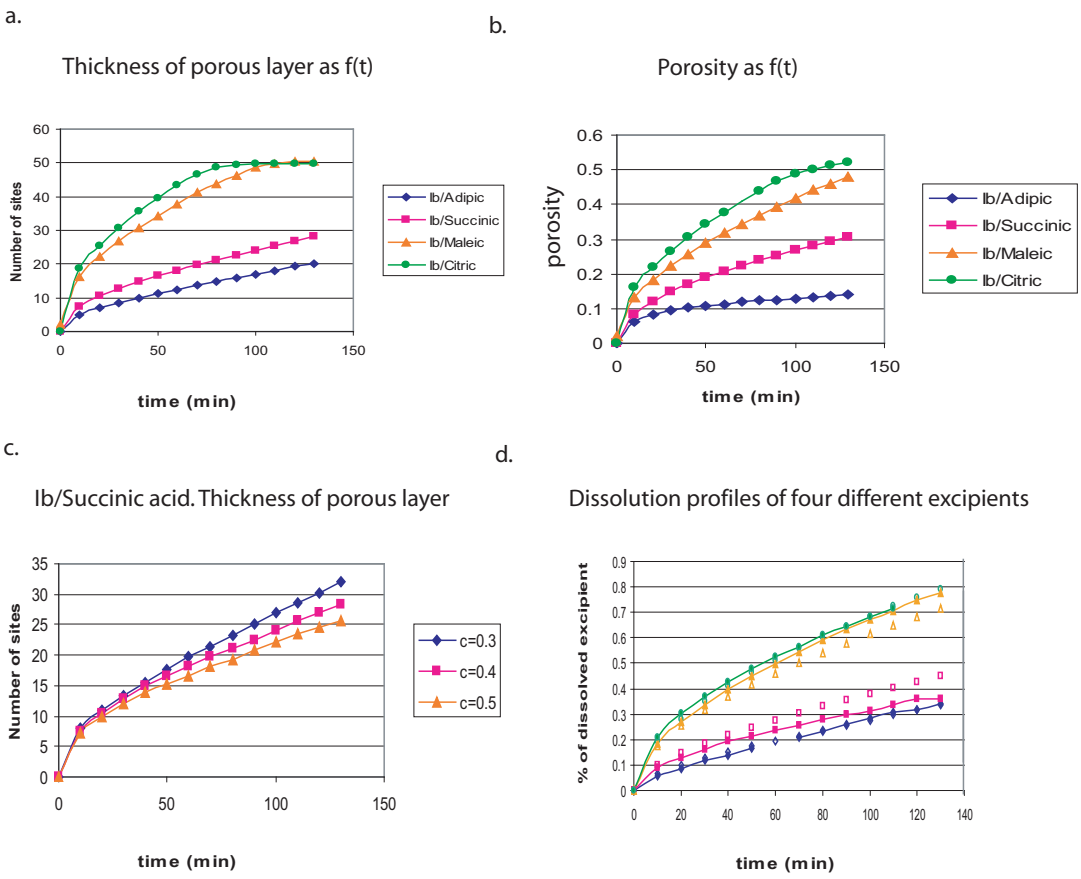

Figure 4.16: Dynamics of the porous layer. a) Thickness of the porous layer as a function of time. b) Thickness of the porosity as a function of time. c) Thickness of porous layer as a function of time for different initial drug loadings. d) Dissolution profiles of the same four excipients, colour and shape code - as for legends of (a) and (b). Continuous lines with filled dots: experimental. Empty dots: the simulated results.

form in 2D and are probably not enough for the excipient to escape. It would be thus a challenging development to extend this work to 3D models to address this further problem. Experimental data appearing in Figures from this and previous sections have been published in Healy and Corrigan (1992); Healy (1995) and details have been kindly provided by the authors.

4.6 Conclusions

With our simple Monte Carlo model, direct consideration is taken of aspects such as time-dependent porosity and thickness of porous layer, dissolution through pores, effects of particle size and distribution, concentration dependent solubilities, receding solid-liquid interface, dissolution over long periods of time and advection due to the *in vitro* environment. Thus, essential features, necessary to reproduce the complexity observed in the real world problem of *in vitro* drug dissolution, are captured. We note that suppression of the advection step from the model leads to simulation results for the drug profiles which do not accord with experiment, hence environment-related features need to be incorporated in any realistic model.

The model can also easily be modified to simulate multicomponent compacts; for example, it can be used to see what happens if a mixture of ibuprofen/acid excipient is compressed in an inert non-soluble matrix of ethylcellulose, (a material used in the present day in the manufacturing of controlled release systems). In this case, it is important to examine percolation phenomena, since both soluble components dissolve in a fractal space determined by the insoluble component. The flexibility of the MC approach has been demonstrated for this type of investigation by the initial models. The next chapter illustrates how a 3D MC model can be used to model dissolution for a controlled-release complex system, which consists of polymer encapsulating an active agent in the form of protein macromolecules.

Chapter 5

3D multi-agent models for simulating protein release from PLGA bioerodible nano- and microspheres

This chapter expands the research, outlined in the previous chapters, to using multi-particle models on more complex systems. Introducing the particulate systems for sustained drug delivery, the chapter opens with a detailed presentation of the types of particulate systems, which are further examined in the thesis, with an emphasis on modelling and simulation needs in the respective fields and the modelling efforts described. Further, a multi-agent model for simulating dissolution of macromolecules from bioerodible spheres is introduced, with a section linking the modelling aspects of the problem to the design and implementation of the simulation. The Results Subsection is a summary of a sensitivity analysis performed on the model developed, discussing the effects of different input parameters on the performance of the simulations. Several hypotheses about the initial state of the system are put forward, making the case for discussing various model variants. The scale of the problem is

discussed, and, finally, a dimensional analysis is performed to validate the model, using real experimental data taken from Sandor et al. (2001). The conclusions highlight the novelty and the advantages of the model, while commenting on the disadvantages, the future work and possible improvements.

5.1 Introduction

The goal of all sophisticated drug delivery systems is to deploy medication intact to specifically targeted parts of the body, through a medium that can control the therapy's administration. To achieve this goal, researchers are turning to advances in the worlds of micro- and nanotechnology, (Vogelson (2001) and others). Nano- and microspheres (composing the nano- and microparticulates respectively) are particulate delivery systems of nanometer or micron size ranges respectively, consisting of biodegradable or bioerodible (see Glossary, Appendix 2)[1]) solids, which can incorporate therapeutic agents, such as small drugs or macromolecules, (Ungaro et al. (2004) and references therein). In what follows, these delivery systems will be referred to simply as *spheres*. During the last decades, particulates have evolved from an alternative experimental type of sustained delivery to a prominent class of drug delivery systems with various applications and many promising future developments, (Merkle et al., 2002). In the past decade, polymeric devices like nano- and microspheres, as well as hydrogels (see Glossary) have been shown to be effective in enhancing specificity of drug targeting, lowering systemic drug toxicity, improving treatment absorption rates, and providing protection for pharmaceuticals against biochemical degradation, (Vogelson, 2001). Currently, polymeric microparticulates have found applications in many key biomedical and drug delivery fields such as: bone repair, tissue engineering and development (Charlton et al., 2006; Ungaro et al., 2004; Göpferich, 1995), vaccine delivery, various chemotherapies for

[1]The glossary of specialist terms is placed, for convenience, at the end of the thesis, in Appendix 2

localized cancer treatment or the treatment of other diseases like AIDS and tuberculosis (Feng and Chien, 2003; ul Ain et al., 2003) and other targeted delivery, (Illum et al., 2001; Kilic et al., 2005).

Depending on the material used, its degradation or erosion kinetics and the size distribution of the spheres, various target drug delivery profiles may be considered, most commonly by administering the spheres through local injections of suitable dispersion, (Merkle et al., 2002). To date, the biomedical potential of particulate formulations is far from being fully exploited and explored (Merkle et al., 2002): the area is growing and expanding, but not as rapidly as it has potential for. Considerable research efforts are needed to exploit the versatile potential of polymeric particulate formulations. The application fields require concomitantly highly specific, nontoxic and functional solutions, characterised by delivery times ranging from weeks to months, making experimental research in particulates extremely time- and resource-intensive. In this context, complementing experimentation with modelling and simulation can be both a scientific challenge and an economically viable solution. The advantages of enriching particulate drug design experimentation with computer models, are evident when using the simulations for predictions and optimizations in design, as well as indicating the trends for choosing the best manufacturing parameters. Despite the fact that modelling the behaviour of bioerodible particulates is far from being a trivial problem due to its complexity, collaborative work can lead to higher performance and improved products in the future, motivating expansion of *in silico* research in the area.

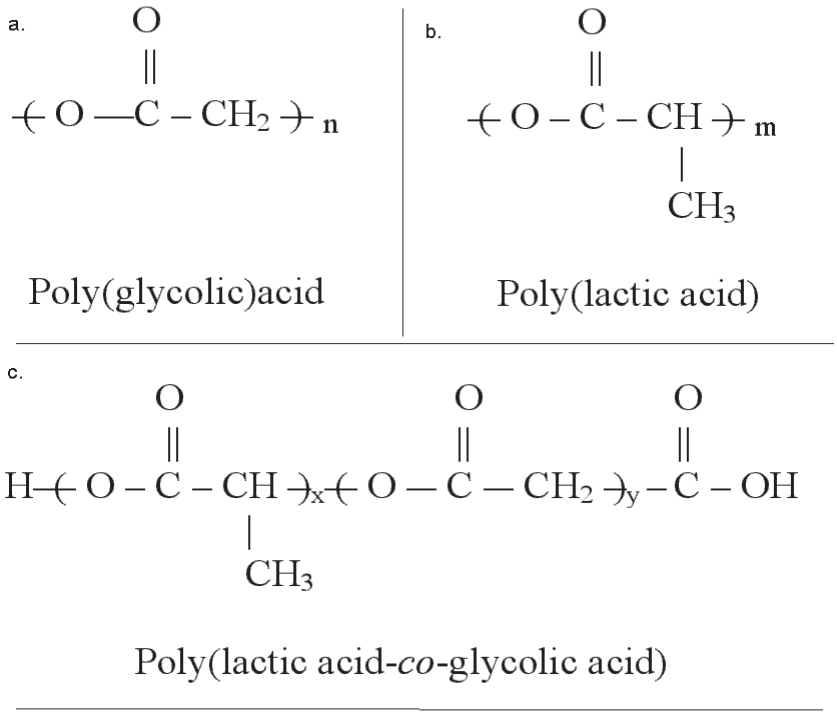

Figure 5.1: Functional groups of: a) PGA b) PLA c) PLGA

5.2 An example of complexity in drug delivery - PLGA spheres

5.2.1 Composition

Particulates are composed of micro- and nanospheres, which embody small drugs or macromolecules. These are made of different biodegradable polymers such as *poly(lactide) (PLA)* (see Glossary in Appendix 2 and Figure 5.1) or *poly(lactide-co-glycolide)* (PLGA) (see Glossary in Appendix 2 and Figure 5.1), or solid lipids such as physiologically cleavable medium and long-chain *diglycerids* or *triglycerids* (see Glossary).

Interest in using biodegradable materials lies in the fact that the products of dissolution of the particles are *biocompatible* (see Glossary) and *biodegradable* (see Glossary), hence do not require further manipulation after introduction to the

body,(Ungaro et al., 2004). This makes particulates suitable for use under minimum invasive surgery (Merkle et al., 2002), providing greater patient convenience and compliance. The inherent physico-chemical characteristics of the materials (e.g. chemical nature, composition, molecular weight, hydrophilicity, degradability), obviously affect the final sphere properties.

5.2.2 Use of PLGA in manufacturing

One of the most successful polymers used to produce micro- and nanoparticulates is PLGA. Besides the fact that it is biodegradable and non-toxic[2], this material has proved capable of easy encapsulation (Feng and Chien, 2003) and subsequent release of different molecules and macromolecules (especially proteins), in a sustained manner. Experimental studies by Lam et al. (2000); Feng and Chien (2003); Sandor et al. (2001), and references therein, demonstrate the potential for encapsulation and sustained release from PLGA micro- and nanospheres, of a wide variety of proteins (such as: lysozyme, insulin-like growth factor I, carbonic anhydrase, bovine serum albumin, alcohol dehydrogenase, thyroglobulin and others).

Another reason for the success of PLGA in particle manufacture is the versatility of its release properties, which can be modified by varying composition (lactide/glycolide ratio), molecular weight and chemical structure (*blocked or unblocked end groups* (see Glossary). In this way, a wide range of *in vivo* life-times of PLGA can be obtained: from three weeks to over a year, (Ungaro et al. (2004) and others). In addition, the release properties of the PLGA spheres can be influenced by the method of fabrication of the protein-loaded PLGA microspheres, because the internal morphology of the particles depends on the *method of microencapsulation* (see Glossary) and Ungaro et al. (2004)). The microencapsulation protocol employed, (Charlton et al., 2006), allows for variable inner pores and channel sizes inside the microspheres. Protocols for PLGA particulates are widely described elsewhere, e.g.

[2]PLGA nanospheres can be 16 times more effective for cell viability than the free drug, (Feng and Chien, 2003)

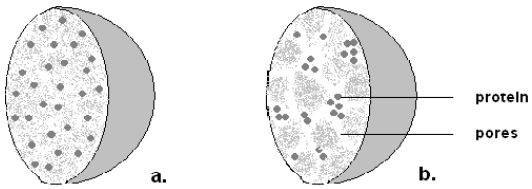

Figure 5.2: a) Sphere morphology obtained by the solid-in-oil-in-water solvent evaporation technique, (see Glossary, Appendix 2). b) Sphere morphology obtained by water- in-oil-in-water solvent evaporation technique (see Glossary). Adapted from Ungaro et al. (2004).

Ungaro et al. (2004); Sandor et al. (2001); Lam et al. (2000); Charlton et al. (2006). Moreover, while one method results in the protein solid dispersion within the polymeric matrix, other methods yield structures where the protein can be located in the occlusions and large pores, formed during the production of spheres, (Ungaro et al., 2004). Figure 5.2 shows different microsphere morphologies. While the *oil-in-water solvent evaporation technique* (see Glossary) usually results in protein solid dispersion within the polymeric matrix (Figure 5.2, (a), *water-in-oil-in-water solvent evaporation technique* (see Glossary) results in a sphere morphology where the protein is initially located within large pores (occlusions). Smaller pores are then formed during PLGA dissolution/erosion, Figure 5.2, (b).

While total control of the pore sizes is still not possible, some studies, such as Charlton et al. (2006), mention good results such as control over the order of pore dimension. This is very important, because, as the simulations from the previous chapter have shown, the porosity of a device can seriously influence its drug release profile.

Due to their popularity and versatility, it seemed an appropriate and a natural extension of our earlier work to develop models for PLGA particulate systems, in the expectation that a large number of practical applications will derive from these developments in the future.

5.2.3 Protein release from PLGA spheres

Protein release from PLGA carriers is the subject of work by many research teams, (Lam et al., 2000; Sandor et al., 2001; Tracy et al., 2001; Ungaro et al., 2004). The literature shows that the area is mainly focused on how manufacturing parameters influence outcomes of dissolution experiments, driven by the need to improve the delivery of effective doses of therapeutic proteins from PLGA spheres.

5.2.3.1 Factors influencing the release of protein

The range of factors responsible for changes (modifications) in the dissolution profiles generated is broad. Sometimes it is not completely clear which of them has a crucial impact on the modification of the final dissolution profile (Sandor et al., 2001) and often the influences of the factors are interconnected:

- In general, the drug release rate from PLGA spheres is controlled by the degradation rate of PLGA co-polymer, (Kang and Singh, 2001; Ungaro et al., 2004; Batycky et al., 1997). Selecting adequate formulation conditions, such as polymer type and preparation method, can generally regulate degradation rate. For example, the use of PLGAs of different molecular weight, hydrophilicity and copolymer composition (the ratio of lactide to glycolide) can change initial hydration and erosion rate for the matrix, (Kang and Singh, 2001; Ungaro et al., 2004).

- Another factor that governs the protein release rate is the structure of the porous environment in the spheres. The sphere processing parameters and copolymer composition (LA:GA ratio) influence the extent of crystallinity and therefore the ratio of smaller to larger pores in the sphere, (Batycky et al., 1997). As already mentioned, the method of sphere preparation and molecule encapsulation plays a basic role in regulating the porosity factor. As we go on to show, the type of encapsulated protein also has considerable influence on

the inner morphology.

- In addition, drug diffusion in the pores influences the drug release profile and is conditioned by a group of factors such as type of molecule (hydrophilicity, size) and drug distribution (size distribution of the encapsulated powder particles and distribution of this powder inside the sphere, Figure 5.2).

It is more difficult to modify the release characteristics of the spheres, once a polymer type and a preparation technique have been selected, (Ungaro et al., 2004). In this case, control over the release rate may be maintained either by modifying the internal morphology of the system (the internal porosity) or adding a third component that alters drug effective diffusivity in the polymeric matrix, (Ungaro et al., 2004). For example, the addition of another polymer and tricaprin[3] would change the surface characteristics of spheres from smooth and non-porous to porous and dimpled, respectively, (Kang and Singh, 2001). The *in vitro* release profiles showed that additives significantly increased the early-stage release of the incorporated protein from the spheres, through increased surface area which enhanced drug passage from internal aqueous phase to external aqueous phase, (Kang and Singh, 2001).

5.2.3.2 Phases of release

Dissolution of the spheres is characterized by several more or less distinct stages, but is most often triphasic. On immersing spheres in an aqueous medium, water penetrates towards the core of the particle and activates drug diffusion through the inherent micropores of the polymer. The water penetration into the sphere occurs over a short time, relative to the total time taken for the polymer to erode, (Batycky et al., 1997).

In the initial release phase, protein adsorbed (see Glossary, Appendix 2) at the surface of the particle and within pre-existing mesopores may give a burst of macro-

[3] a fatty acid ester

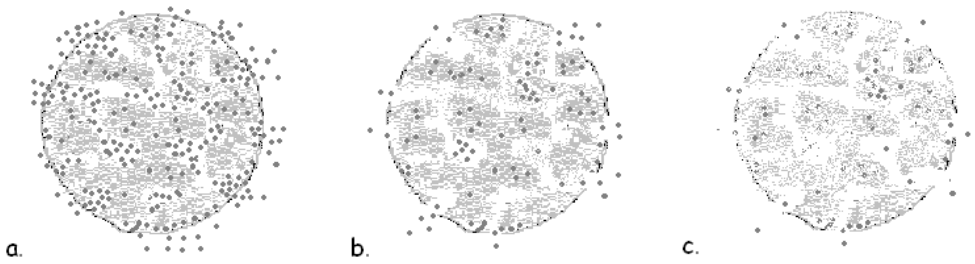

Figure 5.3: Phases of release from PLGA microspheres: a) initial burst related to desorption or dissolution. b) erosion and diffusion. c) mostly erosion and diffusion.

molecule release that is controlled by the rate of macromolecular *desorption* (see Glossary), Figure 5.3, (a).

When the spheres are well hydrated, degradation of PLGA copolymers occurs throughout the volume of the sphere. In the case of a macromolecular drug, the diffusion through the porous network is strictly limited, due to space considerations, hence is extremely slow until the pores attain larger sizes. For this reason, the process of drug release is controlled by degradation rate, and not by diffusion through the pores. The second typical phase is thus characterized by reduced protein release, when interconnected pores are emptied of protein, Figure 5.3, (b). Further release of protein, trapped in the polymer matrix, is largely restricted because of very low diffusivity, (Kang and Singh, 2001).

The third phase of the *in vitro* release of PLGA microspheres takes place as a result of matrix erosion. Usually, the rate in this phase is higher than in the second phase, (Kang and Singh, 2001; Galeska et al., n.d.), Figure 5.3, (c).

Authors like Kang and Singh (2001) and Sandor et al. (2001), note that the total amount of incorporated protein may not be released during the total time needed for the PLGA degradation. It is further suggested that, in some cases, proteins denature and form insoluble aggregates during *in vitro* release.

5.2.4 Example of use of microparticulates in a complex environment

Particulates can be used in conjunction with other polymeric drug delivery systems to achieve the desired therapeutic effects. Often, the initial burst effect (Subsection 5.2.3.2) observed in the release from particulates is undesirable because the aim is to deliver the active molecule at a constant rate, (i.e. linear release profiles). In the case where the drug has to be delivered locally, semi-degradable porous polyvinyl acetate (PVA) hydrogels (see Glossary) can be "seeded" with PLGA micro- or nanospheres (Ungaro et al., 2004), forming therapeutic implants. In this case, the drug does not reach its target directly after escaping the PLGA microspheres, because it first has to diffuse through the larger pores of the implant.

One field where considerable research is being carried out is in the development of implants for the purposes of tissue regeneration. Tissue healing is a complex process, involving the coordinated activity of many different cell types, molecular mediators and cellular processes. If something goes wrong with this regulation, chronic defects and wounds, ulcers and cancers can result. For example, cartilage tissue, once damaged, either regenerates with great difficulty by itself or does not regenerate at all. Thus, implantation of biomaterials at tissue-damaged sites offers a promising solution for the problem of tissue regeneration.

Tissue engineering approaches to this problem typically employ *fully degradable* cell-seeded scaffolds to initiate tissue growth within the defect site. In order to facilitate the ingress of the cells into the scaffolds, these are seeded with growth factors[4] , which initiate cell migration. The ability of the chondrocytes [5] to migrate is influenced by the type and dose of growth factor to which they are exposed and the geometry of the microchannels through which the chondrocytes are expected

[4]These are proteins, normally produced by cells, which are responsible for chemotaxis (migration of cells to the area of injury), mitogenesis (proliferation of cells to the wound site), and synthesis (production of collagen and extracellular matrix proteins).

[5]Cells of cartilaginous tissue.

to move. The new tissue must acquire the *mechanical functionality* of the original tissue, which once filled the defect and *fully integrate* with surrounding cartilage in unison with scaffold resorption. Thus far, efforts *to integrate* engineered tissues with surrounding cartilage have failed.

The concept of using growth factors to encourage chondrocyte migration *into* a hydrogel for the purposes of tissue integration is a new development, currently under investigation at the Hospital for Special Surgery (HSS), New York, USA. On the one hand, *partially degradable* PVA porous hydrogels are used as the main scaffold for providing a similar mechanical basis to that of healthy cartilaginous tissue, helping to avoid extension of the damage by minimising the mechanical effort on the wound. On the other hand, *fully degradable* PLGA microspheres, seeded with growth factors, and inserted into the main PVA scaffold, are used for the *sustained release* of the growth factor, to attract the colonisation of cells into the pores of the scaffold, Figure 5.4. [6]

5.3 State of the art of modelling particulates

The main difficulties in modelling dissolution from PLGA spheres relate first of all to the complexity and heterogeneity of the porous environment, which includes variable concentrations of diffusing species within the pores, hence spatially variable values for diffusion coefficients. Secondly, there is often a lack of detailed knowledge on the inner structure of the nano- or microenvironment. In many cases, neither the experimental researcher nor the modeller can measure such quantities as the protein particle size distribution, porosity within the spheres, percentage weight

[6] Complementing experimentation in this research, computer modelling is required for prediction of the optimum scaffold and microsphere porous morphology and for growth factor dosage to facilitate the cell ingress, because i) some experiments cannot be carried out in an integrated way and/or ii) experimentation is too time-consuming. Modelling both the way in which the drug is dissolved into the medium and the reaction of the cells to the drug would be of benefit to this type of medical research. Future work for this part of the research will thus consist of extending the work done on the PLGA spheres to model diffusion through the scaffold and ingress of cells, and will be carried out in collaboration with the HSS research team, New York.

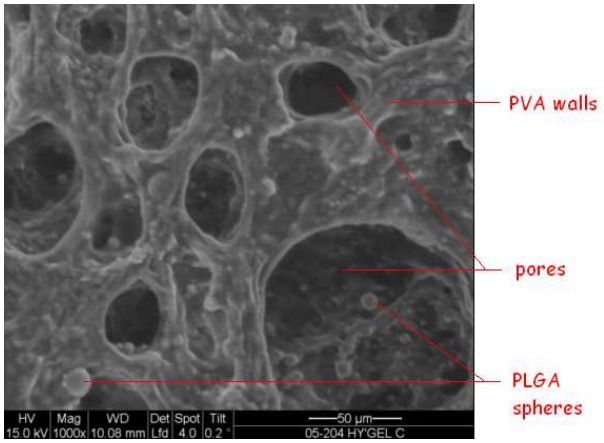

Figure 5.4: Cut through a therapeutical implant seeded with PLGA microspheres, (Charlton et al., 2006).

of the encapsulated drug or the way that drug particles and pores are spatially distributed within the spheres. For example, Sandor et al. (2001) shows that the initial pores are far from being homogeneously distributed inside PLGA nanospheres, but rather they are organised in strata, whereas Batycky et al. (1997) argue that drug distribution is not homogeneous throughout the overall volume of a sphere, but instead coincides with the distribution of the pores. Other information necessary for modelling, (but difficult to obtain), is the rate of growth or coalescence of smaller pores or, in another words, the rate of creation of pores of a certain size. This problem may be susceptible of improvement in future because recently imaging techniques have improved a lot, (Zhao and Rodgers, 2006). For example, transmission electron microscopy (TEM) was recently used to elucidate the transient protein distribution in PLGA microspheres (Zhao and Rodgers, 2006) and the results showed that proteins were not uniformly distributed.

Efforts to model the behaviour of PLGA spheres are ongoing. However, there are presently few reports investigating different modelling techniques for protein dissolution from PLGA spheres. Most of these (outlined in depth below) adapt differential equations based on Fick's second law to describe the concentrations of diffusing molecular species at different space and time points. The problem needs to

be defined on the continuum, i.e. continuous and homogeneous morphology-related variables are required, in order to establish grids for solving the partial differential equations numerically. However, as noted earlier, the environment in nano- and microspheres is rather discrete and heterogeneous. In order to adapt the models to the porous environment of the microspheres, (including initial porosity and time-dependent growth of porosity), these methods consider the porosity (ϵ or p) and the tortuosity (τ) of the microspheres as global parameters, incorporated in the drug diffusion coefficient D.

5.3.1 Main theories and models

The earliest reference attempting to account PLGA sphere complexity dates from 1997, (Batycky et al., 1997). Targeting microspheres in the size range of tens of microns, a theoretical approach was developed, which coupled the erosion of PLGA and monomer release processes to the dissolution of large protein molecules through the dynamically formed pores. If the actual values of the initial parameters could be established, the paradigm can be explored and dissolution profiles obtained. The main assumptions of the model included: all pores taken as randomly distributed throughout the particle and a range of initial pore sizes with time dependent radii. A further assumption was that, as microspheres degraded, drug was released by both desorption and diffusion. Desorption is assumed to originate with the drug, initially distributed both on the external surface of the sphere and in occlusions connected to the external surface of the sphere. It is characterised by an initial surface concentration, C_0, of drug and a rate of desorption k_d:

$$\frac{\partial C_{surface}}{\partial t} = -k_d C_{surface} \tag{5.3.1}$$

Release from the occlusions of the microparticle is prevented until the mean pore radius R (leading from the occlusions inside the particle to the external bath), exceeds the characteristic Stokes-Einstein molecular radius of the drug. Thus, drug

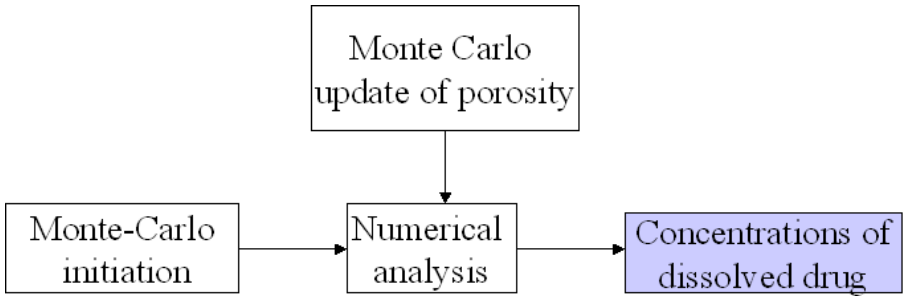

Figure 5.5: Schematic representation of the coupling of the numerical-MC techniques to model dissolution from PLGA microspheres used in Siepmann et al. (2002)

diffusion is delayed by an induction time sufficient to allow the micropores to coalesce and permit passage of the drug. Diffusion is characterised by an effective diffusivity D^* and by the molar fractions of different monomers composing the scaffold polymer.

Based on these assumptions and the calculation of the overall microporosity and macroporosity, a kinetic degradation model was proposed, (Batycky et al., 1997), considering the microspheres as a whole. Expressions for the released mass of monomer and macromolecular drug as a function of time were then derived and used in conjunction with experimental data, to deduce the main parameters of the model such as the rate constant of desorption k_d, the surface concentration of adsorbed drug C_0, the effective diffusivity D^* etc. Given these, the model may be used to make predictions and in fact replicated quite well the dissolution profiles obtained from PLGA microspheres encapsulating glycoprotein 120 (gp 120), with mean radius of the order of 20 micrometers.

Subsequently, Siepmann et al. (2002) proposed a partial differential equations model coupled with a Monte Carlo simulator, (Figure 5.5), to describe drug release from bioerodoble microparticles.

Numerical analysis was performed on a two dimensional pixel grid, similar to that represented in Chapter 2, (Figure 2.2), but which described a rotated hemisphere, with each pixel representing a cylindrical ring. Partial differential equations derived from Fick's second law for cylindrical devices, taking into account axial and radial

mass transfer, were solved on the grid at a sequence of small time intervals. In order to simulate initial configuration of drug/PLGA and subsequent porosification of the device, a Monte Carlo simulation was also carried out on a similar grid. Coupling to the numerical simulation was achieved by making the diffusion coefficient, used in the differential equations, dependent on the porosity calculated in the Monte Carlo simulation, Equation (5.3.2). Monte Carlo direct simulation calculates the porosity as in (Göpferich and Langer, 1995; Göpferich, 1996).

$$D(r,t) = D_{crit}\epsilon(r,t) \tag{5.3.2}$$

In Equation (5.3.2), D_{crit} represents a critical diffusion coefficient, characteristic of a specific drug-polymer combination. The Siepmann et al. model has been validated with experimental data from dissolution of a small molecule (5-fluorouracil) from PLGA microspheres, (Siepmann et al., 2002). Nevertheless, even if using the porosity information obtained from Monte Carlo simulations, it is still an approximation in 2D, since on rotation of the numerical analysis grid each pixel gives a cylindrical ring in 3D. Thus, the matrix structure, which reflects reality, where local effects of both PLGA and pores seem to have a strong influence on the dissolution, (Sandor et al., 2001), is not reproduced in this model.

The most recent complex model for simulation of drug release from biodegradable polymeric microspheres is due to Zhang et al. (2003). This develops a theory based on coexistence inside the microsphere of a virtual solid phase and two real phases: a liquid phase and an effective solid phase. The liquid phase has a constant volume V_0 and the drug enters it by dissolution and erosion and leaves by diffusion. Actual diffusion is taken to occur only in this phase. The effective solid phase is used to simulate actual changes in the solid phase, with its volume V_1 taken to be variable in time. The initial concentration of drug is dispersed in this phase, and leaves it by dissolution - the process by which drug is dissolved from the polymer matrix into the solvent. Thus, the decrease of concentration in the effective solid phase, $C_{sol\_effective}$

depends on the dissolution constant, porosity ε and the drug concentration in the liquid phase C_L as well as saturation concentration, C_{sat}:

$$\frac{\partial C_{sol\_effective}}{\partial t} = -k_{dis}\varepsilon(C_{sat} - C_L) \tag{5.3.3}$$

Hence the rate of dissolution is driven by the difference between the actual and saturation concentrations. However, this equation describes a similar phenomenon to that of Equation (5.3.1), work of Batycky et al. (1997). Finally, the virtual solid phase is introduced to act as a bridge between the two other phases. The concentration of the virtual solid phase is given by:

$$C_{sol\_virtual} = C_{sat}\frac{V_1}{V_0} \tag{5.3.4}$$

In this phase, both erosion and dissolution are responsible for the decrease of the drug concentration. Based on these assumptions, three differential equations are written, describing the variation in concentration of each of the three phases and employing three different terms: erosion, diffusion and dissolution. The sign of the dissolution term can vary depending on whether the concentration of the liquid phase has reached its saturation value or not. The main parameters of the equations are the erosion constant K_{ero} and the dissolution constant. Zhang et al. (2003) took into consideration the three main patterns of polymer erosion found in experiment: linear, hyperbolic and sigmoid, shown in Figure 5.6.

Assuming that these three patterns are conditioned by different erosion mechanisms, the set of three equations for the concentration can be rewritten with specifically derived erosion terms. In the model of Zhang et al. (2003), an initial porosity value only is taken and is not considered to be modified over time. Similarly for the *tortuosity*[7], an interesting point: the drug disperses in the polymer matrix not only because the macromolecules move through the pores, but also because they move

[7] a concept first introduced by Higuchi to refer to the straight or twisted form of the channels

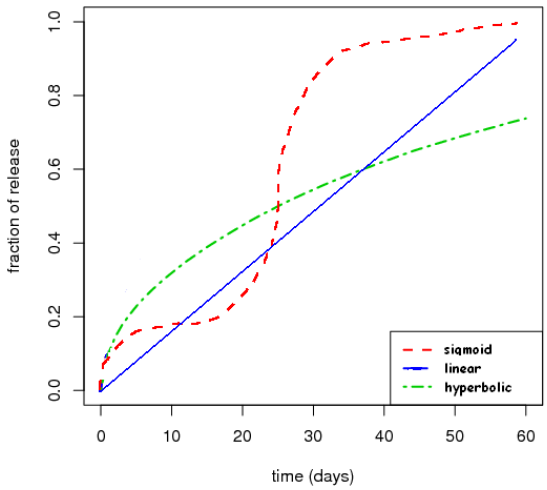

Figure 5.6: Three different patterns of polymer erosion considered in Zhang et al. (2003).

through some bottlenecks that are produced by the vibration of the polymer chains, thus controlling the actual pore size for the passage of macromolecules, (Zhang et al., 2003). Thus in the case of dissolution through polymeric structures, values of tortuosity are much higher than the usual values stated in the literature for other porous systems, for which these range from 1 to 100. In Zhang et al. (2003) the tortuosity was found to range from 10^2 to 10^5. Zhang et al. (2003) assert that the hyperbolic erosion model (Figure 5.6) shows reasonable agreement with BSA (bovine serum albumin) release data, while the sigmoid erosion model shows good agreement with dextran release data. The dissolution constant (similar to the desorption constant in Batycky et al. (1997)) and the tortuosity τ were adjusted by Zhang et al. to fit the experimental result.

5.3.2 Remarks

To the best of our knowledge, no work of integration, generalisation or comparison of these independent methods has ever been performed. The different methods have

been validated for particular experimental situations only, and results of the simulation compared against experimental profiles, often ignoring parallel developments. Future work in the field clearly requires implementation in parallel of the various methods proposed, with modifications in order to generalise to a number of different experimental systems over a range of cases. The work presented here provides further complementarity, as it investigates dissolution from spheres, by considering what happens locally, at each point of the microenvironment, at the chosen scale, so that the microenvironment is taken into account directly. The intent is again to complement experimentation with simulation, (in particular where the former is difficult if not impossible to perform). After calibration of the models to obtain satisfactory quantitative matching with experiment, the use of the calibrated models to solve an inverse problem, is envisaged, as follows: given desired drug dissolution curves, of particular pharmaceutical interest, the aim is to determine optimal manufacture features of the spheres, to meet these requirements. The outcome of our multi-agent approach can then be compared with results provided by the other models. Multiple analysis, based on different viewpoints can increase the knowledge of the way the experimental system works and provide meaningful predictions.

5.4 Modelling

In the present work, we seek to understand the phenomena observed for PLGA spheres, through cellular automata agent-based modeling and probabilistic simulation, where systems are studied both over large temporal scales, (capturing slow erosion of PLGA) and various spatial configurations (capturing initial as well as dynamic morphology and inner structure of the spheres). The remainder of the chapter demonstrates the extent to which the models are able to cover the wide range of situations that arise from the manipulation of PLGA.

5.4.1 Reasons for using multi-agent modelling

The aim, as stated, is thus to implement a multi-agent program simulating the behaviour of the PLGA microspheres as described previously. The core of the program requires design of entities (agents), which have simple properties and characteristics. One advantage of multi-agent modelling is thus simplicity of representation of real space experimental entities by modelled ones. Large protein molecules in a particular PLGA environment surrounded by dissolution medium can be modelled as autonomous computational agents which follow certain rules. Portions of PLGA can also be modelled as agents of a different type, with a separate set of rules. As pointed out in Chapter 3, the major strength of the multi-agent approach is to observe and monitor behaviour directly. In our case, the emergent behaviour is the dissolution profile manifested as a sphere erodes and the proteins dissolve in the dissolution medium.

The dimensions of the experimental entities involved range from several nanometres (proteins) to several microns (spheres), although dimensions of proteins vary. A comparatively simple example like the lysozyme (13.4 kDa), has a diameter of 3.2 nm, (Kisler et al., 2001). Diffusion measurements in PLGA micro- and nanospheres encapsulating lysozymes involve pore sizes < 20 nm, (Sandor et al., 2001), thus it is relevant, in this case, to describe diffusion in terms of individual random walks of molecules rather than by transport of matter through surfaces. Table 5.1 shows the diameters of a number of different proteins across a range of molecular weights. Experimental studies, (Sandor et al., 2001), have revealed that, in general, the initial configuration of pores corresponds mostly to sizes of 20 - 80 nm, (proportional to the size of the encapsulated proteins). On the other hand, other experimental studies have reported on cases of spheres with initial occlusions much larger than the Stokes-Einstein diameter of the microencapsulated molecule, (Batycky et al., 1997; Charlton et al., 2006). However, as long as the proteins undergo very restricted diffusion through pores of i) the same order of magnitude as the proteins themselves or ii)

Protein	Diameter (nm)
lysozyme	3.2
myoglobin	3.5
hemoglobin	5.5

Table 5.1: Examples of protein diameters

slightly larger, but full of diffusing monomers[8]), it is appropriate to treat diffusion by individual random walks of a certain number of agents (Kosmidis et al., 2003b; Nicholson and Sychova, 1998). In such cases, multi-agent systems seem reasonable approximations for the "protein - PLGA - pore" system.

Section 5.7 further discusses the link between the motility of the macromolecules undergoing restricted diffusion and quantities such as effective diffusivities. Finally, the multi-agent approach permits in-depth exploration of the problem. Building up, step by step, nested levels of complexity in the multi-agent system, and comparing the results obtained by simulation, permits the testing of different hypotheses about the system or can be used to confirm recent experimental work on the inner configuration of the spheres.

5.4.2 Model assumptions

The assumptions which apply in all models developed are based on experimental data available. The polymeric particles modelled are considered to be completely spherical and are modelled in 3D space. The spheres are discretised throughout the volume into small sites, (as for Chapter 4). Figure 5.7 represents a section through a sphere during the simulation. The sites are seeded, according to predefined initial concentrations, with PLGA polymer (red sites) or protein molecules (blue, green and black dots are the molecules from different depth levels in the sphere). An initial porosity value in the PLGA bulk material can be considered if necessary (white sites represent initial pores before hydration). Over time, more pores can be formed, (brown sites around the spheres represent the erosion medium and the brown sites

[8]The monomers result from the erosion of the PLGA chains

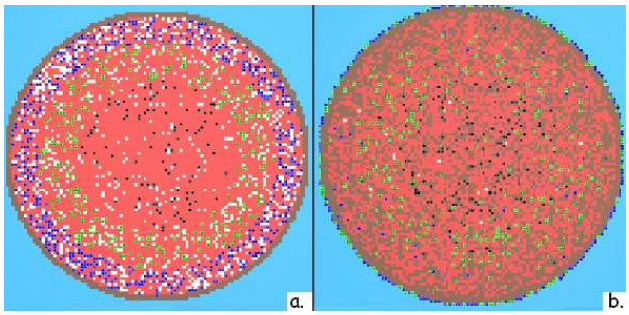

Figure 5.7: Section through a microsphere from the simulation. a) initial configuration. b) configuration when the sphere is dissolving.

inside the sphere represent both initial pores after hydration as well as newly formed pores). Different strategies can be considered for describing the PLGA erosion and the formation of pores. When a site, filled with polymer, reaches a certain stage of erosion, it is considered to be a pore. This is a simplification, because monomers resulting from polymer erosion, occupy the pores as well and restrict diffusion of the drug molecules.

A protein molecule can leave its initial location only in the case where one of the neighbouring sites is a pore (i.e. the molecules can only move through pores). Once in a porous channel, a molecule cannot leave it, except by escaping the sphere. Due to the fact that PLGA microspheres usually have a very low content of molecules and that pores are considered to exist as soon as they are large enough to accommodate molecules, situations where more than one molecule happen to meet on the same site are tolerated. When a molecule escapes the sphere, it is counted as dissolved. The cyan area around the sphere (Figure 5.7) represents the sink solution.

Appendix 1 gives the UML scheme of the C++ program used for the simulation and other implementation details like the chronology of an iteration, graphical issues and description of main functions and classes.

5.4.3 Modelling Erosion

The approach taken to model the polymer erosion is based on Göpferich's theory for polymer erosion (Göpferich, 1996). According to this theory, events which occur independently with some average rate k are modelled by a Poisson process. It is assumed that the chain cleavage is a random event following Poisson kinetics. The waiting times t between k occurrences of the Poisson event are Erlang distributed.

$$f(t,k,\lambda) = \frac{\lambda^k t^{k-1} e^{-\lambda x}}{(k-1)!} \tag{5.4.1}$$

In Equation (5.4.1) k is the shape parameter and λ is the rate parameter. When k=1, the distribution is a first-order Erlang distribution or an exponential distribution for a positive variable (Equation (5.4.2) and Figure 5.8), used to model the times *between* events that happen at a constant average rate:

$$f(t,\lambda) = \lambda e^{-\lambda t} \tag{5.4.2}$$

If the times between bond cleavages are distributed according to Equation (5.4.2), then the mean lifetime of a single bond is given by $t = \frac{1}{\lambda}$. $f(t,\lambda)$ gives the probability that the polymer will erode completely at time t after its first contact with water.

If several Poisson processes are proceeding in parallel, then the whole process is again a Poisson process (Göpferich, 1997*b*). In practise, the lifetime t can be computed using the following relation:

$$t = \frac{1}{\lambda} ln(U) \tag{5.4.3}$$

where U is a random number, uniformly distributed between 0 and 1, (Göpferich, 1997*b*). In order to account for the gradual erosion of the polymer inside the bulk mass and to achieve a desired pattern of pore growth in models for bulk-eroding

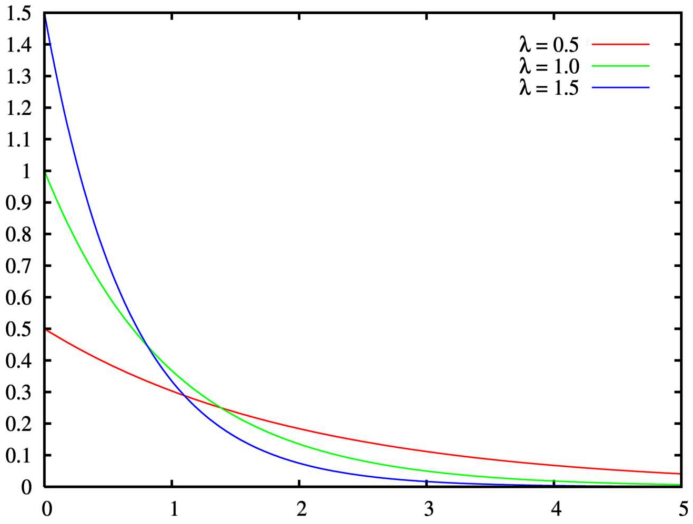

Figure 5.8: Examples of exponential probability distributions, (wikipedia, 2006).

polymeric systems, (Siepmann et al., 2002; Göpferich, 1997*b*) used a probabilistic method based on the concept of dividing the polymeric device into small sites and attributing a lifetime to each site.

Considering that a site on the lattice erodes as a result of several Poisson processes which take place in parallel, the first-order Erlang distribution is used to generate the initial lifetimes of the sites. As the dissolution proceeds, the lifetimes of the polymer sites begin to decrease. When a lifetime reaches zero the polymer from this site is considered eroded and the site becomes a pore. In this way, the porosity of the sphere gradually grows and the release of the drug encapsulated inside the sphere is facilitated by the diffusion through the newly formed pores. This approach permits derivation of a relationship between real time and Monte Carlo time through λ, the inverse of the mean lifetime of a PLGA particle, expressed in s^{-1}.

Theoretically, the rate parameter λ depends only on the nature of the polymer. However, in practice, λ is related to the size of the site chosen for modelling as well. On reaching a lifetime value $t = 0$, the sites are removed from the system, generating pores of the size of the removed site. Thus, in this discrete model, based on representing the system as sites, λ describes *the rate of pore formation.*

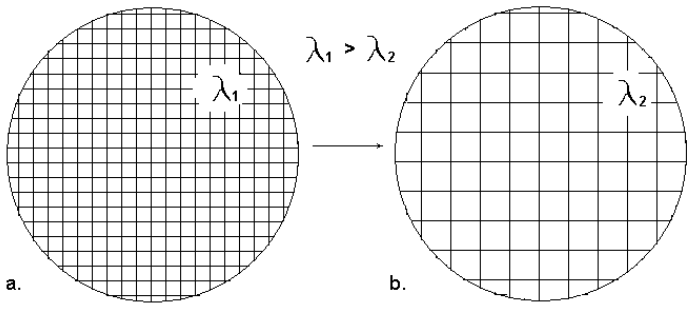

Figure 5.9: Rate parameter as a function of different model resolutions.

Very small pores form quickly. Larger pores form as a result of the coalescence of smaller pores, (Batycky et al., 1997). A pore becomes significant for the present simulation once it reaches sizes reasonably larger than the Stokes-Einstein diameter of a encapsulated drug macromolecule (3-30 nm). Therefore, in the case of nanospheres, the size of the site can be chosen in this range. In the case of microspheres, though, it is possible to opt for coarser grained simulations, with larger sites, because as the number of site in the matrix increases, the problem quickly becomes computationally very intensive.

Thus, the size of the chosen site may vary between 20-100 nm, according to cases of interest. Accordingly, for the same type of polymer, a fine grained model will require larger values of λ than a coarse grained model, Figure 5.9. In conclusion, λ depends on both material characteristics, (the type of PLGA) and model characteristics (the chosen size of the site).

Modern electron microscopy is able to provide information on pore formation, (Sandor et al., 2001; Batycky et al., 1997), therefore the rate of formation of pores of a certain size can be determined. The choice may be that of a site size in the dimensional range of the Stokes-Einstein diameter of the drug molecule, or, for a coarser grained simulation, that of setting the average size of the initial pores in the system to be equal to the size of a site. Thus, the mean lifetime of the sites may range over different values depending on these initial assumptions and corresponding

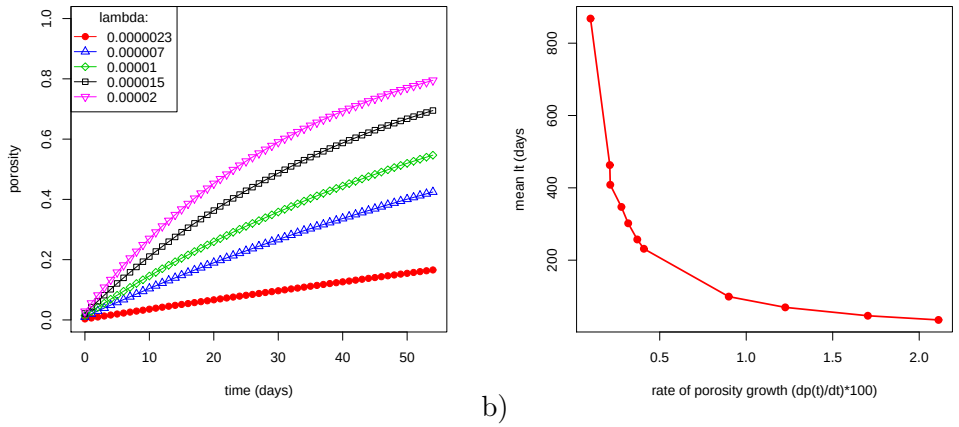

a) b)

Figure 5.10: a) Evolution of the porosity of a sphere with time when the porosity is computed using a zero-order Erlang distribution life-time approach b) Mean lifetime (lt) $\frac{1}{\lambda}$ to use in Monte Carlo simulations as a function of the rate of porosity growth.

model choices. Figure 5.10, (a) represents the dynamics of porosity formation using the model described in the previous sections, on spheres having a diameter of 80 sites and zero initial porosity. At every step, the lifetimes of the sites are decreased by Δt=10 minutes.

It can be seen that the lifetime influences the pattern of porosity dynamics, which is basically hyperbolic, but can be considered linear in the first 15-20 days. This agrees with Batycky et al. (1997), who found that the porosity grows linearly with time for the first 15 days of degradation of PLGA spheres. The figure shows that for λ=0.00002 min^{-1}, (i.e. $\frac{1}{\lambda}$=t=34 days) the porosity of the sphere increases from 0 to 0.8 over 55 days, a typical experimental life-span of PLGA spheres. The pores appear quite quickly and result in a sponge-like topology of the system.

Figure 5.10, (b) represents an empirical relationship deduced between the parameter λ and the initial rate of pore formation. The rate is calculated using the linear part of the porosity dynamics curve (first 20 days).

Figure 5.11, shows how porosity growth dynamics can affect the release of molecules from a sphere. The same spheres used for obtaining Figure 5.10 have

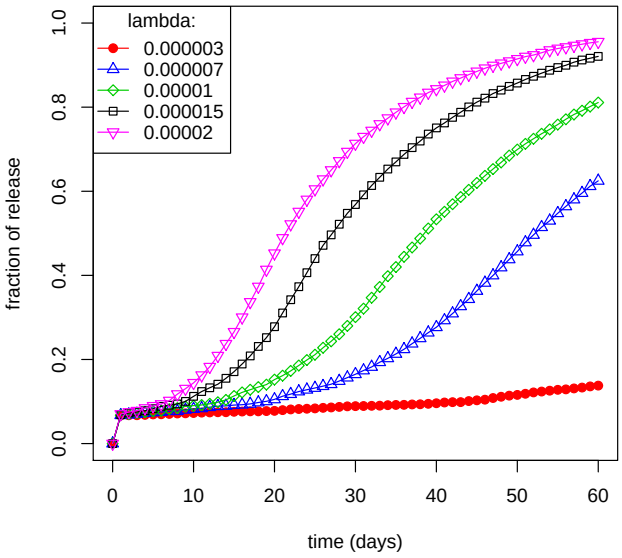

Figure 5.11: Release profiles as a function of the degradation rate λ.

randomly been seeded with particles, from 1 to 4 particles per site, with overall concentration of particles $c = 0.02$. The release profiles obtained correspond to typical experimental profiles of release of macromolecules from PLGA spheres (Sandor et al., 2001; Lam et al., 2000). In all cases, a short initial burst is observed, corresponding to the release of the particles situated on the surface of the sphere. To obtain the curves from Figure 5.11, the initial porosity was $p_0 = 0$. The effects of choice of initial porosity value are discussed in Subsection 5.6.2.

The rate parameter λ affects, for each particle, the time during which it remains trapped in the PLGA. Thus, $t = \frac{1}{\lambda}$ is inversely proportional to the rate of release of the molecules, mainly affecting the convexity of the release curve. With different lifetimes in the input, the model can generate profiles such as those found in Sandor et al. (2001) and Lam et al. (2000). From the discussion in this subsection, the following key points must be considered before setting up the model:

1. The size of molecules encapsulated.

2. The most suitable initial pore size for the given problem. This size then represents the size of a site and *the resolution of the model*.

3. The rate of formation of the pores of interest.

4. Total time of erosion of the spheres and time to when the spheres begin to disintegrate.

5.4.4 Modelling the internal configuration of the spheres

As noted, modelling the internal configuration of the microspheres consists of labelling sites as obstacles or pores in the space delimiting a 3D sphere.

Almost all known modelling approaches available (Zhang et al., 2003; Siepmann et al., 2002; Vlugt-Wensink et al., 2006; Siepmann and Göpferich, 2001) consider homogeneous distributions of the pores and of proteins in the spheres, whereas experiments have indicated that this may not realistically describe most cases (Sandor et al., 2001; Zhao and Rodgers, 2006). The remainder of this subsection presents three different aspects suggesting that the internal configuration of the spheres might be subject to heterogeneity.

In the study conducted by (Sandor et al., 2001) on the effect of microencapsulated molecules on the internal structure of micro- and nanospheres, it was revealed that spheres enclosing smaller proteins appear to have an open branched network throughout. However, those enclosing larger proteins have pores in the outer layers and appeared open near the surface, while having a more dense structure in the inner layers of the sphere, Figure 5.12. At the time of writing, it is still not clear whether the phenomenon of layered porosity happens only in the case of very small microspheres and nanospheres or whether it is a general trend. It might be worthwhile, however, to take this aspect into consideration when designing models.

On the other hand, Batycky et al. (1997) discusses another phenomenon which might happen in the case of microspheres. This reference assumes that adsorption of

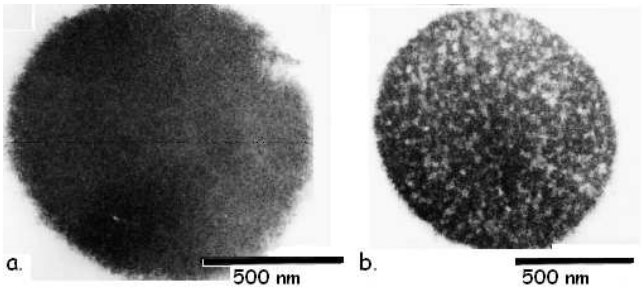

Figure 5.12: a) Control PLGA sphere, no encapsulated molecules b) PLGA sphere encapsulating carbonic anhydrase, adapted from Sandor et al. (2001).

macromolecules to the surface of the microsphere (or to the large occlusions inside the spheres) can occur, suggesting an uneven distribution of the macromolecule in the volume of the sphere. Figure 5.13 shows a recent 3D reconstruction from TEM images of the transient distribution of albumin in PLGA spheres during erosion, (Zhao and Rodgers, 2006). If this uneven distribution is realistic, the values of parameters, obtained by adjusting models premised on a homogeneous distribution to experimental data (like in (Zhang et al., 2003)), will be biased. A more general consideration for modelling should thus be that concentrations of macromolecules in the sphere can be unevenly distributed.

Further, it is necessary to consider whether it is reasonable to assume that PLGA degrades more quickly in the outer layers of the spheres than in the core. From gradient considerations, the degradation products have higher diffusivity in the mantle of the sphere than in the core, thus the porosity generation rate might increase more quickly in the outer layers in comparison to the internal layers.

In this multi-agent investigation, these aspects can be considered in a manner of increasing complexity, i.e. by dividing a 3D sphere into strata and populating these with obstacles, pores and molecules in different ways. Figure 5.14 shows the developmental scheme of the initial model and variants.

To address the stratified initial pore-and-channel configuration problem, (based on (Sandor et al., 2001)), we consider that the spheres, by manufacture, have a

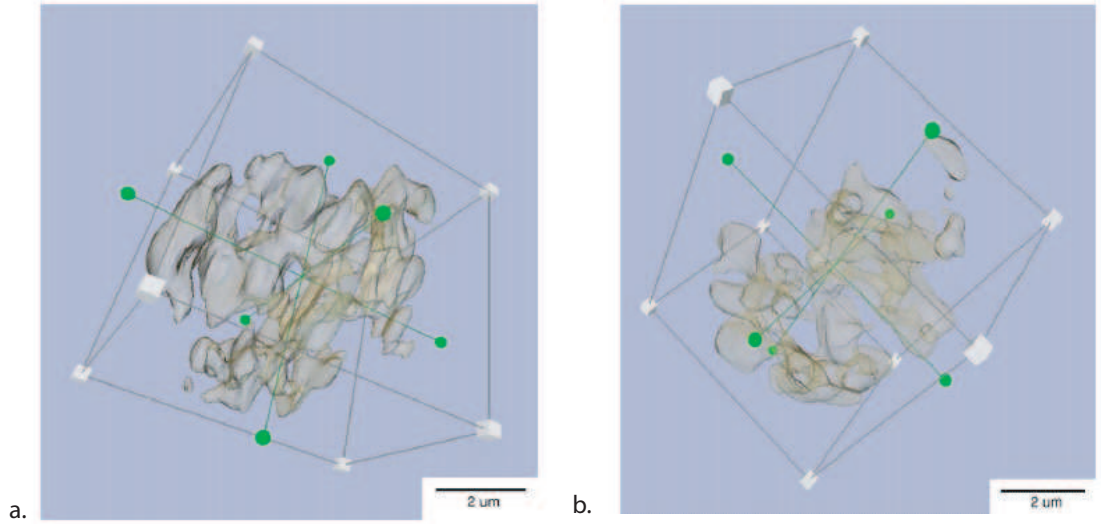

Figure 5.13: Image of the 3D construction of the protein distribution in ovalbumin loaded microparticles at a) 30 days and b) 60 days incubation in an *in vitro* batch process, (Zhao and Rodgers, 2006).

stratified porosity. However, dynamically, the porosity evolves in the same way as described in the previous subsection, depending on a mean lifetime parameter t. The initial porosity p_0 is discretised into three strata with decreasing porosities from the surface to the center, respectively p_{01}, p_{02}, p_{03}. This idea is implemented in model A.1.

The second step was to consider a stratified concentration of the macromolecule in the sphere. For the same three strata as previously, the concentration c_0 becomes discretised: c_{01}, c_{02}, c_{03} (model A.2). This model was considered less realistic than the combination of A.1 and A.2 (variant A1-2), because there is experimental evidence that the concentration of protein is more likely to follow the porosity (Sandor et al., 2001; Batycky et al., 1997).

Finally, it was considered worthwhile to look at whether the effects of discretising λ according to strata could bring benefits to the study (model B).

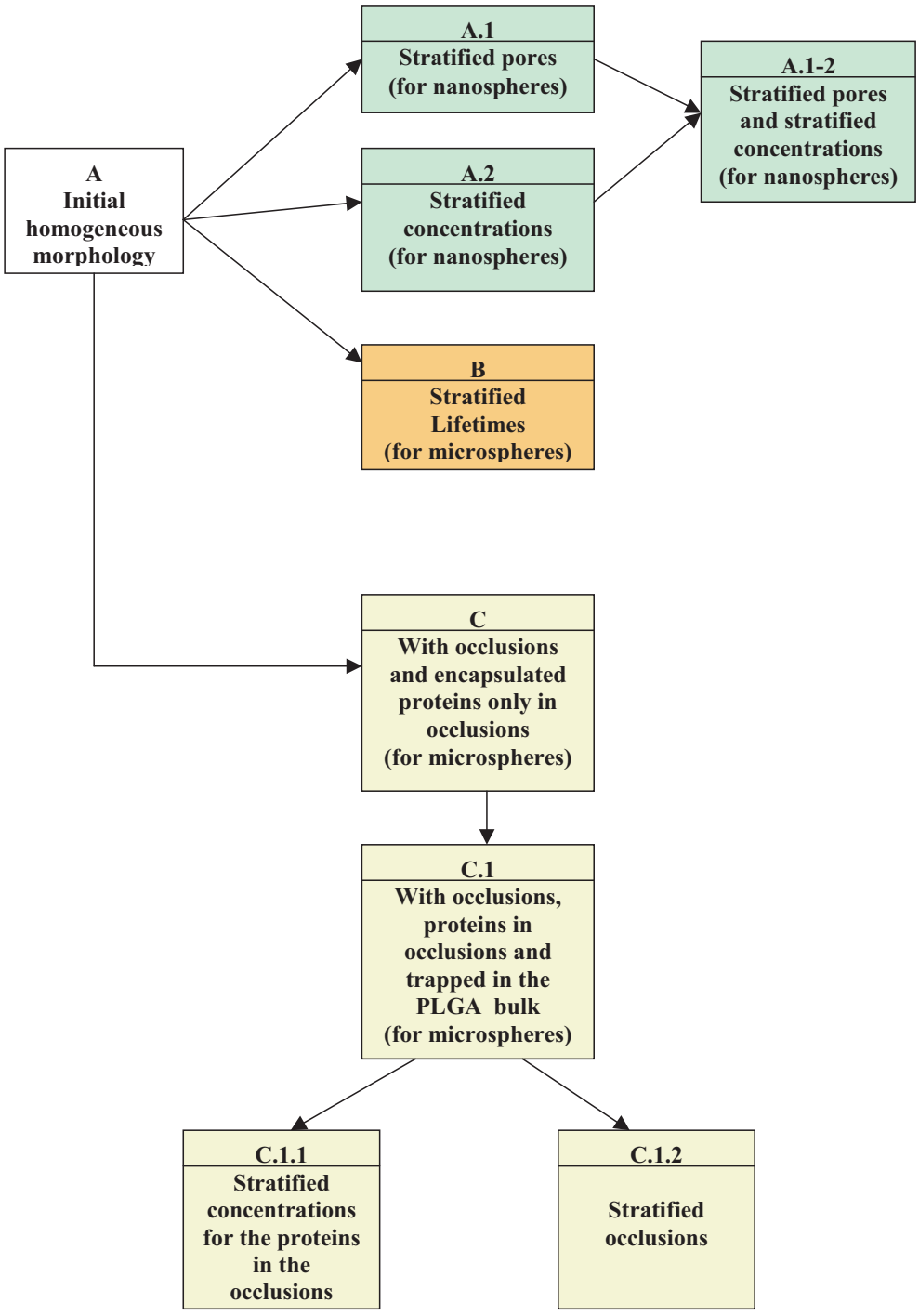

Figure 5.14: Developmental scheme of the models and their variants.

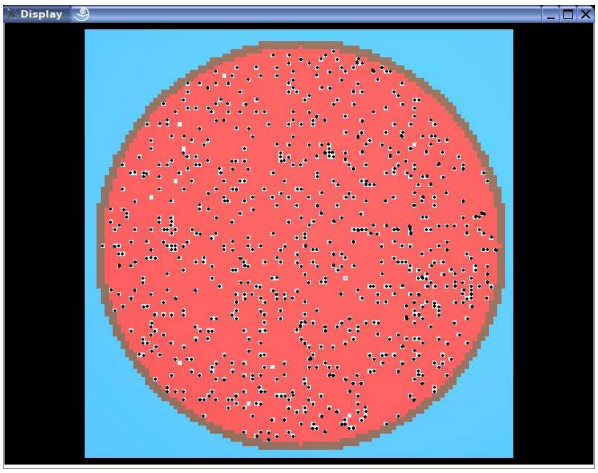

Figure 5.15: Morphology of the spheres in the initial model.

5.5 Results and discussion

A number of dissolution profiles were initially generated with the same settings of the program and with similar inputs and just the seed for the internal random number generator changed for each experiment. The mean and standard deviation of the results were computed in order to verify the reproducibility in generated dissolution profiles. The choice of an appropriate number of runs to be performed, in order to obtain a dissolution profile for a set of input parameters, depended on the variability of the results.

Initially, the choice was made to perform 30 runs with pores the size of one site scattered randomly on the sphere (diameter=100 sites). One site could accommodate not more then one particle (macromolecule). Figure 5.15 represents this initial configuration. These 30 runs with identical inputs and different seeds indicated that variation of the generated results was very low. The variation remained low when a further 30 runs were performed with more then one macromolecule per site. These preliminary runs indicated that simulations were stable and that for each set of parameters, a single run was probably sufficient to generate satisfactory results.

A discussion with illustrative quantitative results is available in Subsection 5.6.5, where the dispersion is discussed as a function of the size of the sphere.

5.6 Sensitivity analysis

This section follows in continuation to the modelling section and is dedicated to verifying the effects of the different input parameters of the simulation. Elements explored in the sensitivity analysis included the distribution of drug particles per site, lifetimes of the sites, initial porosity, macromolecule concentration and distribution in the volume of the sphere, the time interval used in the simulation, the influence of the size of the sphere and the neighbourhood type used in the simulation.

5.6.1 Effect of the distribution of drug particles per site

The method of sphere manufacturing influences protein distribution within the sphere, i.e. it may be scattered throughout or arranged in small blocks, see Figure 5.2. The aim of the further experimentation is to verify the effect of the distribution of macromolecules per site on the dissolution profiles. One question, clearly, is whether simulation shows any difference if a site of the same size accommodates one or more proteins? To examine this, the proportion of sites loaded with drug, i.e. concentration, was kept constant; instead, the number of particles per site was varied. In addition, the mechanism of PLGA erosion was kept constant throughout all experiments and was taken to be independent of the drug loading of the spheres. The lifetimes of the PLGA particles were updated every 10 minutes corresponding to the Monte Carlo time-step and samples were collected every 144 Monte Carlo steps, (corresponding to one day). The number of particles per site was sampled from a uniform distribution between a lower and an upper value: $U(a1, a2), a1 < a2$. At each run, $a2$ was increased. The particles released were considered in terms of the fraction of the initial number of particles in the sphere. From the simulations, it was found that as $a2$ increases, the total drug is released at a slightly slower rate. This may be due to the fact that, while the effective release surface is kept the same for all experiments, the internal drug loading is increased with each experiment. This means that a larger loading will be released in larger quantities, but in slightly

smaller fractions of the total than found for a smaller loading. The next subsections illustrate, however, that in reality, larger loadings are probably very likely to be related, by manufacture, to larger effective release surfaces.

5.6.2 Initial porosity and initial macromolecule loading

Here, the focus is again on the effects of the initial morphology of the spheres. The literature shows that an increase in drug loading results in a corresponding increase in the release rate, (Lam et al., 2000; Sandor et al., 2001). Sandor et al. have measured the protein loadings of the nanospheres, as a percentage of the total weight of nanospheres. The values considered as low loadings were 0.5-1.6 % while high loadings of protein were 4.8-6.9 %, (Sandor et al., 2001). In our simulation, loadings are considered in terms of percentages of sites on the lattice containing one or more particles. Thus, to examine the effects of the initial loadings in a sensitivity analysis framework, concentrations close to experimental loadings could be considered: these were 2 %, as well as a high loading of 15 % of the sites contained proteins. Figure 5.16 shows the effect of the initial concentration on spheres having a diameter d=100 sites and mean lifetime $\frac{1}{\lambda}$ =69.4 days (λ=0.00001). At every step, the lifetimes of the sites are decreased by Δt=10 minutes, Von Neumann neighbourhood being used. Surprisingly, no significant effect is observed to result from modification of the loading value. As the figure suggests, for each of the three different initial values of the porosity, the variations in the concentration do not generate a too wide disparity of results, (Subsection 5.6.5). Indeed, the concentration has unsignificant influence on the dissolution profiles which follow. At all concentrations, the trend is given by the initial porosity p.

In agreement with our simulations, Sandor et al. (2001) suggest that the increase in the release rate at higher loadings occurs due to *initial porosity*: at low loadings (0.5 -1.6 %), small proteins seem to depend on diffusion through pores initially and on degradation at later times. Spheres with higher loadings, are found to have more

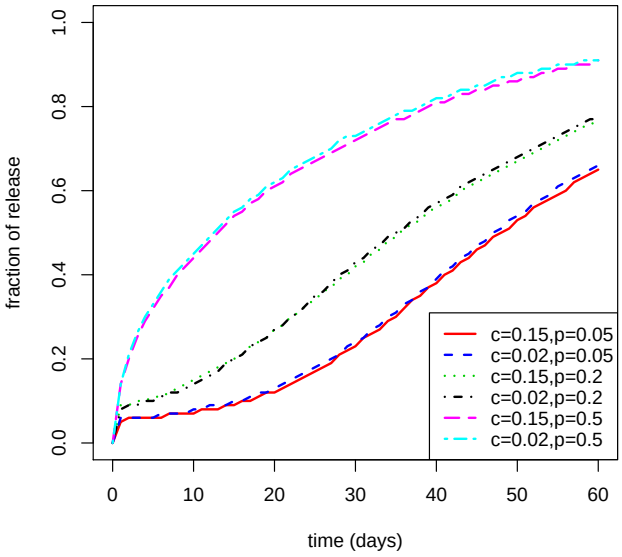

Figure 5.16: For three different initial porosities, p_{01}=0.05, p_{02}=0.2, p_{03}=0.5, the dissolution profile was calculated using two values of the initial concentration, c_{01}=0.02 and c_{02}=0.15. Other model inputs: d=100, λ=0.00001, Δt=10 min, from 1 to 4 particles per site, (von Neumann neighbourhood).

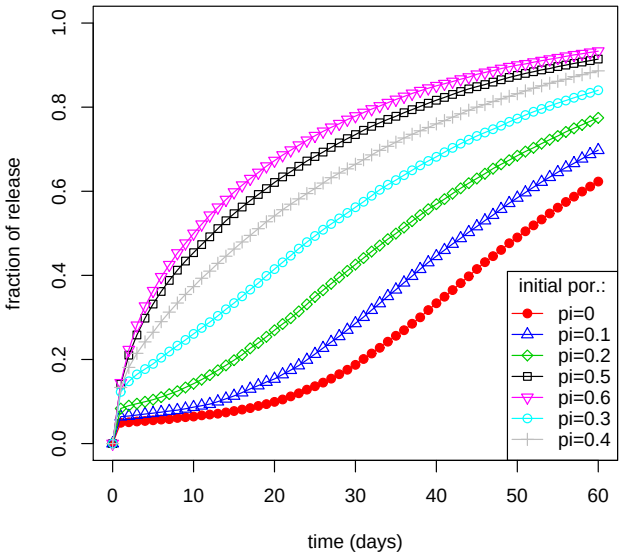

Figure 5.17: Dissolution profile for different values of the initial porosity. The model inputs: d=100, λ=0.00001, Δt=10 min, c_0=0.02, from 1 to 4 particles per site, von Neumann neighbourhood.

interconnecting channels. The authors consider the channels to be the reason why the higher loaded spheres (4.8-6.9 %) do not exhibit the pronounced shift from diffusion based to polymer-based release seen with the lower loaded spheres. Although Sandor et al. (2001) do not provide quantitative evidence on how the initial number of interconnecting pores and channels increases with the initial protein loading, they clearly indicate that not only has the molecular weight of the protein an obvious effect on the initial porosity (larger proteins correlate to larger pores formed in the carrier spheres), but so has protein loading, (larger loadings correlate with larger initial porosities).

Figure 5.17 shows how the spheres, with d=100, λ=0.00001, Δt=10 min, loaded with particles homogeneously distributed through the sphere (c_0=0.02), react to initial porosity modifications in a Von Neumann neighbourhood environment (the pores are homogeneously distributed throughout the sphere).

Simulations were run with porosity values ranging from 5% to 60% sites of the sphere. The initial loadings of the spheres were kept constant throughout the simulations. As can be observed from Figure 5.17, even quite small variations of the initial porosity result in different dissolution profiles beginning with ∼day 1 of dissolution.

There is a threshold value for the initial porosity, p_{th}, which separates two different types of dissolution behavior. For $p<p_{th}$ two distinct dissolution phases can be observed, suggested by the change of shape (from convex to concave) of the release curve:

1. A first phase, corresponding to dissolution governed by diffusion through the initial pores.

2. A second phase where diffusion is generated by two processes: dissolution through the initial pores in conjunction with diffusion through pores created by the erosion process.

In the case of Figure 5.17, p_{th}=0.3. The first phase ends around day 15. Between day 1 and day 15, the dissolution rate is constant and depends on the initial porosity. The second phase begins after day 15 and continues until the molecules are completely released from the spheres, around day 60. The dissolution profiles obtained for $p<0.3$ follow the same pattern as the lysozyme and the carbonic anhydrase at $\simeq$1.5% initial loading, (Sandor et al., 2001).

For $p_0 > p_{th}$, there are no distinct phases of dissolution. On Figure 5.17, for p_{th}=0.3, the profiles obtained have a kinetics pattern like the lysozyme, c_0=6%, alcohol dehydrogenase (1.1 % and 6.9 %) and thyroglobulin (0.5% and 4.8 %).

In relation to experimental values, there is reason to believe that it is not variation in concentration, but rather *the variation of initial porosity*, which is the main basis for modification in dissolution profiles.

In conclusion, as outlined earlier, the simulations strongly support the view that initial concentration only *indirectly* influences dissolution profiles. More evidently,

	Stratum1	Stratum2	Stratum3
Depth of stratum (sites)	$0.15r$	$0.25r$	$0.6r$
Porosity	$1.5p_0$	$0.7p_0$	$0.3p_0$
Concentration	$1.5c_0$	$0.7c_0$	$0.3c_0$

Table 5.2: Details on the stratification of the spheres used to obtain the results from Figure 5.18. r represents the radius of a sphere in number of sites, p_0 and c_0 are, respectively, the input porosity and concentration.

there is a correlation with initial porosity resulting, in all probability, from the way the spheres are manufactured, (with the given combinations of polymer-protein, see Section 5.2). In general, as the literature provides rather little information on the porosity in the PLGA spheres used as drug carriers, it can thus be seen that simulation can be a useful tool from this point of view. The above discussion suggests that it would be useful to dedicate more attention to porosity studies, while investigating release from PLGA spheres, and better describe the connection that exists between the concentration of the loaded molecule and the initial porosity resulting from it. Manufacturing would then be a compromise between the desired quantity of drug released per unit of time and the desired dissolution profile over the time.

5.6.3 Stratified spheres

It has been shown above that there are grounds to consider cases where pores and protein concentrations are not homogeneously distributed throughout the sphere, but, for example, where large porosities at the surface gradually decrease towards the core of the spheres. Figure 5.14 presents three different variants on the initial model A. Version A.1 considers only stratified pores, with the porosities decreasing from the surface towards the centre. Version A.2 considers stratified concentrations of protein also decreasing from the surface to the core. However, as discussed in Subsection 5.4.4, it is reasonable to assume that layers with large initial porosities are correlated with correspondingly larger concentrations too, as described in Batycky et al. (1997); Ungaro et al. (2004). This is incorporated in version A.1-2.

Figure 5.18 shows a comparison between the basic model A and its variants A.1 and A.1-2. Table 5.2 details the width of the strata, deliberately chosen in such a way that in each variant initial porosity of the generated spheres was almost the same. Figure 5.18, (a) shows how the three variants behave with reduced initial porosity. Figures 5.18, (b) and (c) illustrate the behaviour of the three variants for larger porosities. These results suggest that stratification of the porosity plays a smaller role than stratification of the concentrations of the molecules. It also argues for the fact that the internal morphology of the spheres is an important factor to take into consideration at modelling. According to our model findings, the spheres illustrated in Figure 5.2, (a) and (b) would provide very different dissolution profiles when exposed to a dissolution medium.

5.6.4 Influence of the time interval for updating the particles

The physical meaning of the time interval, in which the particles of the model move, is directly related to the mobility of the particles within the structure. In the case of a multi-agent model such as the present one, Δt does not completely reflect the diffusivity or the *effective diffusivity* of the macromolecule, but it rather reflects the potential for diffusion conditional on the pores of the device.

This simulation actually indicates more clearly the mechanisms behind the profiles. The smaller Δt is, the more often the particle is given the chance to update, i.e. to move to a neighbouring site. Figure 5.19, (a, b, c), (t>20 days), shows that in the case where the environment permits mobility,(right hand side of the graphs), different values for Δt can considerably change the rate of dissolution profile. This means that even though the PLGA does present an obstacle, the porosity spans the whole system and on increasing the mobility, the molecules are released extremely rapidly. We will say that a *sphere is said to reach the percolation threshold* when there is a cluster of *connected pores* spanning the whole sphere. For the left-hand side of the graphs the situation is very different: Δt has no effect on the dissolution

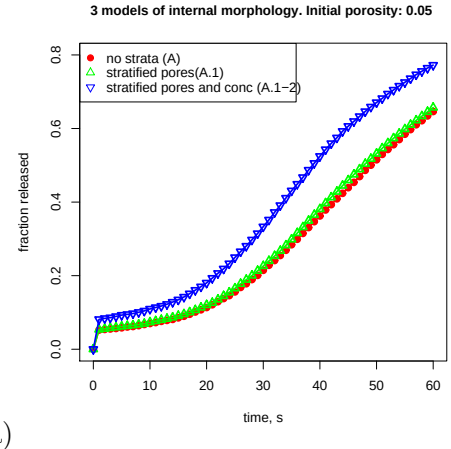

a)

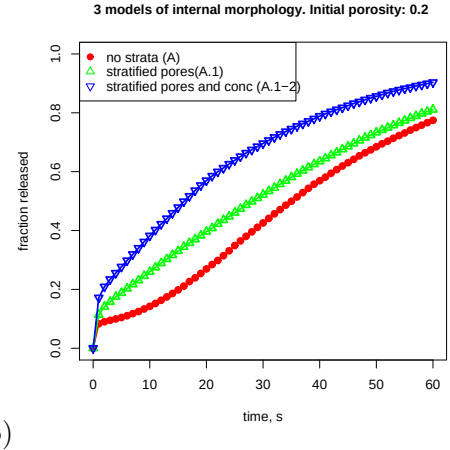

b)

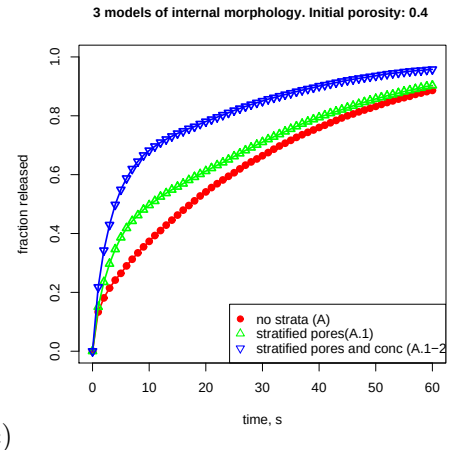

c)

Figure 5.18: Comparison between dissolution through spheres with homogeneous porosity and spheres with stratified porosity and stratified concentration. The concentration strata are superposed on the porosity strata.

rate, demonstrating a reduced dissolution through unconnected channels.

Figure 5.19, (a) is a particularly good example: the spheres start at zero initial porosities, but a small initial burst can still be observed. Further, porosity is allowed to increase slowly, (λ=0.00001). At day 16, when the value of the porosity reaches the threshold value of p_{th}=0.2, the profiles split according to the different values of Δt used, as there are clusters of pores spanning the whole sphere which begin forming at this point in time.

The following figures show behaviours in stages. These stages are due to the sequential percolation through the three strata by connected pores. The first stratum is initially percolated and is the origin of the initial burst. The second stratum is apparently percolated very quickly after dissolution begins, (before day 10), while the stage, which can be observed by day 20, is caused by the last stratum reaching its percolation.

The dissolution patterns obtained with different Δt are again in good qualitative agreement with a number of profiles obtained experimentally in Sandor et al. (2001): lysozyme 6.9 %, bovine serum albumin (0.9 % and 5.1 %), Figure 5.19, (c) or lysozyme (1.6 %) , Figure 5.19, (a).

The choice of Δt is in agreement with the effective diffusivity of a molecule in a medium filled with erosion products, such as different monomers. Smaller molecules have larger effective diffusivities, while larger molecules will be characterised by very reduced diffusivities, (Sandor et al., 2001).

5.6.5 Influence of the sphere size

Each of the two curves in Figure 5.20 is obtained by calculating the standard deviation over 10 program runs with the same inputs. The figure shows that with the increase of size of spheres considered, the standard deviation for different runs of the program converges to a stable value. Even for small spheres, the standard deviation is very small in comparison to the data values on release. This justifies performing

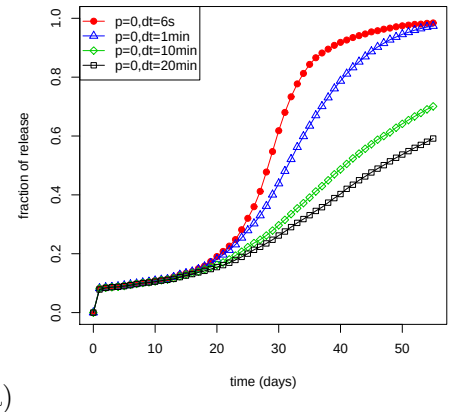

a)

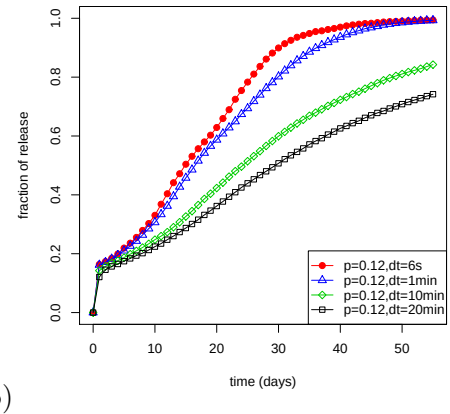

b)

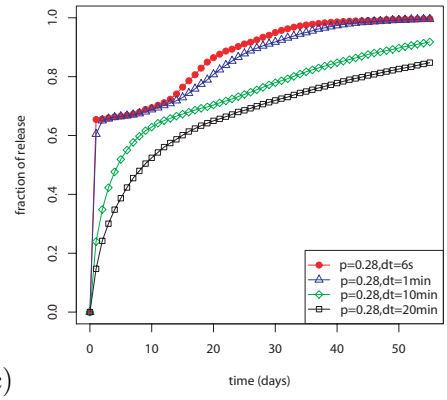

c)

Figure 5.19: Effect of the time step used to perform the updating in the simulation. Model used: A.1-2.

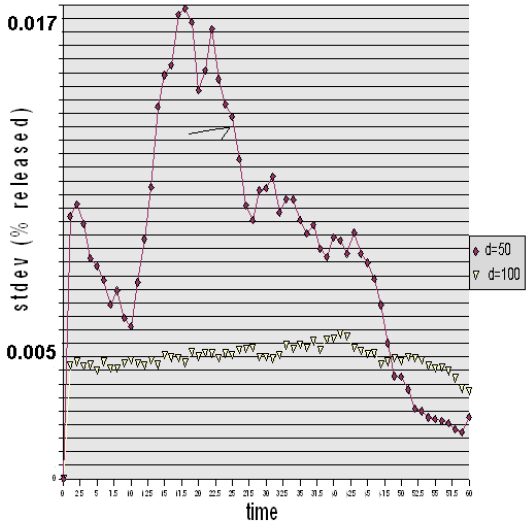

Figure 5.20: Dynamics of the standard deviation calculated for ten different runs with the same input parameters for two different sizes of the sphere: d=50 and d=100 sites.

only one run for each different input situation.

Obviously, particles will be released more slowly from a larger sphere: Figures 5.21, (a) and (b). Usually, the PLGA particulates come in batches of spheres characterised by a certain size distribution, thus it is interesting to use simulation to analyse the effect on the size distribution on the release profiles. It addition, it is useful to investigate how variations in the size distribution can affect the overall dissolution curves. The differences in the profiles obtained with d=50, d=100 and d=150 suggest that small shifts in the size distribution would result in significant changes in the release profile.

5.6.6 Influence of the neighbourhood used

The simulation has again been adapted for both Von Neumann and Moore neighbourhoods. The patterns obtained using Moore's neighbourhood (results not shown) have the same forms as those obtained with Von Neumann neighborhood. However, we find that the rate of formation of porous channels has to be extremely slow in

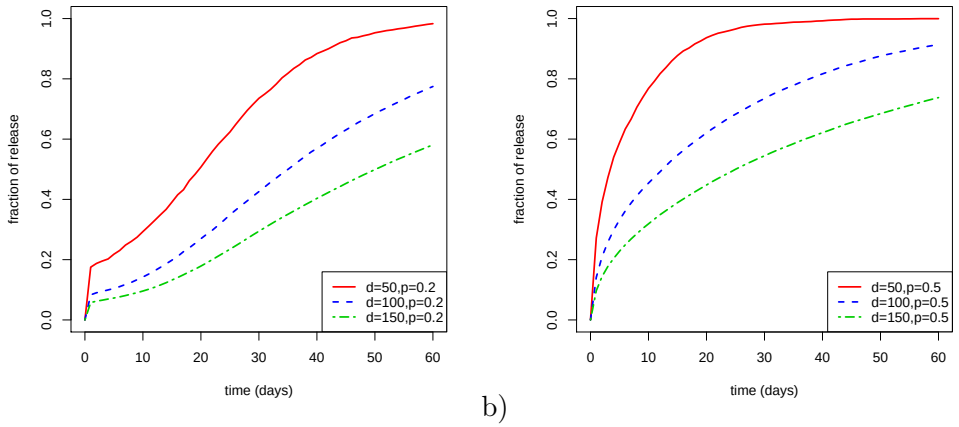

a) b)

Figure 5.21: Effect of the size of the sphere on the release profiles. a) initial porosity p_0=0.2 b) initial porosity p_0=0.5.

order to obtain sigmoid profiles such as described by Zhang et al. (2003) and illustrated in Figure 5.6, (b). The Moore neighbourhood in 3D involves 18 nearest neighbours (degrees of freedom) in comparison with only 6 considered with von Neumann neighbourhood and as indicated in Chapter 4, considering a larger number of nearest neighbours signifies higher degrees of freedom for the molecules movement. A neighbourhood providing a larger degree of freedom to the molecules could be of interest when adapting the model to coarser grained simulations, where the size of the pores considered is of the order of 10^{-7}-10^{-8} m. Thus, protein macromolecules can gain access to the pores from more directions, whether by virtue of the inner sphere structure, or through dissolution through micropores. Intuitively, macroporosity grows much slower than microporosity, thus a combination of the Moore neighbourhood and slow porosity growth rates can be useful for coarse-grained simulations. Small molecules have larger effective diffusivities than larger molecules, thus, the former would be characterised by smaller Δt and the latter by larger Δt for the same initial size of the pore. Additional information is needed about the time when the spheres disintegrate since this accelerates molecule release.

Description	Variable
Size of the sphere	d
Effective diffusivity/mobility of the macromolecules through the pores	D_{eff}
Diffusivity of the macromolecules in the solvent	D_0
Diameter of the macromolecules	a
Sphere loading	c
Concentration of the macromolecule at different depths od the sphere	c_{01}, c_{02}, c_{03}
Size of the pore one wish to consider	p_d
Initial porosity	p_0
Pattern of repartition of pores in the volume of the sphere	p_{01}, p_{02}, p_{03}
Rate of formation of pores	r_p

Table 5.3: List of variables desirable to set up correctly the simulations

5.7 Validation with experimental data for quantitative measurements

To use the model developed for quantitative evaluations or making predictions, initial knowledge about the microspheres is needed. Table 5.3 gives a list of variables, characterising the spheres, although as the next subsection shows, not all of these variables are absolutely necessary to determine dissolution profiles of the spheres.

5.7.1 Dimensional analysis

The target here was to establish a relation between the diffusion coefficient of the encapsulated species in the matrix and the time interval Δt, determining how often the model particles from the spheres need to be updated.

In their article, Zhang et al. (2003) mention two diffusivities: D_0 which is the solute diffusion coefficient in the solvent and D_{eff} the effective solute diffusion coefficient in the polymer matrix, depending on the internal morphology of the latter. Based on this work, the following expression gives the effective diffusivity of a chemical species in a porous medium:

$$D_{eff} \sim \frac{D_0 p}{\tau} \tag{5.7.1}$$

p is the porosity and τ is the dimensionless tortuosity of the medium. The porosity is one measure of the dimensions of the internal morphology, usually in the range 0.2-0.7 (fraction of volume) for polymers, (Zhang et al., 2003). As stated, the value of τ is usually between 1 and 100, (Zhang et al., 2003), but in the case of the PLGA τ reaches much larger values, in the range of $10^3 - 10^5$, because the drug molecule has to move through some narrow passageways which are produced by the vibrations of the polymer chain and control the actual pore size for the passage of macromolecules, (Zhang et al., 2003).

To verify independently the value for the tortuosity, the literature was examined for diffusion coefficients and effective diffusion coefficients experiments on PLGA spheres. Batycky et al. (1997) obtained the effective diffusivity of a protein in PLGA: $D_{eff} = 2.00 \times 10^{-13} \frac{cm^2}{s} = 2.00 \times 10^{-17} \frac{m^2}{s}$. Goodhill (1997) stated that $D_0 = 3 \times 10^{-7} \frac{cm^2}{s} = 3 \times 10^{-11} \frac{m^2}{s}$ for the diffusion coefficient of a protein of 17 kD (IL-1 beta). Zhang et al. (2003) mention references which published $D_0 = 8.3 \times 10^{-11} \frac{m^2}{s}$ for BSA (bovine serum albumin). With these values of D_0, D_{eff} and p and Expression (5.7.1) the tortuosity τ indeed appears to be of the order of 10^5.

Fick's first law can be expressed as the following equation:

$$J = D\frac{dC}{dx}\ [\frac{kg}{m^2 s}]\ or\ [\frac{mol}{m^2 s}] \tag{5.7.2}$$

where $dC = C_{sat} - 0$. Zhang et al. (2003) give C_{sat} in the range 1-100 $\frac{kg}{m^3}$. If the site of the sphere is Δx , then, for very small sizes of the site, such as 10 nm, the flux J is in the range of $10^{-8} - 10^{-7}[\frac{kg}{m^2 s}] = 10^{-26} - 10^{-25}[\frac{kg}{nm^2 s}]$. This quantity can be expressed as mass per surface of the site: $10^{-24} - 10^{-23}\ [\frac{kg}{site\_surface \times s}]$.

Zhang et al. (2003) give an example of concentration saturation $C_0 = 13.5[\frac{kg}{m^3}] = 13.5 * 10^{-27}[\frac{kg}{nm^3}] \simeq 10^{-24}[\frac{kg}{site}]$. Thus the time for a site of 10 nm to reach saturation is $t \simeq \frac{10^{-24} kg/site}{10^{-24} kg/(sites)} \simeq 1s$. This means that the time a site is occupied by a diffusing species is of the order of seconds. In conclusion, choosing Δt for the model in the range of seconds should provide realistic simulations. Choosing much larger time-

Variable	Value	Model
d	200-250 nm	50 sites
D_{eff}	N/A	Δt =10min, 1min and 6 sec
D_0	N/A	not needed here
a	$\simeq$3 nm	-
c_0	1.6% and 6.9%	c_{0low} =0.016 c_{0high} =0.069
c_{01} /c_{02} /c_{03}	N/A	c_0 /0.5c_0/0.2c_0
p_d	>20 nm	5 nm/site
p_0	N/A	p_{0low} =0 p_{0high} =0.3
p_{01} /p_{02} /p_{03}	N/A	p_0 /0.3p_0 /0
r_p	N/A	$\lambda = 5 * 10^{-6}$

Table 5.4: Summarises the knowledge available on the nanospheres loaded with lysozyme and the corresponding modelling decisions taken after evaluating this data

steps will slow down the release of the particles, whereas too small time steps will slow down the run-time of the model. Figure 5.19, (a, b, c) shows how choosing too large a Δt, such as 10 and 20 min, influences the dissolution profile, making it much slower. The effect of choosing Δt is especially visible when the sphere reaches percolation and the molecules gain mobility (Subsection 5.6.4) .

5.7.2 Validation with experimental case 1: lysozyme

In this subsection, the models are validated by comparing their performance to real data. The first experimental data set due to Sandor et al. (2001) relates to a set of nanospheres encapsulating a very small protein, the lysozyme. Table 5.4 specifies the knowledge available on this system. It has been decided to use the model labeled as A.1-2 (stratified pores and stratified concentrations) for the simulation of this case.

The spheres have been analysed by electron microscopy and they appear compact and non-porous. This means that the pores, if these exist, have diameter $<$ 20 nm i.e. below the resolution levels of the microscopy technique, (Sandor et al., 2001). For the simulations, we chose to consider the existence of very small pores of 5 nm in diameter, just above the Stokes-Einstein diameter of the lysozyme (3 nm). Given

the diameter of the sphere d and the diameter of the pore p_d it was decided to run the simulations with spheres of 50 sites in diameter, (i.e. taking 5 nm as the diameter of one site). The λ parameter was chosen to be $5 \times 10^{-6} s^{-1}$. It was not known if the pores were organised in strata or not, but given that in slightly larger nanospheres, (encapsulating larger molecules, such as carbon anhydrase), porosities are known to be stratified, it is assumed here that spheres carrying lysozyme have stratified porosities as well. The strata in the model are organised as:

1. A surface stratum to the depth of r_1 =3 sites, characterised by maximum porosity and maximum concentration (Table 5.4)

2. A second stratum (r_2 =12 sites) with a lower porosity hence a low concentration.

3. A core of a radius r_3 of 10 sites which is not porous at all and encapsulates a correspondingly reduced concentration of molecule.

As information about the effectiveness of the lysozyme in PLGA matrix is unknown, three different values of $\triangle t$ are chosen, close to the approximate value obtained by dimensional analysis (see Subsection 5.7.1). The best results are still obtained with the smallest time step: $\triangle t$=6 s, (Figure 5.22). In this Figure, the points indicating a slow release experimental curve correspond to an initial loading of 1.6% and the curve of very fast release has been obtained by Sandor et al. (2001) with an initial loading of 6.9%.

5.7.3 Validation with experimental case 2: carbonic anhydrase

This subsection summarises results obtained with the model calibrated to simulate release of carbonic anhydrase from microspheres of size $\simeq$1 μm, described, like previous spheres, in Sandor et al. (2001). This type of sphere has a different initial internal morphology to the case examined previously. Transmission electron micrographs of PLGA microspheres encapsulating carbonic anhydrase are shown in Figure 5.12, (b).

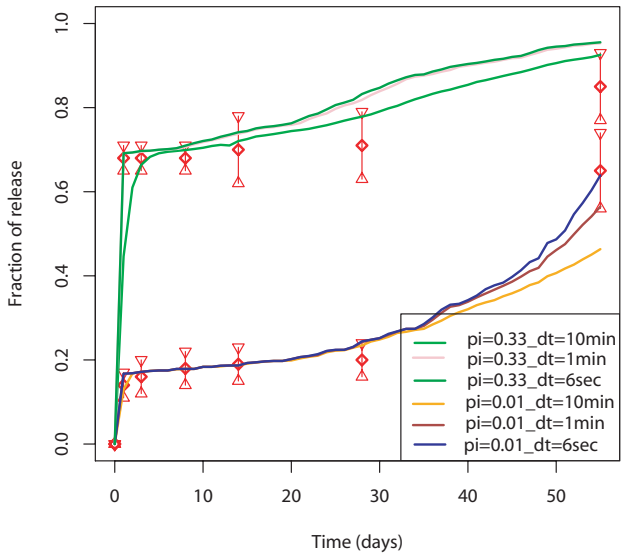

Figure 5.22: Experimental lyzosyme release versus simulated drug release from biodegradable microspheres. Red rhombi represent the experimental points from Sandor et al. (2001). Continuous curves show simulated results obtained with different Δt values.

These spheres have larger diameters than the previous ones and a somewhat different internal morphology to those encapsulating lyzosyme. Figure 5.12, (b) shows that the spheres are characterised by quite large internal pores and channels, which appear to be much larger then the protein diameter (carbon anhydrase). It is for this reason that in models C to C.1.2, (Figure 5.14,) models the initial pores were permitted to be larger than one site in size. Figure 5.23, (a) shows a cross-section through a sphere generated with model C. In addition, it is considered that most molecules are initially concentrated in these pores, as argued in Batycky et al. (1997); Ungaro et al. (2004). To simulate carbonic anhydrase release, model variant C.1.2. (Figure 5.14) has been used. In this version, most of the proteins are situated in the occlusions, but some are trapped in the bulk PLGA as well. The occlusions are slightly stratified, such that they are more prevalent at the surface of the spheres, in order to replicate the pattern observed in Figure 5.12, (b). Table 5.5 shows the information available on spheres as well as corresponding decisions about the model parameters.

a)

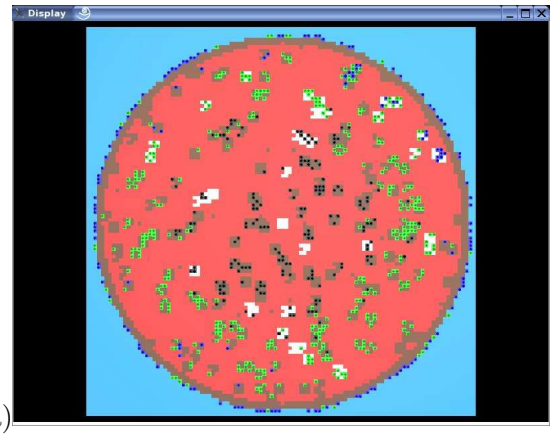

b)

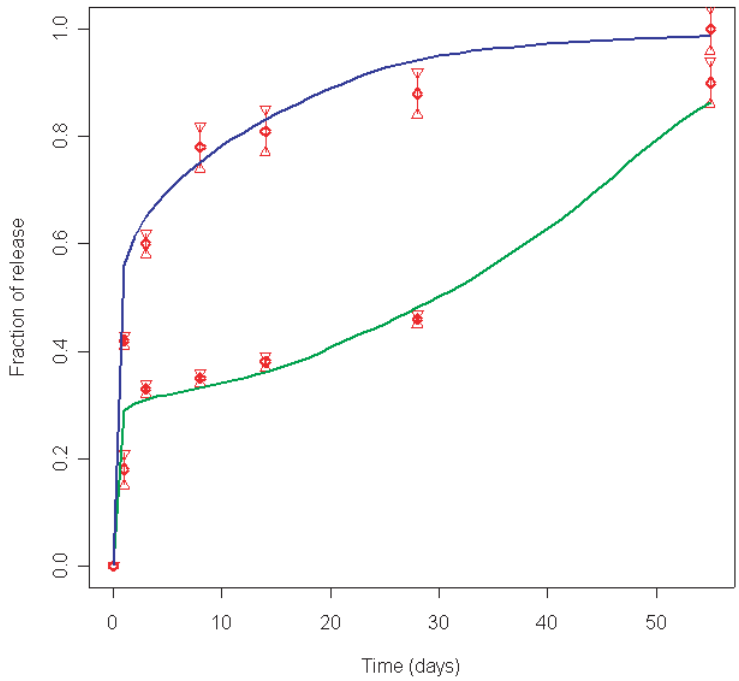

Figure 5.23: a) Internal morphology of the spheres for simulating dissolution of carbon anhydrase from PLGA spheres of $\simeq 1\mu m$ diameter. b) Experimental carbonic anhydrase versus simulated drug release from biodegradable microspheres. Red rhombi represent the experimental points from Sandor et al. (2001). Continuous curves show simulated results obtained with different Δt values.

Variable	Value	Model
d	1000-1200 nm	100 sites
D_{eff}	N/A	Δt =10min and 1min
D_0	N/A	not needed here
a	~10 nm	-
c_0	1.2% and 6%	c_{0low} =0.012 c_{0high} =0.006
$c_{01}/c_{02}/c_{03}$	N/A	follows the occlusions
p_d	1-60nm	10 nm/site, 30 nm/occlusion
p_0	N/A	p_{0low} =0.14 p_{0high} =0.33
$p_{01}/p_{02}/p_{03}$	N/A	2strata: $r_1 = 5,\ r_2 = 45$ sites and $3p_0/p_0$
r_p	N/A	$\lambda = 5 * 10^{-6}$, but could have used a smaller value

Table 5.5: Summarises the knowledge available on the nanospheres loaded with lysozyme and the corresponding modelling decisions taken after evaluating this data

Figure 5.23, (b) illustrates performance of model version C.1.2 to simulate the experimental data obtained by Sandor et al. (2001). The simulated slow release curve has been obtained with an initial porosity of 0.14 and the quick release curve: with initial porosity p_0=0.33. The curves have been obtained by running the model for a single sphere. The experimental data were based a population of spheres with average diameter of 1 μm. It should be noted that models A and B (see Figure 5.14) did not succeed in obtaining the types of curves provided by model C and its variants.

5.8 Conclusion

This chapter presented an exploratory framework for modelling dissolution of proteins from PLGA microspheres. It has been shown that the initial model (A) can be modified to simulate a number of experimental situations. For the PLGA microspheres, the results obtained in the work presented above are in good agreement with the original experimental work of Sandor et al. (2001). The two experimental cases discussed in the validation subsection were the most problematic for modelling. The models developed can be easily used to simulate other cases of other protein dissolu-

tion from PLGA microspheres presented in Sandor et al. (2001) and elsewhere. We elaborate on three different aspects of future work related to the PLGA micro- and nanospheres in Chapter 7, considering:

- Optimisations from a technical point of view making possible broader use of models A-C and their variants.
- Extending the models to other types of bioerodible nanospheres as the role of the latter grows in modern pharmaceutics.
- Project outline for a particular case: using and extending the models developed to simulate the experimental work described in the example from Subsection 5.2.4, where the bioerodible spheres are used in conjunction with other type of polymer to form therapeutical implants for damaged tissues.

Chapter 6

Reconstruction of particle size distributions of particulate polydisperse systems from *in vitro* dissolution data

6.1 Introduction

This chapter continues investigation of drug delivery systems which are composed of many particles for all or part of their dissolution process. In the previous chapter, the way in which bulk eroding spheres for sustained release show different release profiles as a function of their size was demonstrated. While the previous chapter concentrated on the microscopic behaviour of each component of a particulate system, following interaction with the dissolution medium and ways by which the carrier particles release their active content, the present chapter, on the other hand, examines a delivery system composed entirely of particles. In other words, the dissolution

profiles, obtained from such systems, are treated both in terms of (i) size distribution of the component particles and (ii) interactions of these particles in the *in vitro* or *in vivo* environments for dissolution.

In contrast again with the previous chapter, (which dealt with *direct problems*, with solution based on a complete description of cause and effect), this chapter looks at an *inverse problem*, where solution implies determination of *unknown causes* behind certain dissolution profiles, based *on observation of outcomes*.

The chapter begins by examining the problems related to the dissolution profiles from multisized multiparticle systems, focusing on multiple sources of noise in these data. Next, the Bayesian paradigm is proposed for *reconstruction of unobserved parameters* and *noise quantification* for these data. An Inverse Monte Carlo technique is put forward to handle the inverse problem, using sampling. A proof of concept algorithm is described for a general case of a particulate system, in order to extract information from the experimental dissolution profiles. The aim is thus to reconstruct the parameters of the system (e.g. the size distribition), and to assess its noise levels, at different stages of the dissolution.

In order to validate the theory, in the absence of detailed experimental data, dissolution data *are simulated* within known parameter values and against known endpoints. Finally, the Inverse Monte Carlo algorithm is adapted for these particular "artificial" cases and a sensitivity analysis is carried out to evaluate algorithm performance. Finally, conclusions are drawn and future work outlined.

6.1.1 Examples of multi-particle drug delivery systems

Many kinds of particulates, not just those composed of micro- and nanospheres (presented in Chapter 5), are made up of multiple particles. Many solid dosage forms, such as the majority of immediate release tablets, are other than non-disintegrating. Rather they disintegrate into smaller fragments and particles during the course of the dissolution test *in vitro* or during *in vivo* dissolution. In contrast to bulk eroding

particulates, these particles decrease in size as the dissolution proceeds, changing the thickness of the dissolution boundary layer at each point in time. Another example of dosage forms that consist of separate particles are *in-suspension* formulations or *solid-liquid dispersed* systems.

Studies have shown (Simoes et al., 1996*a*; Almeida et al., 1997) that the particle size distribution strongly influences the dissolution profiles, as the size of the particle is obviously related to the surface exposed to the dissolution medium. Noting that the dissolution of powdered drugs was far from well understood, Almeida et al. (1997) evaluated a number of existing models on multi-particle systems in conjunction with an extensive experimental study. This provided detailed information about the size distributions involved. More precisely, three different size fractions of a widely-used sparingly soluble drug - ibuprofen - were fully characterised with regard to particle size distribution, specific surface area, density, solubility and diffusion coefficient. Dissolution profiles were obtained using a technique that counts and sizes particles - the Coulter counter technique (see ref. Coulter (2006)) - which is capable of directly tracking the number and size of the particles in suspension throughout time. The study (Almeida et al., 1997) concluded that most of the assumptions of the evaluated models were actually not valid for the experimental conditions, thus the profiles generated by the models fitted the data extremely poorly, (Almeida et al., 1997).

For other cases, however, it is harder to verify directly the assumptions of existing models and postulate more correct hypotheses, as the only visible (or observed results) are the dissolution profiles, (see example below, Subsection 6.1.2). In such cases, the problem can be *inversely* posed: *"what are the unobserved system parameters, which result in the observed dissolution profile?"*. The undetermined parameters this study focuses on are the size distribution of the constituent particles and the dynamics of this distribution during the dissolution process.

6.1.2 Nature and quality of *in vitro* obtained data

The backward or retrospective study aims to reconstruct unobserved parameters using observed dissolution data. Thus it is worthwhile examining more closely the data observable from multi-particle pharmaceutical systems and discussing their nature and *quality*.

The USP Type II Apparatus is widely used in performing *in vitro* dissolution testing of newly developed drug delivery systems, (Chapter 4). Typically, experimental data from the USP apparatus II would be dissolution profiles, representing i) the time series of fractions of dissolved solute in the solvent or ii) the time series of solid matter remaining in the solvent.

Numerous reports in the literature describe high variability in test results, even for dissolution apparatus calibrator tablets, (Baxter et al. (2005) and references therein). Healy et al. (2002), Crane et al. (2004a), Baxter et al. and other studies show that, under normal stirring conditions, flow behaviour is both time-dependent and highly heterogeneous. Hydrodynamic conditions, while not turbulent, are directly related to the strain and shear rates, which determine the thickness of the dissolution boundary layer, which in turn limits the mass transfer rates on tablet or particle surfaces. Thus, fluctuations in the flow introduce variability in the evolution of the processes, which are affected by hydrodynamics: shearing of the tablet surfaces, disintegration of tablets and de-agglomeration rate of the particles, suspension and mixing of tablet fragments and, finally, mass transfer from the solid to the liquid.

In illustration, Baxter et al. (2005) have performed experiments with three distinct types of tablets: non-disintegrating, slowly-disintegrating and rapidly-disintegrating. All were found to exhibit statistically significant dissolution rates when the tablets were fixed in two different locations. In particular, rapidly-disintegrating tablets, containing the drug prednisone, have the greatest sensitivity to tablet position in the vessel, (e.g. an off-centered position yields an almost

two-fold difference in the dissolution rate).

In many cases, published experimental dissolution profiles are averages of profiles obtained for different trials, performed under similar conditions, so that they represent the *general* behaviour of the system, but are contaminated with noise from the point of view of determining underlying unobserved parameters.

Generally, the number of parameters relating to the dissolution profile is large relative to the number of available data points in the resulting dissolution profile. For example, one can imagine all possible trajectories that the different types of particles can take, crossing regions in space, characterised by different shear rates etc. and the different ways size distribution can evolve according to flow conditions in different locations of the vessel. In conclusion, noise in the dissolution profiles is thus associated both with the measurement procedures and the system state fluctuations through the different experiments performed. Therefore, when modelling the dissolution process, rather than being entirely deterministic, it can be considered to consist of *a deterministic* part and *a stochastic part*, by incorporating a level of uncertainty into the model.

The Appendix 3 gives a complete list of the notations and the abbreviations used throughout this chapter. The notations are as well introduced at the appropriate places as the discussion progresses, thus the reader can take note of the titles of different subsections classifying the symbols, and return to the appropriate one if necessary.

6.2 Theoretical Bayesian framework for the dissolution problem

In this section, a Bayesian framework for parameter reconstruction and noise quantification is proposed for drug delivery systems which exhibit certain amounts of variability in their dissolution profiles, consistent with a set of data for the dosage

form used, and the USP dissolution apparatus. The target types of drug delivery systems, as noted, are:

- soluble or surface eroding particulate polydisperse systems
- disintegrating tablets

The objective is to examine the effects of changing particle size, particle size distribution and particle density on inversely simulated results, as compared with experimental results. Mass transfer rates or cumulative proportions of solute for different kinds of particulate systems or disintegrating systems can be determined experimentally and compared with the predictions made by modelling and simulations.

The problem posed is a good example of an inverse problem (for a review see Mosegaard and Sambridge (2002)), because in some cases of DDS in the USP apparatus II and other conditions it is difficult and time-consuming to assess the size distributions and other parameters at different times of the dissolution. Moreover, the time-dependent flow conditions of the dissolution apparatus are such that it is not completely obvious towards what particular distribution the particles will evolve to at any next time step. As in many other inverse problems, the problem of a multi-particle system dissolving in the USP apparatus is thus *underspecified*: i.e. many initial states could produce similar fits to the data. It can be assumed that the parameters characterising the size distribution at a given time-step are not fixed but follow some *probability distributions*, whereas the transition from one distribution to the next one, associated with the next time step, *is a stochastic process* rather than a deterministic one, (Subsection 6.1.2). In other words, the aim of the following is to estimate model parameters, related to the size distributions and their variability, from experimental measurements. The assumption is that these parameters are not fixed but *follow some statistical distribution.* Posing the problem in this way satisfies the Bayesian framework, (Meyer and Millar (1999a); Meyer and Christensen (2000*a*); Ramachandran and Kandlikar (1996); A. Voutilainen and Kaipio (2001).

The Bayesian theory has been described and studied in many instances, e.g. Davies (1998), the review of Mosegaard and Sambridge (2002) and references therein. It permits the production of a large range of possible initial states, by reporting on posterior distributions or confidence intervals of parameters. Finding posterior probability distributions amounts to finding the conditional probabilities that certain values of the unobserved parameters are taken, after the relevant experimental evidence is taken into account. The Bayesian view of a measurement is that of a process of extracting additional knowledge from it, consisting of refining previous knowledge of physical parameters by:

1. narrowing their distribution of probability, by repeatedly sampling from it,
2. assessing the posterior distribution of the model parameters, given this measurement.

The following subsection develops these ideas.

6.2.1 Observation model and time evolution model

Probability distributions corresponding *to parameters of the particle size distribution at each time step* are explored. The unobserved data are modelled by the state parameters or *the vector state* $\overrightarrow{\theta_t}$ at time t. If y_t represents the experimental data, the problem amounts to how to relate the vector state $\overrightarrow{\theta_t}$ to y_t. This relationship can be built up using a number of factors. Mainly it is a deterministic relating the concentrations of solute in the solvent and the size of the particles. Additional information, such as that originating from e.g. visual images of disintegrating or disintegrated dissolving compacts or powder might also be incorporated if available. But usually this is not enough, because there are factors, whose effect on y_t unknown, and as stated above, y_t might contain noise, related to either of:

- spatially heterogeneous hydrodynamic conditions

- measurement error.
- model-related error.

The inverse model can take the form:

$$y_t = F(\overrightarrow{\theta}_t) + u_t$$

$F()$ is a deterministic functional relationship between the state parameters at time t. u_t is some noise component. For simplicity, it can be chosen to be Gaussian with zero-mean, but this is not always the case. For example, at each point in time the variance of u_{y_t} can be weighted by the experimental measurement error range exhibited in the experimental part, as in Meyer and Millar (1999a,b).

In order to introduce into the model the system's time evolution in time and to be able to use feedback mechanisms (such as a Markov Chain[1]), the following can be introduced:

$$y_t = F(\overrightarrow{\theta}_t, \psi) + u_{y_t} \tag{6.2.1}$$

$$\overrightarrow{\theta_{t+1}} = G(\overrightarrow{\theta}_t) + \overrightarrow{v_t} \tag{6.2.2}$$

where ψ represents some extra parameters, the nature of which can be related e.g. to particle shape. Equation (6.2.2) describes the time evolution of the model. It is composed of two terms: a stochastic term $\overrightarrow{v_t}$ and a deterministic term $G(\overrightarrow{\theta}_t)$. The deterministic term is a functional relationship describing update of the vector state

[1] A Markov chain describes at successive time steps the states of a system. The changes of state are called transitions. The Markov property means that the conditional probability distribution of the state in the future, given the state of the process currently and in the past, depends only on its current state and not on its state in the past.

between time j and $j+1$. The stochastic term, v_t, accounts for additive dynamical noise factors, which can be related to either of:

- the speed of evolution of the states of the system.
- the time-dependent flow conditions.
- the correctness of the time-evolution model G.

The extra Equation (6.2.1) also provides the basis for intervention in the simulation on the basis of *a priori* knowledge or gross deviations of the new $F(\overrightarrow{\theta}_t, \psi)$ from expected results. Figure 6.1 gives a schematic representation of the material described above.

The previous knowledge of the parameters can be refined by through comparisons with the data, by performing what is called*empirical updating*. It can be performed on the basis of the classical Bayesian paradigm, which relates probability distributions as presented in the methodology chapter (Chapter 3). In this particular case the measurements are a time-series of dissolution data, with a single value for each time-moment t: y_t and $\overrightarrow{\theta}$ represent the unobserved physical quantities of interest, or the state parameters, seeking to give confidence intervals estimates for them.

Assuming that the noise u_t is Gaussian and depends on y_t, then at each discrete time step j, the likelihood probability distribution is given by:

$$P_{post}(y_j|\overrightarrow{\theta}) = \frac{1}{\sigma_{y_j}} exp(-\frac{1}{2\sigma_{y_j}}(y_j - F(\overrightarrow{\theta}_j)^2) \tag{6.2.3}$$

where σ_{y_j} is the variance of the random variable u_t.

Generally, sampling $P_{post}(\overrightarrow{y}|\overrightarrow{\theta})$ can be performed by generating values for $F(\overrightarrow{\theta})$ corresponding to a sample of $\overrightarrow{\theta}$ taken from $P(\overrightarrow{\theta})$. The functional relationship $F()$ for different $\overrightarrow{\theta}$ is accepted or rejected depending on whether it predicts the experimental data $\overrightarrow{y}$ within a certain *tolerance threshold*. This is an example of

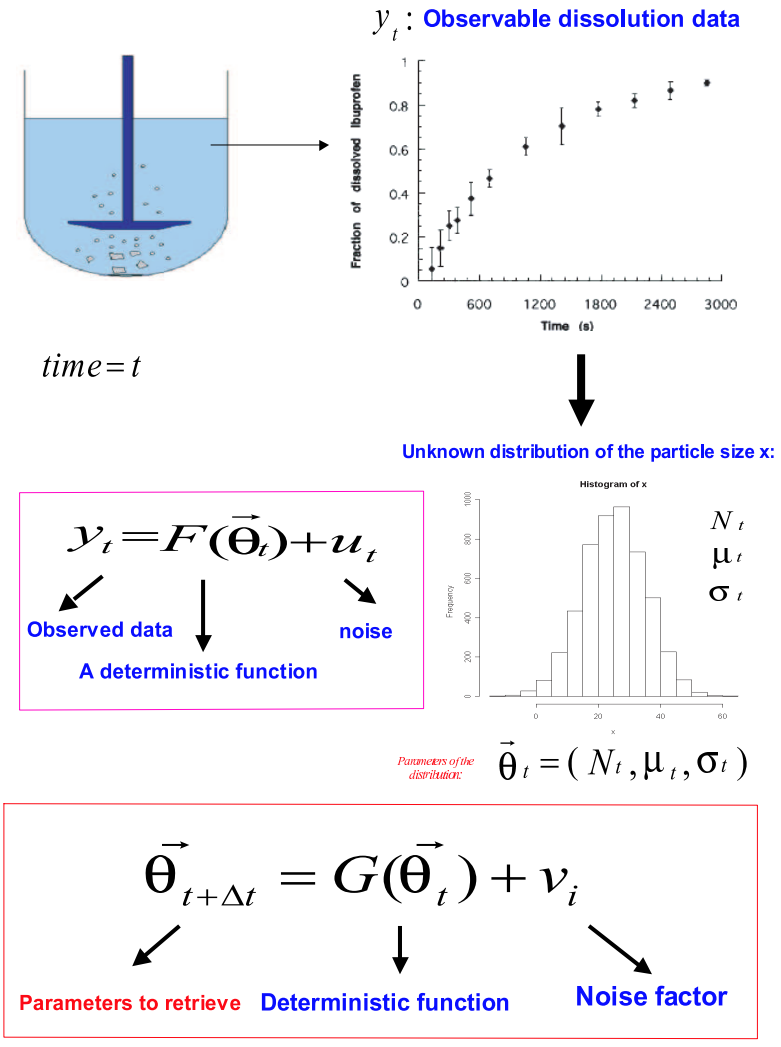

Figure 6.1: Diagram summarising the concept of modelling the problem of particulate dissolution from a stochastic point of view.

feedback mechanism. Section 6.4 provides more details on how different $\overrightarrow{\theta}$ can be sampled.

6.2.2 Time evolution model

6.2.2.1 Particle size distributions

Parametric distributions Despite their tendency to be oversimplistic, *log-normal* and *normal* parametric distributions are quite good as first approximations for modelling the particle size distribution of different systems consisting of many particles. As well, there are examples in literature, where *log-normal* and *normal* distributions are used to describe different pharmaceutical polydisperse systems (Almeida et al. 1997 and references therein).

The log-normal function has also been used by Ramachandran and Kandlikar (1996) and Voutilainen and Kaipio (2005) for estimation of aerosol size distributions. Here is an illustration of practical application of the log-normal distribution as a parametric approximation for the size distribution function. The distribution is assumed to vary over time as the dissolution takes place, while, for simplicity reasons, at each new time step $j+1$, the distribution has again a log-normal shape, characterised by *a new* vector of parameters $\overrightarrow{\theta}_{j+1}$. From the previous section, the objective is clearly to estimate these parameters as the solution of a time-discrete problem: i.e. to estimate values of the unknown parameters $\overrightarrow{\theta_j}$ at each time instant j, $j = 1, ..., m$.

For a log-normal distribution, the number concentration of particles in a size range $[x,\ x + dx]$ is:

$$N_{tot_j} = f(x;\ \overrightarrow{\theta}) = \frac{N_{tot_j}}{\mu ln\sigma_j\sqrt{2\pi}} exp(-\frac{1}{2}(\frac{lnx - ln\mu_j}{ln\sigma_j}))dx \tag{6.2.4}$$

where N_{tot_j} is the total number of particles at time j, μ_j and σ_j are the mean and standard deviation of the distribution at time instant j, respectively. Thus, for each

time instant j, there are these unknown parameters to determine, and the vector of unknown parameters at the instant j is defined as follows: $\overrightarrow{\theta}_j = (N_{tot_j}, ln\mu_j, ln\sigma_j)$, as in Ramachandran and Kandlikar (1996); Voutilainen and Kaipio (2005). Throughout the rest of this study, *normal* distributions will be considered because it will be based on data from Almeida et al. (1997), who argue for normal size distributions on the particles used in their study. Hence, hereafter $\overrightarrow{\theta}_j = (N_{tot_j}, \mu_j, \sigma_j)$.

Equation (6.2.2) relates the parameters characterising the particle size distribution at instant j to those, characterising it at $j+1$. The equation thus describes the transition $(N_{tot_j}, \mu_j, \sigma_j) \rightarrow (N_{tot_{j+1}}, \mu_{j+1}, \sigma_{j+1})$. In order to find a way to define this transition, a technique to update the decreasing diameters of the particles deterministically, as they dissolve, is needed, i.e. the function $G()$ from Equation (6.2.2). The subject of the following subsection is to discuss ways in which classical diffusion models can contribute to writing the deterministic part of Equation (6.2.2) for the time evolution of the size distribution.

Non-parametric distributions In cases where experimental data are not amenable to modelling by parametric distributions, non-parametric models can also be used to model the size distributions in the case of polydisperse systems. In practice, these distributions are represented by using a discretisation of the range of particle sizes (diameters in this case) in n intervals, as in A. Voutilainen and Kaipio (2001). Each interval is characterised by the minimum, $x_{min,i}$ and maximum, $x_{max,i}$ or by the mean value, $x_i = \frac{x_{max,i} - x_{min,i}}{2}$, where $i = 1...n$. The idea is to associate with each size interval ($x_{min,i}$, $x_{max,i}$), the number of particles in this size range, N_i, or the proportion of particles is this size range, $\frac{N_i}{N_{tot}}$.

It is possible to deduce the parameters of the associated normal or log-normal distributions using definitions for the geometrical mean and variance:

$$\mu = \sum_{i=1}^{n} x_i \frac{N_i}{N_{tot}} \tag{6.2.5}$$

$$\sigma^2 = \sum_{i=1}^{n} (x_i - \mu)^2 \frac{N_i}{N_{tot}}, \tag{6.2.6}$$

6.2.2.2 Dissolution models

Classical dissolution models have proved quite satisfactory when applied to short dissolution periods and equally sized particles (Almeida et al., 1997). Most diffusion models describing the dissolution kinetics for particulate systems are a result of the integration of the Noyes-Whitney equation (Noyes and Whitney, 1897):

$$\frac{dC}{dt} = \frac{D\alpha}{hV}(C - C_S) \tag{6.2.7}$$

where $\frac{dC}{dt}$ is the rate of variation of concentration of solute, C_S is the concentration at saturation, D is the diffusion coefficient, independent of the concentration and normal to the solid surface, α is a shape factor related to the general shape of the particle and h is the thickness of the diffusion layer outside the solid surface (the boundary layer).

The boundary layer is the result of a simple two state model where two types of molecular flux (from the particle surface, along the surface normal, into the bulk and the opposite) are considered. The two types of molecular flux are diffusive (near the surface) and convective (in the bulk liquid) (Rost and Quist (2003); McMahon et al. (2003); Crane et al. (2004a)). The boundary layer thickness at a point varies inversely with the stirring rate. Rost and Quist (2003) considers that, since the boundary layer is a result of a simplification, it's exact thickness is of little interest. References in (Rost 2003) indicate that the boundary layer thickness is in a range

$h \simeq 30 - 60\ \mu m$ under normal stirring conditions. However, recent studies (Crane et al. 2004a; McMahon et al. 2003) show that the boundary layer thickness depends both on the stirring conditions and the shape and size of the solid immersed into a stirred liquid. In the case of the USP apparatus II, as mentioned above, the boundary layer thickness depends strongly on the flow conditions in the apparatus. Some assumptions of the Noyes-Whitney model are:

- fairly intense stirring
- monosized particles
- constant area available for dissolution

A number of models have been obtained by integrating Equation (6.2.7), but the three conditions mentioned are still required for all models deduced.

The following relations give, for a *fixed* number N of very small monosized particles, the *total weight of suspended solids* at the time $j+1$, w_{j+1} :

$$w_{j+1}^{\frac{2}{3}} = w_j^{\frac{2}{3}} - N^{\frac{2}{3}} k\Delta t,\ k = \frac{2D}{3k}\alpha(\frac{6}{\pi\rho})^{\frac{1}{3}} C_S \tag{6.2.8}$$

As the particles are assumed monodisperse, their area, exposed to the dissolution buffer, is directly proportional to a fraction of the weight of the solid: $w^{\frac{2}{3}}$. It was noted (Higuchi and Hiestand, 1963), that the boundary layer is proportional to the particle diameter, especially for quite small particles. Thus $h = kd$ in this particular model, Δt is the time elapsed between two consecutive time points j and $j+1$ and d is the diameter of the particle (other parameters are defined as for Equation (6.2.7)).

For larger particles, the following equations were found to be more suitable:

$$w_{j+1}^{\frac{1}{3}} = w_j^{\frac{1}{3}} - N^{\frac{1}{3}} k\Delta t,\ k = \frac{2D}{3hx_{crit}}\alpha(\frac{6}{\pi\rho})^{\frac{2}{3}} C_S \tag{6.2.9}$$

In this model, h is considered constant, thus approximately independent of the particle size. x_{crit} is the critical diameter. The model given by Equation 6.2.9 can

be applied for particles larger than this critical value.

Simulations based on models, where the surface exposed to the dissolution medium does not vary with time, give good agreement with experimental data, but only for short time periods, corresponding to the beginning of the dissolution process. Simoes et al. (1996*b*) clearly indicate that truly monosized systems do not exist in practice and rules, which account for the polydisperse nature of the real powders, have to be followed.

In order to satisfy the three conditions under which the diffusion model can be applied (intense stirring, monosized particles, constant surface area), time discretisation and a split of the particle size distribution in classes can be performed. Equations (6.2.8) and (6.2.9) can be applied to each size class at each time point, as in Almeida et al. (1997). After each time interval, a new value of x_i can be computed:

$$x_{new,i} = (\frac{6\omega_{t+\Delta t,i}}{\rho N_i \pi})^{\frac{1}{3}} \tag{6.2.10}$$

For each time step, it is thus possible to analyse the initial distribution, and for each size class, to apply the diameter updating equation (6.2.10) as $G(\overrightarrow{\theta_j})$, beginning with the upper range of diameter values. If $x_{new,i} < x_{min,i}$, then a number of particles, N_i, is discarded from the class i and assigned to another size class, or completely discarded from the system if the particles are too small.

Because of fluctuations in the hydrodynamics in the apparatus, this updating may not reflect particularly well the exact way in which the particles pass through different size classes. As stated earlier, this is one of the reasons why the stochastic term $\overrightarrow{v}_t$ is being used in Equation 6.2.2.

With the newly-obtained distribution, Equations (6.2.5) and (6.2.6) can be used to calculate the following new vector of parameters:

$$\overrightarrow{\theta}_{new,j} = (N_{newtot_j}, \mu_{new,j}, \sigma_{new,j}) = G(\overrightarrow{\theta_j})$$

The following transition probability from one state of the system to the another, is also refereed to as *transition kernel*, i.e. a "probability distribution"-oriented interpretation of Equation (6.2.2):

$$P(\overrightarrow{\theta}_{j+1}|\overrightarrow{\theta_j}) = N(G(\overrightarrow{\theta}_{j+1}), \Gamma_j) \tag{6.2.11}$$

$$\Gamma_j = \begin{pmatrix} \gamma^2_{Ntot_j} & 0 & 0 \\ 0 & \gamma^2_{\mu_j} & 0 \\ 0 & 0 & \gamma^2_{\sigma_j} \end{pmatrix} \tag{6.2.12}$$

It represents the probability distribution of the vector of parameters $\overrightarrow{\theta}_{j+1}$, given the value of $\overrightarrow{\theta_j}$. The matrix Γ_j represents the noise term v_t from Equation 6.2.2. In order to obtain the probability distribution for $\overrightarrow{\theta}_{j+1}$ one has to solve Equation (6.2.11), which is far from being a trivial task, (Meyer and Millar, 1999b; Voutilainen and Kaipio, 2005). Examples of techniques to solve it are sampling the joint distribution given by Equation (6.2.11), using a Monte Carlo Technique like the Gibbs Sampler or Particle Filtering, ((Mosegaard and Sambridge, 2002; Meyer and Millar, 1999b; Voutilainen and Kaipio, 2005).

6.2.3 Particle Filtering

As mentioned in Chapter 3, *particle filtering* is a Sequential Monte Carlo method, for sampling from a sequence of probability distributions. Here, particle filtering is adapted for our specific drug dissolution problem.

Equation (3.4.1) can be developed in the following way:

$$P_{post}(\overrightarrow{\theta_j}|y_{1:j}) = \frac{L(y_j|\overrightarrow{\theta_j})P(\overrightarrow{\theta_j}|y_{1:j-1})P(y_{1:j-1})}{P(y_{1:j}|y_{1:j-1})P(y_{1:j-1})} = \frac{L(y_j|\overrightarrow{\theta_j})P(\overrightarrow{\theta_j}|y_{1:j-1})}{P(y_{1:j}|y_{1:j-1})}$$

$$\sim P(y_j|\overrightarrow{\theta_j})P(\overrightarrow{\theta_j}|y_{1:j-1}) \tag{6.2.13}$$

$$P(\theta_j|y_{1:j-1}) = \int P(\overrightarrow{\theta_j}|\overrightarrow{\theta}_{j-1})P(\overrightarrow{\theta}_{j-1}|y_{1:j-1})\mathrm{d}\overrightarrow{\theta}_{j-1} \tag{6.2.14}$$

The probability of the state parameters at time j or the *proposal density* is given by Equation (6.2.14), where the probability of the current state is driven according to a family of independent events which are all possible: $\overrightarrow{\theta}_{j-1}$, or all possible previous states and $P(\overrightarrow{\theta}_{j-1}|y_{1:j-1})$ is the posterior probability at step $j-1$. As solving Equation (6.2.13) is a multidimensional integration problem, Monte Carlo techniques can again be used.

The distribution $P(\overrightarrow{\theta}_{j-1}|y_{1:j-1})$ can be represented by a rich sample, which approximates it. Suppose such a sample is available, and let $\{\overrightarrow{\theta}^{(k)}_{j-1},\ k = 1, ..., p\}$ be such a sample from the marginal distributions $p(\overrightarrow{\theta}_{j-1}|y_{1:j-1})$ [2]. Using the evolution density, a sample $\{\overrightarrow{\theta}^{k}_{j}\}$ can be obtained. If $\overrightarrow{\theta}^{k}_{j-1}$ is one member of the sample $\{\overrightarrow{\theta}^{k}_{j-1},\ k = 1, ..., m\}$, then we first compute the corresponding values of $w^k_{t+\Delta t,i}$, then update the corresponding particle size distribution and use the evolution density $P(\overrightarrow{\theta}_j|\overrightarrow{\theta}^{k}_{j-1})$ in order to generate a new value for $\overrightarrow{\theta}^{k}_{j}$, as described in the previous section. To summarise:

$$\overrightarrow{\theta}^{k}_{j-1} \rightarrow w^k_{t+\Delta t,j-1} \rightarrow G^k(\overrightarrow{\theta}_{j-1}) \rightarrow \textit{transition kernel} \rightarrow \overrightarrow{\theta}^{k}_{j} \rightarrow w^k_{t+\Delta t,j} \tag{6.2.15}$$

Having generated the new sample, we approximate $P(\overrightarrow{\theta}^{k}_{j1:j})$:

[2] We consider the distribution of $N_{tot_{j-1}}$,μ_{j-1} and σ_{j-1} (and as the remainder of the chapter will show, possibly other parameters) which are *jointly distributed* random variables. The marginal distribution of one of the members of the vector $\overrightarrow{\theta}_{j-1}$ is the probability distribution of , say $N_{tot_{j-1}}$, ignoring information about the other members of the vector, such as $\mu_{j-1}$and σ_{j-1} A marginal distribution would be theoretically calculated by summing or integrating the joint probability distribution over $\mu_{j-1}$and σ_{j-1}.

$$P(\overrightarrow{\theta}^k_j|y_{1:j}) = \frac{L(y_j|\overrightarrow{\theta}^k_j)}{\sum_{k=1}^{p} L(y_j|\overrightarrow{\theta}^{(k)}_j)} \tag{6.2.16}$$

The likelihood for each member of the sample is calculated according to Equation (6.2.3) where

$$F(\overrightarrow{\theta}^k_j) = \sum_{i=1}^{n} w^k_{t+\Delta t,j,(i)} \tag{6.2.17}$$

This represents the total quantity of mass transferred into the solution at time step j, given the size distribution $\overrightarrow{\theta}_j$ for all size classes i and the dissolution model defined by the Equations (6.2.8) and (6.2.9).

So, at the end of one step, an array containing the couples $\{\overrightarrow{\theta}^k_j,\ P(\overrightarrow{\theta}^k_{j\,1:j})\}$ is available. This can be used to draw the marginal probability distributions for each element (for the next step) in the vector $\overrightarrow{\theta}^k_j$ and to compute:

- The maximum likelihood estimate, given by the mode of the obtained posterior distribution.
- The minimum variance Bayes estimate or the minimum *a posteriori* estimate:

$$\hat{\theta}_j = \sum_{k=1}^{p} (\overrightarrow{\theta}^k_j P(\overrightarrow{\theta}^k_{j\,1:j})) \tag{6.2.18}$$

The standard deviation of the expected value is given by:

$$\hat{s}_{\overrightarrow{\theta}_j} = \sum_{k=1}^{p} ((\overrightarrow{\theta}_j^k - \hat{\theta}_j)^2 P(\overrightarrow{\theta}|_j^k y_{1:j})) \tag{6.2.19}$$

6.3 Data

Situations for which inverse modelling is suitable vary from case to case. In the absence of real and complete dissolution data, it was decided to simulate a dissolution experiment and to use the results for testing/validating the modelling technique presented for reconstruction of unobserved data.

Subsection 6.2.2.2 presented the deterministic theory suggested in Almeida et al. (1997) to model dissolution in a particulate system, by updating the particle size distribution as the particles dissolve. Almeida et al. (1997) used the Coulter multisizer experimental technique to count and size the particles from the powders used. The results showed fairly normal distributions of the particle sizes. The methodology proposed to describe the dissolution of these powders, uses the experimentally-determined characteristics of the drug and takes into account the polydisperse nature of the powder.

As the size distributions experimentally-determined are not available, the Almeida et al. method was used to generate the data for the validation of the proposed inverse theory. As real distributions of ibuprofen particles were found to be normally distributed, the size distribution is kept normal in the direct simulation. The generated normal distributions are discretised: the numbers of particles are recorded for each interval Δx of the size range.

6.3.1 Inputs and outputs

The direct simulation needs as input the following parameters:

- the mean of the initial distribution, μ_0

- the standard deviation of the initial distribution, σ_0
- the total number of particles from the initial distribution, N_{tot0}
- the range of the distribution
- the length of the intervals Δx for the discretisation of the distributions
- the total time of simulation, t_{tot}
- time interval for the time discretisation, Δt_{direct}
- time interval for sampling the parameters, $\Delta t_{sampling}$

The outcomes are four vectors available to the user:

Simulation of observed data:

- the weight of the solid mass in the solvent at each $\Delta t_{sampling}$: $y(t) = (y_1, ..., y_k, ..., y_p)$.

Simulation of unobserved data:

- the means of the distributions at each $\Delta t_{sampling}$: $\mu(t) = (\mu_1, ..., \mu_k, ..., \mu_p)$
- the standard deviations of the distributions at each $\Delta t_{sampling}$: $\sigma(t) = (\sigma_1, ..., \sigma_k, ..., \sigma_p)$ - unobserved.
- the total number of particles in the solvent at each $\Delta t_{sampling}$: $N_{tot}(t) = (N_{tot\,1}..., N_{tot\,k}, ..., N_{tot\,p})$ - unobserved.

6.3.2 Data generation

To generate the data, the initial distribution of particles is generated first, using μ_0, σ_0 and $N_{tot\,0}$. Figure 6.3 shows two examples of initial distribution of the particle size. The orange solid circles, in Figures 6.3, (a) and (b), show the initial distribution

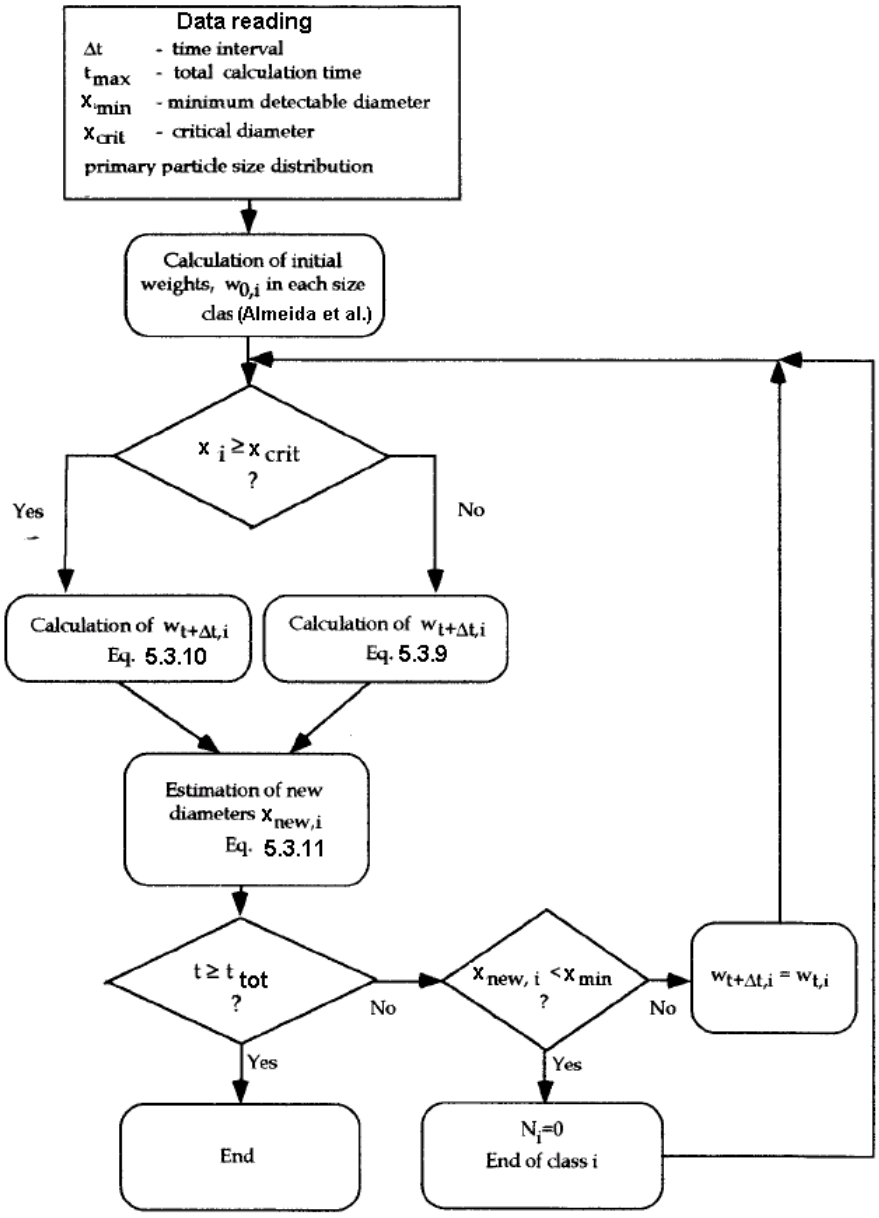

Figure 6.2: Flowchart of the algorithm used to generate the initial data. Adapted from Almeida et al. (1997).

of particles with μ_0=25 μm, $\sigma_0 = 10$ and $N_{tot\,0} = 2 \times 10^6$. Figures 6.3, (c) and (d) show, in orange solid circles as well, the initial distribution with μ_0= 45 μm, $\sigma_0 = 10$ and $N_{tot0} = 10^6$. Each size class, defined by $(x_{min,i}, x_{max,i})$, contains a number of particles N_i. The flowchart in Figure 6.2 summarises the algorithm used in the data generation.

After the initial distribution is generated, the weight of each of these size classes is calculated using formulas proposed by Almeida et al.:

$$w_{0,i} = N_i \rho \frac{\pi(x_{max,i} - x_{min,i})/2}{6} \tag{6.3.1}$$

where N_i is the number of particles in class i, ρ is the density and $x_{max,i} - x_{min,i}$ is the diameter of the particles from the class i.

Once the initial weights of each class are available, Equations (6.2.8) and (6.2.9) are used to update the weights as a function of $\triangle t_{direct}$, the previous weights, the diameters, the number N_i of particles in each size class, the density of the solid ρ, the diffusion coefficient D, the thickness of the diffusion layer h and the shape factor α.

After the updated weights in each size class are calculated, Equation (6.2.10) is used for updating the diameters in each size class. If the updated diameters do not belong to their previous size class any more, a corresponding swap of class follows. If the updated diameters are smaller than a critical value, the particles are considered as dissolved. In this way, both the weights of each size class and the shape of the histogram have undergone modification corresponding to Δt_{direct} and the system is ready to be re-updated at a new increment of the time counter.

Figure 6.4 shows two **examples** of generated data sets. Table 6.1 summarises the input parameters used for generating the data sets. The difference between them depends on the input value for Δt_{direct}. Ten different simulations have been performed with the same inputs, but with different seeds for the random number generator, which was used in the method for generating the initial distribution. The

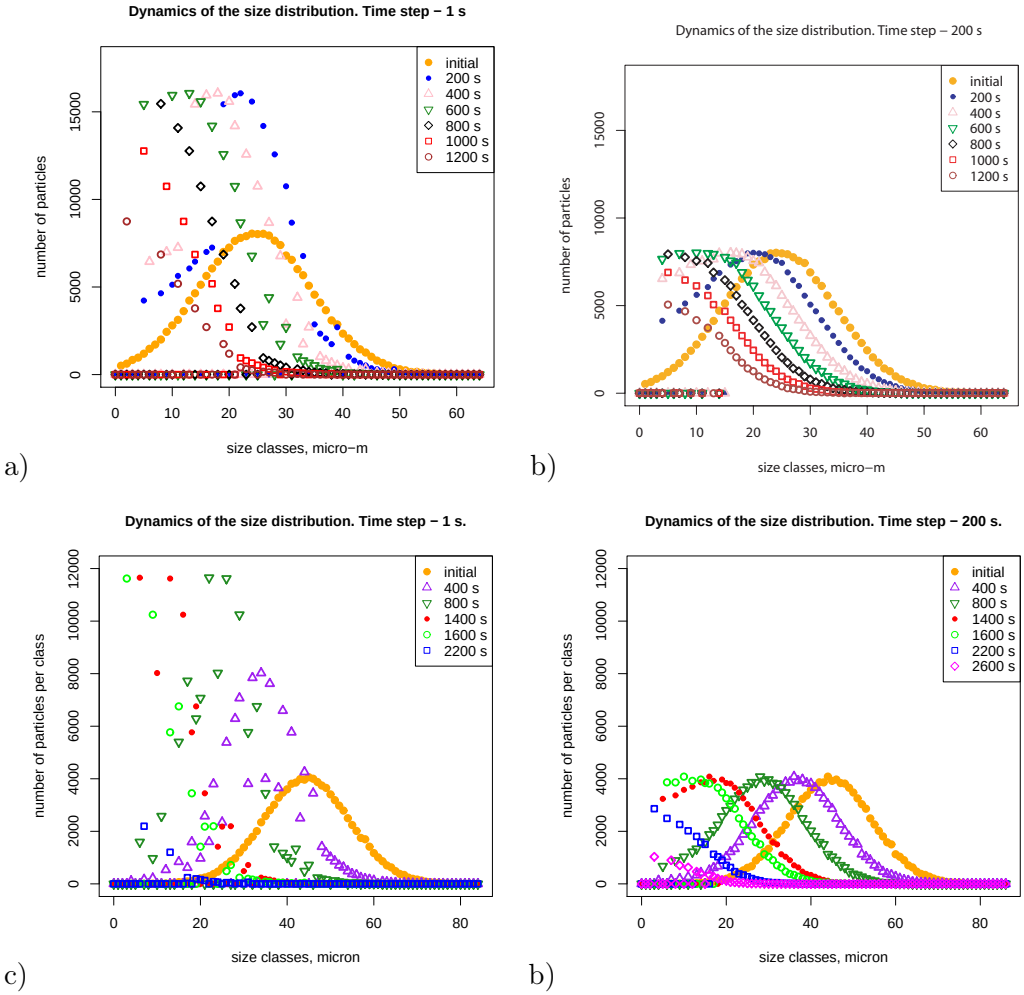

Figure 6.3: Dynamics of the size distribution.
a) $\mu_0 = 25\mu m$, updating each Δt_{direct}=1s.
b) $\mu_0 = 25\mu m$, updating each Δt_{direct}=200s.
c) $\mu_0 = 45\mu m$, updating each Δt_{direct}=1s.
d) $\mu_0 = 45\mu m$, updating each Δt_{direct}=200s.

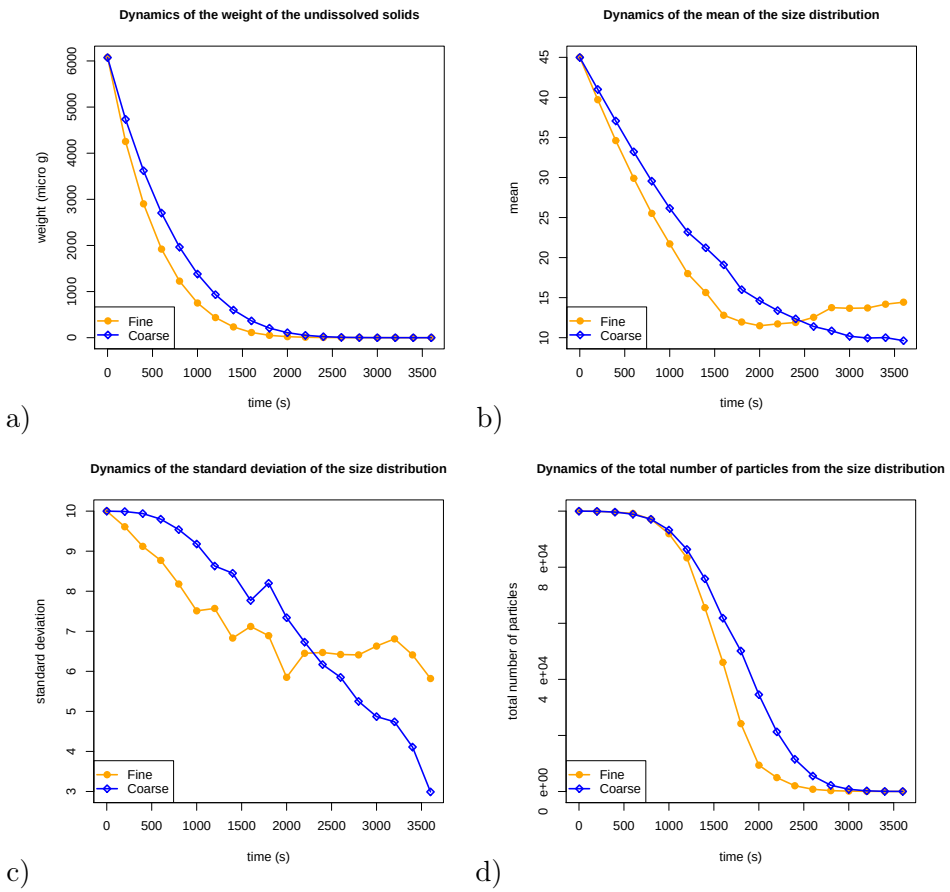

Figure 6.4: Two data sets obtained by simulation with the input parameters indicated in Table 6.1. The fine data set corresponds to $\Delta t_{direct} = 1$s and the coarse data set corresponds to $\Delta t_{direct} = 200$s.

N_{tot0}	μ_0 (μm)	σ_0	$t_{tot}(s)$	$\Delta t_{direct}(s)$	$\Delta x(\mu m)$	$t_{sampling}$
100000	45	10	3600	1 and 200	1	200 in both cases

Table 6.1: Inputs for the direct simulation.

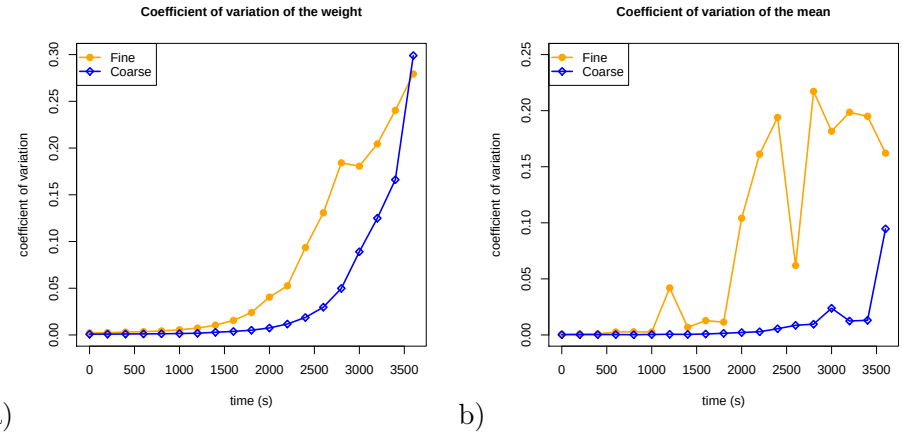

a) b)

Figure 6.5: Coefficient of variation for a) the weight of the particles b) the mean of the size distribution.

curves represented in Figure 6.4 are obtained by computing the averages for the four output parameters: the weight of the solid $w(t)$, the mean of the distribution $\mu(t)$, the standard deviation of the distribution $\sigma(t)$ and the total number of particles in the distribution $N_{tot}(t)$. The variability of the generated data, related to the initial histogram, is much reduced, in comparison with the means of the values, as shown by the coefficients of variation [3] illustrated on the Figure 6.5.

6.3.3 Discussion

6.3.3.1 Data structure

As indicated in Table 6.1, the sampling is done, in both directly simulated data sets, at a sampling interval $t_{sampling}$= 200 s. As seen in Figure 6.4, there is a difference between the data simulated using a small time step (referred to as *fine-grained direct simulation*) and the data obtained using a larger one (referred to as *coarse-grained*

[3] Coefficient of variation cv is a measure of dispersion of a probability distribution. It is defined as the ratio of the standard deviation σ to the mean μ.

direct simulation). In the case of fine step simulations the same number of particles dissolves more quickly. In addition, the fine step simulations show more variability in the tails of the distribution compared to the coarse step simulations. The remainder of this section first discusses the structure of the data, giving some interpretations of its dynamic behaviour and then concludes how can it be used for verifying the inverse algorithm.

The fine simulations therefore seem to represent more exactly what happens in the solution. In the algorithm for the generation of the direct data, (presented in the previous section, at every time step Δt_{direct}), the new weight for each size group of particles is computed. Two cases can occur for group i:

1. $w_{t+1} > 0$. Based on this, the new diameter is established and N_i particles are moved, if the case, to the corresponding size group. This case is most likely to occur when Δt_{direct} is small enough, and the N_i particles are large enough not to completely dissolve during this value of Δt_{direct}.

2. $w_{t+1} = 0$. This means that N_i particles have dissolved completely during Δt_{direct}. In this case, all of the particles are directly discarded from the system. The problem of large Δt is that this situation occurs very often and, as a result, the system is solving *more slowly*.

In fine step simulations, case 1 mostly applies. Most particles, especially large ones, smoothly move from class to class until they are discarded. Conversely, when a large time step is used, in the case of coarse step simulations, case 2 occurs more often. For example, size class i contains N_i=15 particles which can dissolve in 50 s. With Δt_{direct}=1 s, the particles dissolve completely only by passing from class to class, over 50 s. However, with time step Δt=200 s the particles lose their weight instantly without traveling through size classes and the rest of the time left in this time step nothing more happens.

This implies that, if one computes the weights using a coarser algorithm, *accu-*

mulation of error is inevitable. Figure 6.4 shows the dissolution profiles in coarse and in fine simulations. The fluctuations of the μ at tail end of the fine step simulation is probably due to the small number of size classes remaining populated at the end of the dissolution. In Figure 6.3, which illustrates how the shape of the distribution changes over the time, it can be seen that, especially at the end of the dissolution, fine step simulations tend to have fewer populated size classes then coarse step simulations. In simulations where Δt_{direct}=1 s, size distributions tend to organise themselves into fewer classes than when simulating with coarser time steps. In fact the distributions obtained with fine and coarse time steps are almost equivalent, but coarse simulations supress the detailed picture. The difference is that size distributions from coarse step simulations tend to organise into more classes.

Figure 6.6 shows how the number of populated classes varies with the time as a function of the chosen Δt_{direct}.

The distributions generated with fine time steps are closer to the real data because they satisfy the conditions[4] for which the Equations (6.2.8) and (6.2.9), used in the algorithm, apply, (Subsection 6.2.2.2 and Almeida et al. 1997). However, the fact that for $\Delta t_{direct} = 1$ s the distributions are not well defined, with fewer populated size classes, argues for the fact that the simulated data which are closest to the real data are probably those with $3\,s < \Delta t < 10\,s$.

In addition, Figure 6.3 illustrates how the distributions switch from being normal to disordered at the end of the dissolution, as the number of unpopulated classes increase. Correspondingly, sampling from a normal distribution at all dissolution times while performing inverse simulations will affect the quality of the reconstruction.

6.3.3.2 Implications for inverse simulations

In inverse simulations, comparison needs to be made with observed data (y_j) at every $\Delta t_{inverse}$, whether the (y_j) are either directly simulated or experimental results.

[4] constant area available for dissolution is assured by the small time steps in the simulation

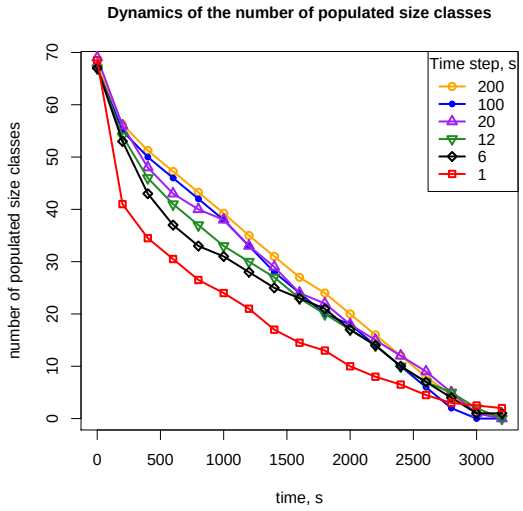

Figure 6.6: Number of populated classes of the size distribution as a function of time and the time step used for the simulation.

Consequently $\Delta t_{inverse}$ is dictated by available experimental Δt. In real experiments these data are collected at quite sparse time intervals. For example, in Almeida et al., data on the state of the system is collected every 100 or 200 s. The time step of experimental data collection implies that the likelihood can be evaluated only at those time points, where data are available to perform computation. For this reason this work supplements sparse experimental points by using directly simulated data and Δt_{direct} is input by the user.

As discussed above, it is better to generate this data (y_t) with rather small Δt_{direct}, as $\Delta t_{direct}>$ 10 s is shown to generate error-prone results. In contrast, for inverse simulations, distributions are re-updated and re-sampled at $\Delta t_{inverse}$ which is quite large, meaning that the model definitely accumulates error. This error is part of the error v_t (Equation 6.2.2), related to the validity of the evolution model $G(t)$.

The target here is to check if the inverse simulation will permit reconstruction of the original, fine-step generated unknown parameters.

6.4 Modelling

6.4.1 Adapting the Particle Filtering algorithm to the problem

Subsection 6.2.3 presented the theoretical premises for inverse Monte Carlo sampling. It has been shown how a dissolution problem can be put into a Bayesian framework and how it's dynamic part can be handled through a "transition kernel". The target of Bayesian analysis is to determine the posterior probability distribution $P_{post}(\overrightarrow{\theta}|y)$, w (the probability distribution of the parameters of interest given the model and the observed data). It has also been shown that $P_{post}(\overrightarrow{\theta}\,|\overrightarrow{y})$ can be written as a product (Equation 6.2.13) of the likelihood density $P(y_j|\overrightarrow{\theta}_j)$ and the *prediction density* $P(\overrightarrow{\theta}_j|\overrightarrow{y}_{1:j-1})$, of the set of parameters $\overrightarrow{\theta}$ at time point j, given previous experimental data $\overrightarrow{y}_{1:j-1}$. This distribution is also referred to as the *prior distribution* at each time step j. In most cases it is not possible to analytically solve the stochastic Equation (3.4.1) (Meyer and Christensen, 2000*b*; Voutilainen and Kaipio, 2005), and this is why various sampling techniques have been developed and applied (for review on various sampling techniques see Mosegaard and Sambridge, 2002). For example, one could employ a basic importance resampling (SIR) filter (Mosegaard and Sambridge, 2002) so that the prediction density $P(\overrightarrow{\theta_j}|y_{1:j-1})$ is first sampled and the likelihood density $P(y_j|\overrightarrow{\theta_j})$ is then evaluated at each sample to obtain importance weights (Voutilainen and Kaipio, 2005), which are a measure of the likelihood of the given sample. Figure 6.7 summarises the process described in this subsection.

In order to avoid evaluating the likelihood density at each sampled point and getting trapped in the neighbourhood of local maxima of the likelihood distribution, an alternative way of performing the computations has been presented in Subsection 6.2.3. The remainder of this subsection summarises the way in which particle filtering was applied in the algorithm written for this study.

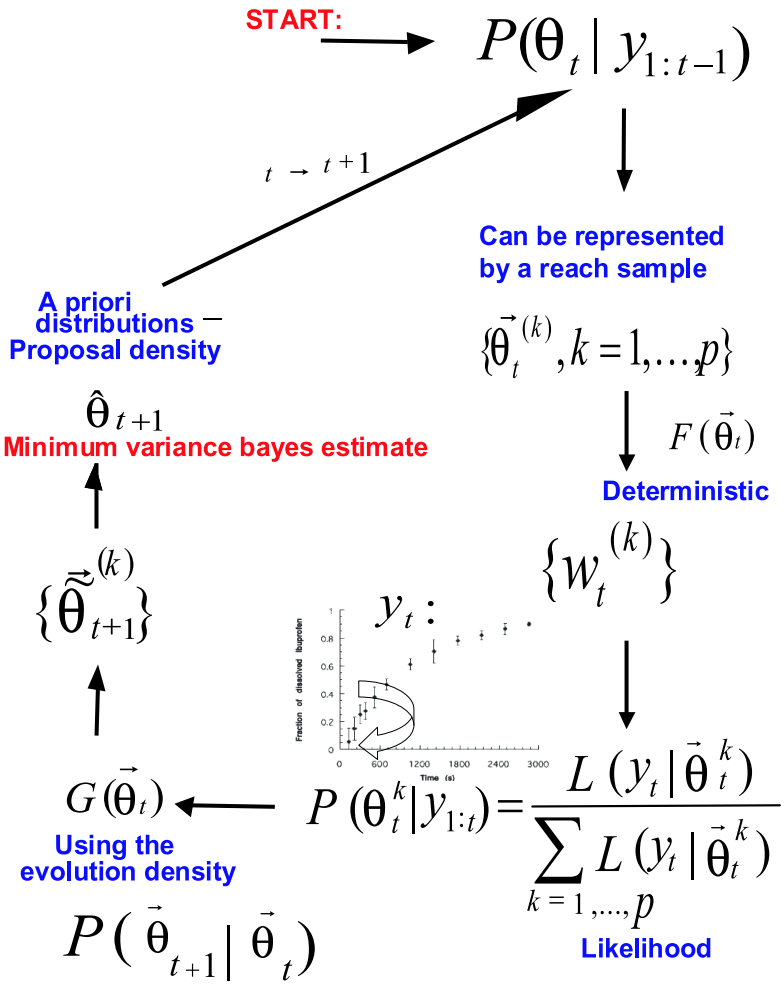

Figure 6.7: Diagram summarising the particle filtering process used in this chapter.

Assuming that:

$$\{ \overrightarrow{\theta}_j^{(k)},\ k = 1, ..., p\} \tag{6.4.1}$$

is a sample from the marginal filtering density $P(\theta_j|y_{1:j-1})$, a population of size p of quadruplets of the parameters of interest $(N_{tot_j}^k, \mu_j^k, \sigma_j^k, \alpha_j^k),\ k = 1, ..., p$ is then available. The parameter α is the shape factor, (discussed in detail in the following subsection). Each quadruplet defines a possible discrete particle size distribution at time j. These size distributions will be further referred to as "histograms", to avoid confusion with the probability distributions for parameters discussed in this section.

For each histogram from the population, k, the theoretical weight w_j^k (given by Equation (6.2.17)) at time j is computed. In comparing w_j^k to y_j, given by the experimental points, an *importance weight* ω_j^k (*omega*) is assigned to each sample $\overrightarrow{\theta_j^k}$, using the normal likelihood density, defined in Equation (6.2.3) and Equation (6.2.16). The minimum variance Bayes estimate is given by the expectation of the posterior density function (joint filtering density), $P(\overrightarrow{\theta_j}|y_{1:j})$, which can be approximated by a weighted sum of the samples, Equation (6.2.18) , i.e:

$$\hat{\theta}_j = \sum_{k=1}^{p} \overrightarrow{\theta_j^k}\omega_j^k \tag{6.4.2}$$

The sample $(\overrightarrow{\theta}_j^{(k)})$ from the marginal prediction densities $P(\overrightarrow{\theta}_j|\overrightarrow{y}_{1:j})$ is used to generate a sample $(\overrightarrow{\tilde{\theta}}_{j+1}^{(k)})$ from the *prior* prediction density at the next time step $P(\overrightarrow{\theta}_{j+1}|y_{1:j})$, using the deterministic part defined by the Equations (6.2.8), (6.2.9) and (6.2.10) and the *transition kernel* defined by a modified form of Equation (6.2.11):

$$P(\overrightarrow{\theta}_{j+1}|\overrightarrow{\theta}_j) = N(\hat{\theta}_{j+1}, \Gamma_{j+1}) \tag{6.4.3}$$

where $\hat{\theta}_{j+1}$ is the minimum variance Bayes estimate for the sample $(\overrightarrow{\tilde{\theta}}_{j+1}^{(k)})$ and

Γ_{j+1} are some conveniently chosen standard deviation values. Now the loop is closed because a new sample, given in Equation (6.4.1) for time $j+1$ is obtained by sampling from Equation (6.4.3).

6.4.2 Shape factor

The shape factor α features in both Equations (6.2.8) and (6.2.9), and is needed to calculate the evolution of the weight of the particulate system over time. It is normally an unknown constant parameter and the inverse simulation will be used to estimate the distribution of its most probable values.

At the beginning of the simulation, the shape factor is sampled from a uniform distribution. The difference between this parameter and other estimated parameters is that it does not undergo any modification by transition to the following step, i.e. in the next time step it can be sampled from the same uniform distribution as initially, or from a normal distribution centred on the previous estimate. The uniform distribution leads to the most conservative estimate of uncertainty; i.e., it gives the largest standard deviation. The value of the shape factor, obtained (Almeida et al., 1997) by fitting simulated data to experimental points, is found to be α=4.1.

6.4.3 Credibility intervals

In a Bayesian framework, *credibility intervals* are the equivalent of confidence intervals in normal inference. Finding a $100(1-\beta)\%$ credibility interval means finding an interval of the form $(\overrightarrow{\theta_a}, \overrightarrow{\theta_b})$ such that:

$$\int_{\overrightarrow{\theta_a}}^{\overrightarrow{\theta_b}} p_{post}(\overrightarrow{\theta}\,|\,\overrightarrow{y})d\theta = 1-\beta, \tag{6.4.4}$$

where β is small, usually chosen such that there is at least 95% probability of the estimated parameters being in the intervals $(\overrightarrow{\theta}_a, \overrightarrow{\theta}_b)$. Suppose the unknown (posterior) distribution is $N(mean, stdev)$, with known $stdev$ and the prior distribution is

$N(mean_0, stdev_0)$. In order to find out the credibility interval, an independently and identically distributed sample, $(\overrightarrow{\theta^1}, ..., \overrightarrow{\theta^p})$ from $N(mean_0, stdev_0)$ has to be available.

In this context, the posterior distribution for the *mean* is, (Small, 2006):

$$N\left(\frac{\frac{mean_0}{stdev_0^2} + \frac{p\bar{\theta}}{stdev^2}}{\frac{p}{stdev^2} + \frac{1}{stdev_0^2}}, \frac{1}{\frac{p}{stdev^2} + \frac{1}{stdev_0^2}}\right) \tag{6.4.5}$$

where $\bar{\theta}$ is the average the sample $(\overrightarrow{\theta^1}, ..., \overrightarrow{\theta^p})$ and the 95% credibility interval for the *mean* is, (Small, 2006):

$$\frac{\frac{mean_0}{stdev_0^2} + \frac{p\bar{\theta}}{stdev^2}}{\frac{p}{stdev^2} + \frac{1}{stdev_0^2}} \pm 1.96\left(\frac{p}{stdev^2} + \frac{1}{stdev_0^2}\right)^{\frac{1}{2}} \tag{6.4.6}$$

In the context of the present model, samples from the posterior distribution $P_{post}(\overrightarrow{\theta}|y)$ are not directly available. This distribution is sampled using the following distribution $P(\overrightarrow{\theta_{j+1}}|\overrightarrow{\theta_j}) = N(\hat{\theta}_{j+1}, \Gamma_{j+1})$. In addition, a particle filtering technique is used to compute the minimum variance Bayes estimates $\hat{\theta}_j$ (Equation (6.2.18)) and its standard deviation $\hat{s}$ (Equation (6.2.19)), using the weights evaluated for the previous sample. Then, the interval $(\overrightarrow{\theta^1}, ..., \overrightarrow{\theta^p})$ consists of a single value which is $\hat{\theta}_j$. $mean_{prior}$ is used to designate the mean of the prior distribution for sampling at the given step, thus $mean_{prior} = mean_0$. In this case Equation (6.4.6) becomes:

$$\frac{\frac{mean_{prior}}{\gamma^2} + \frac{\hat{\theta_j}}{\hat{s_j}}}{\frac{1}{\hat{s_j}} + \frac{1}{\overrightarrow{\gamma}^2_{j+1}}} \pm 1.96\left(\frac{1}{\frac{1}{\overrightarrow{\gamma}^2_{j+1}} + \frac{1}{\hat{s_j}}}\right)^{\frac{1}{2}} \tag{6.4.7}$$

where $\hat{s_j}$ is the standard deviation for the minimum Bayes estimate and $\overrightarrow{\gamma^2_{j+1}}$ is the standard deviation of the prior distributions, (the values from the diagonal of the matrix Γ_{j+1}).

6.4.4 Results and Discussion

This section shows results from the implementation in C++ of the material presented above. First, the choice and influence of the prior distributions for the parameters are discussed, the likelihood distribution is introduced, then the effect of the size of the sample populations chosen to perform the inverse simulations is analysed. Results, obtained with directly simulated data obtained using both fine and coarse time steps are then presented. At the end of the section, the obtained results on the credibility intervals, together with the distributions for the parameters, are illustrated.

In the following reconstructions, based on inverse simulations, the sampling time step was chosen at $\Delta t_{inverse}$=200 s (see Subsection 6.3.3.2), while the sampling time step used in the directly simulated data for the prior distribution, $\Delta t_{direct} = 1$s (fine-grained time step) and the number of samples $p = 2000$, unless otherwise specified in the text.

6.4.4.1 Effect of the prior distributions

From Section 6.4.1, the transition from one step to another is achieved by using the transition kernel, and is described by the expression: $P(\overrightarrow{\theta}_{j+1}|\overrightarrow{\theta_j}) = N(\hat{\theta}_{j+1}, \Gamma_{j+1})$ (Equation 6.4.3). This equation describes how each of the parameters is sampled, at a new time, by first performing a deterministic dissolution step (Equations (6.2.8), (6.2.9) and (6.2.10)), based on the parameters sampled at the previous step and their *weights*, (obtained using a normal likelihood distribution, specified in Equation (6.2.17) and discussed in Section 6.4.4.2) and finally, by calculating and *applying* the minimum Bayes estimate (Figure 6.7). In the first step, initial distributions for the four parameters need to be specified. Table 6.2 shows the prior distributions used to obtain the results shown in the following sections.

To avoid confusion with values from the other sections, $mean_{prior}$ is the mean of the prior distribution for sampling at the given step, (the four values of the vector $\hat{\theta}_{j+1}$), γ's are the standard deviation of this distribution (figuring on the diagonal of

Parameter	Distribution	$mean_{prior}$	γ	min	max
N_{tot_0}	Normal	100000	100	90000	110000
μ_0	Normal	45	2	0	47
σ_0	Normal	10	1	8	12
α	Uniform	NA	NA	1	7

Table 6.2: Initial prior distributions for the parameters $\overrightarrow{\theta}_0$.

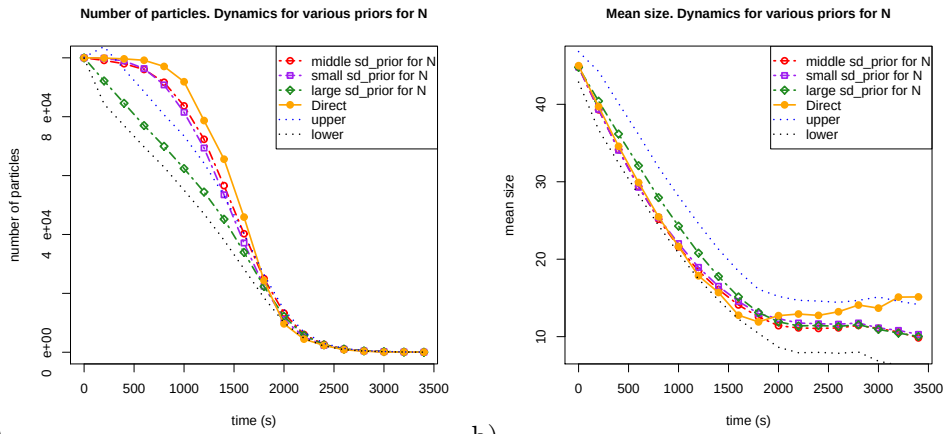

a) b)

Figure 6.8: Effect of the prior distributions on the total number of particles N_{tot}.

the matrix Γ_{j+1}: $\gamma_{N_{tot_j}}$, γ_{μ_j}, γ_{σ_j} and γ_{α_j}) and min and max are the minimum and the maximum limits of the distributions (in the case where they are truncated).

Table 6.3 specifies the prior distributions used for all following steps of the simulation. They have been chosen, based on the structure of the data and on best-performance basis as well. In the case of the parameter N_{tot}, the standard deviation of its prior distribution is chosen to be directly proportional to its predicted value, because throughout the dissolution process, this parameter spans a very large range of values. In the case of the other parameters, their standard deviation γ_{j+1} can also be set proportional to the value of the predicted values $\hat{\theta}_{j+1}$. However, in comparison to N_{tot}, these do not take a large range of values, so constant values for γ_{j+1} have been chosen, based on the mean values.

Figure 6.8 shows the effect of different priors for the parameter N_{tot}, characterised by their different standard deviations, in the inverse simulation. As shown in

Parameter	Distribution	$mean_{prior\,j+1}$	γ_{j+1}	min_{j+1}	max_{j+1}
$N_{tot_{j+1}}$	Normal	$\hat{N}_{tot_{j+1}}$	$0.001\times\hat{N}_{tot_{j+1}}$	0	$\hat{N}_{tot_{j+1}}$
μ_{j+1}	Normal	$\hat{\mu}_{j+1}$	3	0	45
σ_{j+1}	Normal	$\hat{\sigma}_{j+1}$	3	$0.5\times\hat{\sigma}_{j+1}$	15
α_{j+1}	Normal	$\hat{\alpha}$	3	0	10

Table 6.3: Initial prior distributions for the parameters $\overrightarrow{\theta}_{j+1}$.

	Case 1	Case 2	Case 3
$\gamma_{Ntot_{j+1}}$	$0.001 \times \hat{N}_{totj+1}$	$0.01 \times \hat{N}_{totj+1}$	$0.1 \times \hat{N}_{totj+1}$
Label on Fig. 6.8	small	middle	large
Quality of fit to the data	good	best	poor

Table 6.4: Three cases of marginal prior distribution for N_{tot}.

Table 6.4, the prior chosen for Case1 has the smallest value among the three cases examined: $\gamma_{Ntot_{j+1}} = 0.001 \times \hat{N}_{totj+1}$. In Figure 6.8, (a) it can actually be seen that Case2 tends to perform better than Case 1, yielding a result which is the closest to the direct N_{tot} profile. However, as the overlapping credibility intervals of the Case 1 and Case 2 experiments show, these are not significantly different. On the other hand, Case 3 demonstrates that when the prior for N_{tot} becomes too general, this produces a too rapid decrease of the value of the parameter N_{tot} over time, Figure 6.8, (a). The credibility intervals shown in Figure 6.8 are those obtained for this last experiment and it can be seen that the direct N_{tot} profile is outside these intervals. The wrong direction for reconstruction, as illustrated on Figure 6.9 (left-hand side), is "fuelled" by picking smaller N_{tot} in combination with larger values for the mean μ of the size distributions, Figure 6.8, (b). Thus, a "loose" prior distribution for N_{tot} conditions a good reconstruction of the evolution profile of the "observed" weights y_j in the system, but does not reconstruct correctly the distributions of more problematic parameters like those included in the vector $\overrightarrow{\theta_j}$.

6.4.4.2 The likelihood distribution

As mentioned earlier, at each step of the inverse simulations, the marginal conditional distributions (for the parameters included in the vector $\overrightarrow{\theta_j}$) are sampled and the likelihood distribution is used in conjunction with sample values in order to obtain importance weights, (Equations (6.2.3), (6.2.17) and (6.2.16) and Figure 6.7). The likelihood distribution used for the testing of the theory here is equivalent to the following: $w_{ij} - y_j \sim N(0,\, 0.1y_j)$ for all j except the last two values ($j = 3200$ s and $j = 3400$ s) because for these particular values the distribution is very variable and not Gaussian any more, so we choose $w_{ij} - y_j \sim N(0,\, 2)$.

Actually, it is not strictly correct to use a Gaussian likelihood distribution in the case where we use directly simulated data with a fine time step, rather than an experimental dissolution profile. This is because fluctuations obtained with the coarse-grained time step of the inverse simulation are definitely biased, (the coarse time stepping makes the dissolution slower, see Figure 6.4). However, in this work the normal distribution has been chosen for the likelihood because the target is to investigate performance of the theoretical Bayesian reconstruction approach for a drug dissolution problem, rather than to fine-tune for acceptable levels of bias. The results of the simulations have shown quite good performance for the Gaussian-based likelihood used.

6.4.4.3 Effect of the size of population on variability of the estimated parameters

At each time step of the particle filtering, a population, size p, of histograms is generated by the inverse simulator. Typically, the value of p (chosen by the user) has to be large enough to assure convergence of the simulation, but small enough not to render the simulation too computationally intensive. In this subsection, sensitivity analysis on the effects of the size of the sample (population) is performed.

The simulation was allowed to run for five different sizes: p_1=100, p_2=500,

N_{tot0}	μ_0 (μm)	σ_0	$t_{tot}(s)$	$\Delta t_{inverse}(s)$	$\Delta x(\mu m)$	p
100000	45	10	3601	200	1	100, 500, 1000, 2500, 5000

Table 6.5: Inputs used for verifying the effects of the population size used in the inverse simulations

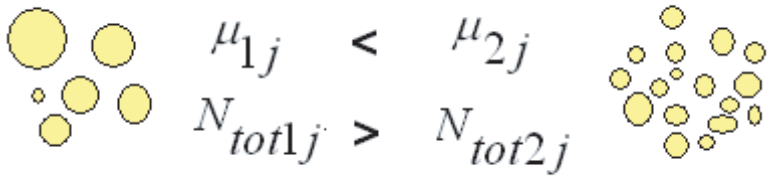

Figure 6.9: Typical error source due to using marginal distributions instead of joint distributions for the priors. Both size distributions are likely to be selected by the algorithm.

p_3=1000, p_4=2500, p_5=5000, with the fine-grained simulated data as input, Table 6.5. For each size p, the program was computed over 25 runs with different seeds. The average $M_{25\,runs}$ and the standard deviation $sd_{25\,runs}$ for each of the estimated parameters were computed. These results have been compared for the five different population sizes and over the entire period of dissolution.

The main observation from the results is that, with increase of population size, the simulations converge better, as shown in Figure 6.10 and 6.11, (b, d). These Figures illustrate that standard deviations obtained over 25 runs decline as the number of individuals in the population increases up to p_5=5000. It can be observed that parameters μ, σ and shape parameter α are quite stable, especially in the first two thirds of the dissolution process. In the last third of the simulation, higher standard deviations are observed. This is due to the structure of the data: note that it was shown that at the end of the dissolution process the size distribution departs from Gaussian and becomes quite disordered (see the distribution from Figure 6.3, (c, d) and the coefficients of variation in Figure 6.5, (a, b)). From this point of view, the data is reconstructed well with p larger then 100. The parameter N_{tot} behaves differently to the other three parameters: it is most variable in the middle of the

reconstruction. Reasons for this are that at the start and end the number of particles is respectively very large and very small, but in the middle it can fluctuate because of the way the likelihood of the sampled parameters is computed. For simplicity reasons, the marginal probability of the whole quadruplet is considered, meaning that both situations indicated on Figure 6.9 may still be possible. The parameter σ and well selected marginal prior distributions specified at each step keep this effect under control though. Figures 6.10, (a, b) show, however, that the variability of N_{tot} in the middle of the simulation does not distort results in a major way and the adopted strategy of particle filtering is still valid.

6.4.4.4 Effect of the quality of the data presented to the inverse simulation

In this subsection, two different prior dissolution profiles are used for the inverse MC simulator. The first $y_1(t)$ is generated with $\triangle t_{direct}$=1s and sampled at $\triangle t_{sampling}$ =200 s. The second set of direct data, $y_2(t)$, is generated with a coarse time-step $\triangle t_{direct}$= 200 s and sampled at the same intervals as previously: $\triangle t_{sampling}$ =200 s. This second $y_2(t)$ contains more "measurement error" than $y_1(t)$.

From Figure 6.12 it can be observed that the inverse simulation reconstructs fine-grained $y_1(t)$ with more difficulty than coarse-grained $y_2(t)$, because for $y_2(t)$: $\triangle t_{direct}$=$\triangle t_{inverse}$. However, even if the time-step of the kernel of inverse simulations is coarse, the figures show that the simulation is able to reconstruct the parameters due to the priors. It can also be observed that the correction is made gradually, so that the estimated values for the number of particles get better towards the end of the simulation. The average shape factor α obtained with fine-grained time step prior, is 4.6 and with a coarse-grained time step prior is 4.7, (compared to the real shape value $\alpha = 4.1$).

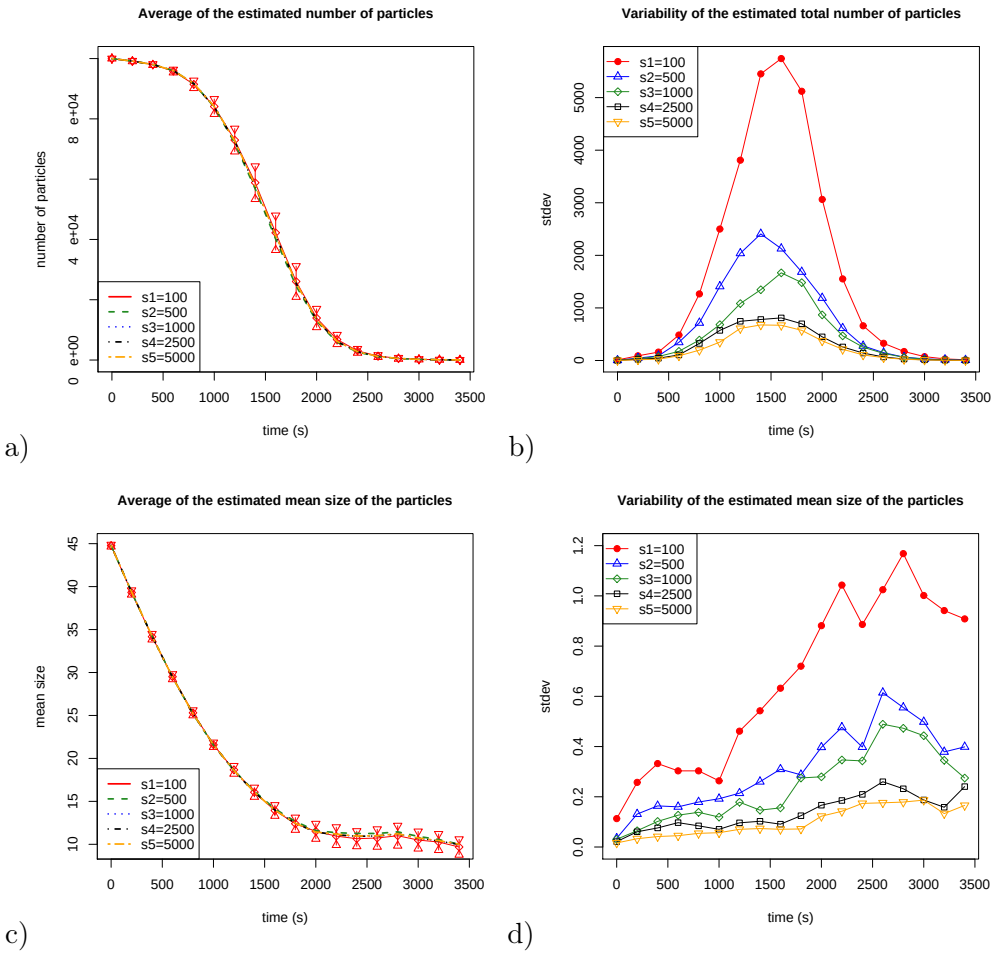

Figure 6.10: Effects of the population size on the average values of the estimated parameters N_{tot} and μ. Figures show the parameters averages over 25 simulations (a, c), the standard deviations indicated on the curves correspond to the standard deviations obtained for the smallest population p_1=100.

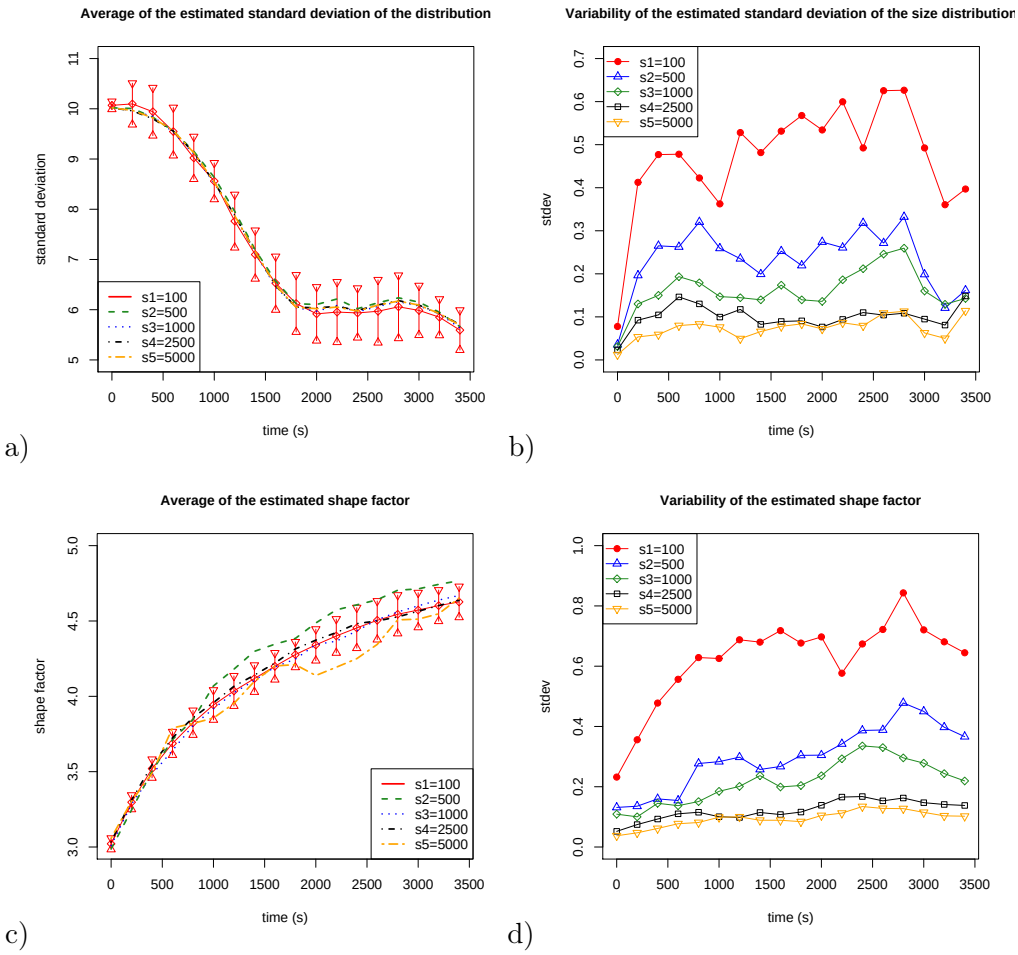

Figure 6.11: Effects of the population size on the average values of the estimated parameters σ and α. Figures show the parameters averages over 25 simulations (a, c), the standard deviations indicated on the curves correspond to the standard deviations obtained for the smallest population p_1=100.

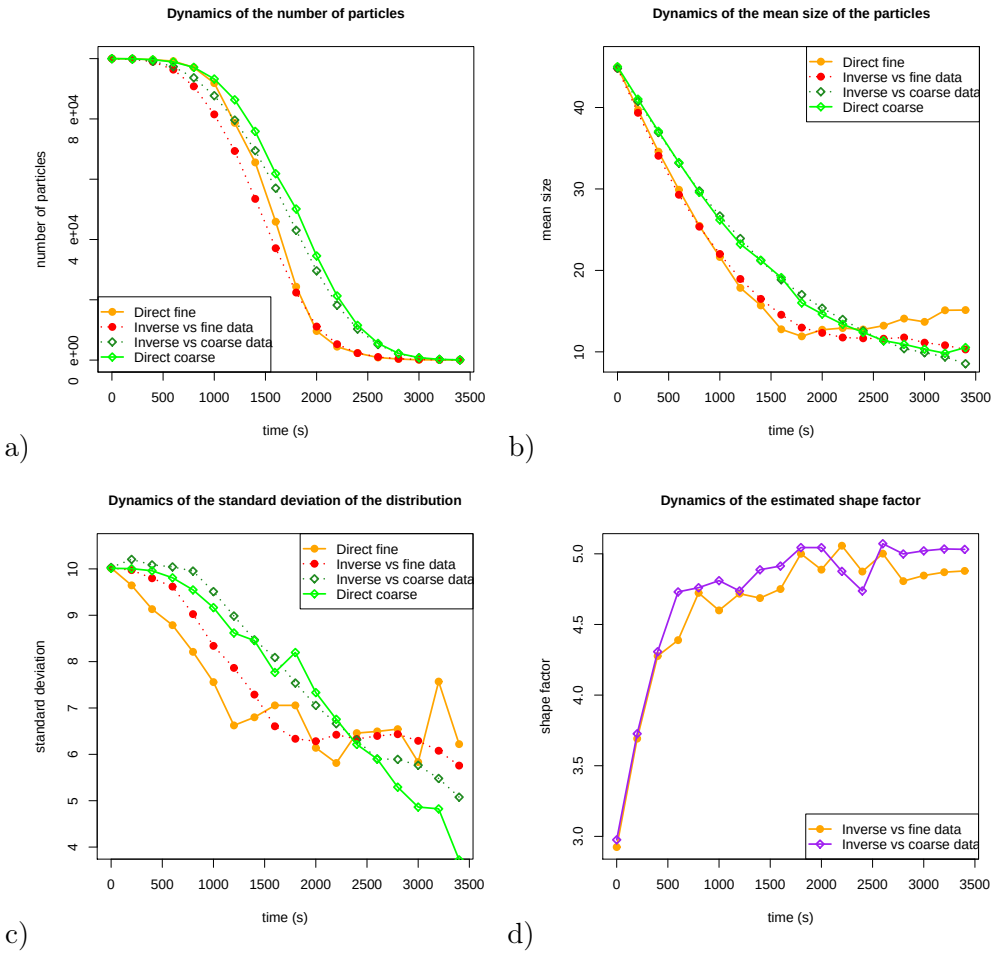

Figure 6.12: Comparison between inverse simulations obtained using a fine time step prior dissolution profile and inverse simulations obtained, using a coarse time step prior dissolution profile.

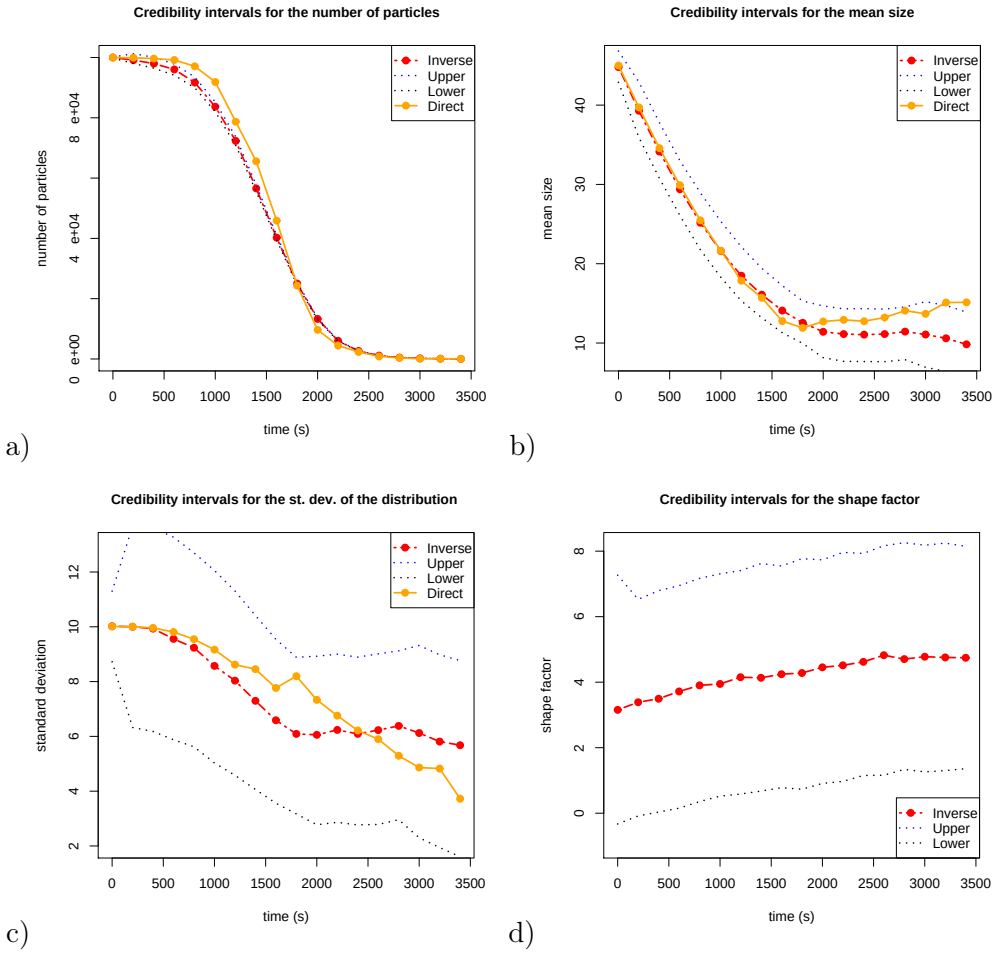

Figure 6.13: Credibility intervals for the estimated parameters are given by the dotted curves.

6.4.4.5 Credibility intervals

Credibility intervals depend strongly (Section 6.4.3) on the prior distributions (Subsection 6.4.4.1) chosen for the parameters at each time step. Figure 6.13 shows the variation in the credibility intervals obtained over the whole period of dissolution for the four analysed parameters. The direct data presented for the inverse simulation was the fine-grained time step direct simulations.

6.5 Summary, conclusions and ideas for future work.

This project involved the use of MC simulations to model drug dissolution from DDS consisting of a large number of small particles. Regardless of the specific purpose of the DDS (immediate or sustained release), its physical properties (soluble or bioerodible) or the medium of dissolution (various *in vitro* environments or *in vivo* environment), multi-particle Drug Delivery Systems result, at dissolution, in variability related to their particle-size distribution and the way different particles interact with the dissolution medium. The aim of this work was to increase our understanding of how the multi-sized dissolving particles cause variability in the dissolution profiles.

In this purpose, a theoretical Bayesian framework has been proposed. The distribution of particles at different times of the dissolution, as well as the noise components it gives rise to, are considered unknown and stochastic. The stochastic part is incorporated in the deterministic relationship between the dissolution parameters and the dissolution profiles. The prototype inverse MC program, implemented to validate the theory, and needing subsequent upgrading for various specific experimental settings, was tested using simulated dissolution data. This data was considered to be sufficiently variable to be used by the inverse MC. Hence, no variability specific to any dissolution medium was added at the data generation.

Nevertheless, the inverse MC model is intended to aid in elucidating dissolution

of multi-particle systems in the widely-used paddle dissolution apparatus, in order to understand the inherent variability associated with its test conditions therein, as well as with the particle distribution.

The inverse MC model developed here was shown in conjunction with well-detailed sensitivity analysis, in order to illustrate its function and was shown to perform quite well at reconstructing time-series of particle size distributions. The results of the sensitivity analyses suggest that prior knowledge about the system is of utmost importance for model performance, because it is involved in setting the marginal prior distributions for the unobserved parameters for sampling at each new time step. Therefore, in the case of modelling any particular *in vitro* or *in vivo* system, any extra knowledge about it is extremely valuable. Some ideas related to using extra knowledge about particulate systems dissolving in the USP apparatus are proposed in the Future Work Section from the following overall concluding Chapter 7.

In spite of the proposed theory and the fact that the implemented prototype deals with a non-disintegrating particulate system, both theory and inverse MC model can benefit from integrating the behaviour of disintegrating pharmaceutical systems. The most interesting and challenging part of modelling a disintegrating system will correspond to building up the transition kernel of the model, because it will involve abrupt jumps in the number of particles at each time step considered.

Chapter 7

Summary, Conclusions and Future Work

7.1 Introduction

The purpose of this research was to explore complex system modelling in the field of stochastic drug dissolution. Many methods have been applied to model different aspects of the dissolution problem, but increasing research on biomaterials and their potential for sustained drug release is continuously challenging modellers to focus their energies on the development of new simulation techniques and new models to help optimise but also to complement the large amount of experimental work performed. This thesis begins with a description of the multi-factorial problems posed by drug dissolution and underlines a number of cases which required particular attention from modelling, which are the multi-component soluble devices for immediate release, bioerodible swellable polymeric (PLGA) for sustained release and drug delivery systems composed of a large number of small particles (particulates) for any kind of release. Next it concentrates on the reasons for choosing to explore *probabilistic techniques* in the field of drug dissolution. Novel modelling efforts using direct and indirect Monte Carlo techniques for pharmaceutical or other systems showing some similarity are described subsequently.

This body of research either develops the work of others or breaks new ground in the area of probabilistic methods for drug dissolution. The thesis takes an *exploratory approach* to the problem by developing multiple versions of probabilistic models for various cases of DDS. Throughout the previous chapters it has been clearly shown that the internal morphology of many drug delivery systems plays a key-role in the release of the active molecule. Multi-particle direct Monte Carlo methodologies were considered appropriate for the investigation for three main reasons:

- they permitted the internal configurations and physical properties of many drug delivery systems to be accessed, described and modelled in a straightforward way.
- they permitted treating the physical phenomena, which are unobserved and unquantified, as distributions of probability.
- they have a very high potential for modelling increasing complexity and can be implemented on parallel architectures for more optimal results.

This thesis builds on the idea, initially proposed by Kosmidis et al. (2003b), of representing drug delivery systems as multi-particle systems. Direct Monte Carlo methods were proposed by these authors as appropriate techniques to simulate the processes undergoing at dissolution of a drug carrier, while subsequently partially developed by Göpferich and Langer (1995); Zygourakis and Markenscoff (1996) and others. The present work is based on the consideration that multi-particle MC methods have received insufficient attention to date, and can, with appropriate formulation and implementation (specific to both experiment and targeted goals and outcomes), prove to be a useful tool for many practical applications in drug dissolution. The principal focus of modelling drug delivery remains that of reducing the costly and time-consuming experimental work. Advanced models can help reduce the amount of animal testing involved. Used in conjunction with other methods or by themselves, MC simulation methods are shown to be capable of eliminating possible gaps

in the knowledge of the devices in question, by validating the modeller's theoretical assumptions about them.

7.2 Summary of findings

7.2.1 Internal insight into Drug Deliver Systems

In the light of findings to date, two new experimental situations were explored from the point of direct Monte Carlo modelling.

Much of the focus in this work has been on an experimental binary system, consisting of poorly-soluble drug, dispersed in a matrix of highly-soluble acid excipient (with experimental results from School of Pharmacy, TCD). On dissolution, the acid excipient develops certain mechanisms, based on local changes in the pH of the medium, which strongly influence drug release. The model developed directly accounts for effects, such as local interactions of the dissolving components, development of wall-roughness at the solid-liquid interface, moving concentration boundary layer and solid-liquid interface and mass transport by advection. This model is totally novel, because multi-component soluble systems for immediate release have never been analysed using multi-particle CA and MC modelling, even if the internal morphology of such DDS represents a typical physical system which can be analysed with CA. Considering the heterogeneous nature of the *in vitro* environment, the probabilistic approach to advection was shown to be an appropriate tool for handling the problems encountered. The sensitivity analysis on the method and quantitative results illustrated that this approach has a large potential for future work. In particular, the work related to probabilistic way of analysing advection, (even if the idea was simple), showed very good agreement with experimental data. Hence, making the existing models more sophisticated we could anticipate considerable benefits in modelling more delicate *in vitro* situations.

The second experimental system examined was that of bioerodible micro- and

nanospheres encapsulating large molecules such as proteins (with results from Sandor et al. (2001). It has been shown that these drug carriers can only be modelled with difficulty. Thus, original work in this thesis involves modelling dissolution of PLGA spheres using 3D multi-agent computational systems. The Direct MC models developed showed qualitative results which were in strong agreement with experimental dissolution profiles. Subsequently, the models were refined in order to take account of details characterising particular experimental systems. Major attention and modelling work has been directed towards implementing multiple theoretical hypotheses about the PLGA nanospheres, such as: distribution of protein in the spheres, distribution of pores in the spheres, distributions of protein in the pores, resulting in several versions of the main implementation.

Results demonstrated that Direct MC models can give very good quantitative agreement with experiment and hence can be used by the pharmaceutical researcher for predictions and optimisations. The following modelling features are innovative and open new ground for large amounts of future work:

- very fine-grained modelling for PLGA nanospheres.
- effects of different internal morphologies can be examined very closely.
- use of agents for modelling the proteins.

As this research concluded, other very recent work by a research team from Holland ((Vlugt-Wensink et al., 2006)) came to light. They approach a similar problem of proteins encapsulated in a polymer with different properties to that of PLGA, through a similar methodology of treating the encapsulated drug molecules as moving particles. In parallel with the work carried out in DCU, this demonstrates the increasing interest of MC multi-particle models in this context. Nevertheless, the work presented in this thesis demonstrates an in-depth investigation of a number of aspects of the sustained release PLGA DDS problem, specifically by implementing

model's versions for spheres with stratified porosities, spheres initially characterised by large occlusions and spheres encapsulating molecules of different sizes.

The computational requirements of both models mainly depend on the size of the lattice. For example, the multi-agent model for protein dissolution from PLGA spheres runs on an Intel(R) Pentium(R) 4 CPU, 2.8 Ghz, 512 MB RAM processor for about 30 min for cube lattices with edges of 50 sites and about 90 min for cube lattices with edges of 100 sites. The computational requirements of this model equally increase proportionally to the number of agents present in the system. Thus, as already stated, parallelisation of the two models can be interesting if fine-grained simulations of relatively large drug delivery systems are necessary.

7.2.2 Populations of DDS

In the final part of the thesis, an alternative viewpoint has been taken. As opposed to Chapters 2, 4 and 5, which mostly investigated the drug carriers in relation to their internal morphology and physical properties, Chapter 6 considers how the drug delivery system, composed of an agglomeration of small units, behaves as a whole, in order to analyse the effects of the distributions of different entities present, on the drug release curves. A Bayesian framework has been proposed for analysing these *particulate systems* and Inverse Monte Carlo techniques have been used to explore features of the problem.

The model reported was shown to be capable of retrieving knowledge from experimental data, specifically time series of dissolved quantities of drug, originating from a system composed of many particles dissolving simultaneously. At different time-steps of the dissolution, the parameters of the particle size distribution are considered as random variables. A deterministic function based on classical equations for drug dissolution is used to assess the relation between the particle size distribution and the amount of dissolved drug in the solution. The inaccuracy in the dynamics of the model is considered stochastic and represented by noise factors.

In comparing simulated results and experimental dissolution results, the unknown particle size distributions are re-updated in order to obtain their reconstruction at the end of the simulation, within a previously specified error range.

This approach not only serves to round off and complement existing research, it also brings to the area of drug dissolution similar work from other areas, and serves to demonstrate how the little information available from experimentation may be separated from the various noise sources. While, up to now, the dissolution process has produced data containing relatively little information and considerable error, the work in this thesis has shown how the former can be increased and the latter minimised through the use of novel or existing probabilistic methods.

7.3 Future Work

This research substatially advances the field of drug release modelling through a number of new developments based on both Direct and Inverse MC methods, which also demonstrate their considerable potential for future in this context. Some of these features are presented in what follows.

7.3.1 Optimisation and technical enhancements for the direct MC models

As a 3D multi-agent program, the dissolution simulator is very computationally intensive and time consuming. The computing resources needed grow extremely rapidly with the 3D matrix size and as the concentration of molecules in the spheres increases. Future work will involve optimisation of the program in order to obtain better performance on larger lattices. The results, presented in Chapter 5, for example, have been obtained from simulations with single spheres. However, as noted previously, microsphere populations are typically large. In most studies involving PLGA spheres, efforts are made to maintain variability as low as possible for the

micro- or nanospheres size distributions, (Kilic et al., 2005), in order to have more prediction control over the release profiles obtained. However, in some particular cases, the spheres have extensive size distributions[1]. Hence it is ultimately of interest to monitor how a larger population of spheres behaves. Running the simulations for any model (A to C), for populations of spheres of different sizes, can be partitioned to run on a distributed memory cluster. For example, the Irish Centre for High-End computing (ICHEC, 2006) offers researchers use of two clusters consisting of more than 300 computing nodes (CPUs). A considerable amount of work has already been done in this direction, in the form of a number of programs generating code to simulate the dissolution of a distribution of spheres of different sizes, or of different internal morphologies on a PC cluster. The simulation for each sphere runs on a separate CPU. One problem with using a remote cluster is related to the fact that it is often the case that the simulation is interrupted for technical or other reasons. Thus, important future work will also be to implement and incorporate program tools for saving the current states of the simulation in the event of a crash and for re-reading this information from a file, in re-loading the parameters and re-launching the the simulation. Several save files (corresponding to different types of objects) are necessary to re-launch the simulation.

Another interesting optimisation which permits time-saving is use of the MPI (Gropp et al., 1999) components or tools in order to parallelise the simulations. As these use very small time steps, they are very time-consuming. The model for the matrix soluble systems would also benefit from an MPI parallelisation as well, because it simulates quite large delivery systems composed from microgranules requiring a very fine-grained approach. A lot of memory is needed for such a simulation, thus using parallel processors would facilitate the task and permit simulations for more life-like internal morphologies untreatable by a single processor.

[1] see Figure 5.4 from the example given in Subsection 5.2.4, (Charlton et al., 2006)

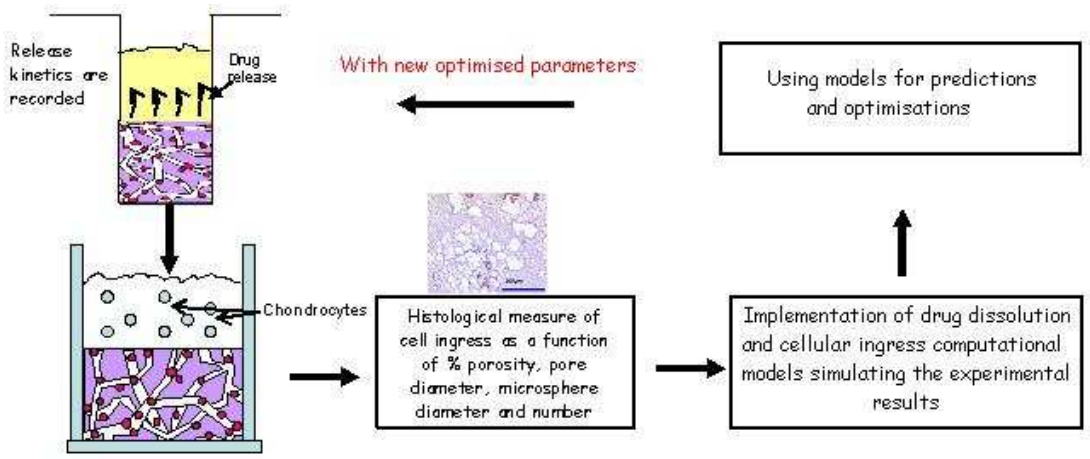

Figure 7.1: Schematic representation of the main phases of the research related to the therapeutical implants seeded with PLGA microspheres for sustained release of growth factors. The figure shows at what level the modelling and simulation will intervene.

7.3.2 Bioerodible implants

As described in Subsection 5.2.4, PLGA protein-loaded microspheres are used not only on their own, but also in conjunction with other delivery systems. The model presented in Chapter 5 will be used in future for optimising the experimentation undertaken to design therapeutical implants for damaged cartilage. To facilitate this, the present work must be enhanced through more flexible coding.

The PVA scaffold seeded with microspheres is a porous material where the proteins escaping from the microspheres diffuse in order to facilitate the ingress of cells. The case is described in Subsection 5.2.4 and schematised in Figure 7.1.

Protein diffusion through the pores of the scaffold is a problem on a different scale to that treated in Chapter 5. In the scaffold, diffusion takes place at a much larger scale and can be tackled more easily in terms of mass transport and concentrations rather than random walks of individual particles. A differential equation-based model will be solved on a computational grid and one of the Monte Carlo models presented above will be used to simulate, at each time step, the quantities of protein

made available by the erosion of the PLGA microspheres.

Once the approximate concentration of growth factor in the pores of the PVA scaffold is available, these results will be redirected to a 3D multi particle Monte Carlo simulation where the particles will represent the cells moving according to the concentration gradients. Figure 7.1 illustrates this future research plan.

7.3.3 Perspectives in PLGA nanospheres research

An important point to make here is that the existing models are readily adaptable to modifications in order to account for properties of other types of DDS. In this section we outline other possible applications.

Presently, nanotechnology is beginning to play a considerable role in drug design. PLGA nanospheres offer a very promising and very powerful technique for drug transport in many important medical fields. Given the major challenges this methodology is now facing, careful and detailed studies are required for every example case. In contrast to existing models for bioerodible spheres discussed earlier, the models presented in this thesis are specifically designed for very small scales (i.e. nano-level).

The study of Kilic et al. (2005) proposes PLGA nanospheres as one approach to improve both pharmacokinetics and pharmacodynamics of large size neuropharmaceuticals for the treatment of the diseases of the central nervous system (CNS). These results demonstrate that a stable drug formulation could be prepared, utilising PLGA nanospheres as a potential delivery system, (and with the potential to perform much better than other drug delivery methods). The results of this study showed that formulations with different neuropharmaceutical content exhibited different release profiles. Most anti-cancer drugs have limitations in clinical administration due to their poor solubility and other physicochemical and pharmaceutical deficiences. They require the use of additives or excipients, which often cause serious side effects. Moreover, intravenous injection and infusion are unavoidably associated with consid-

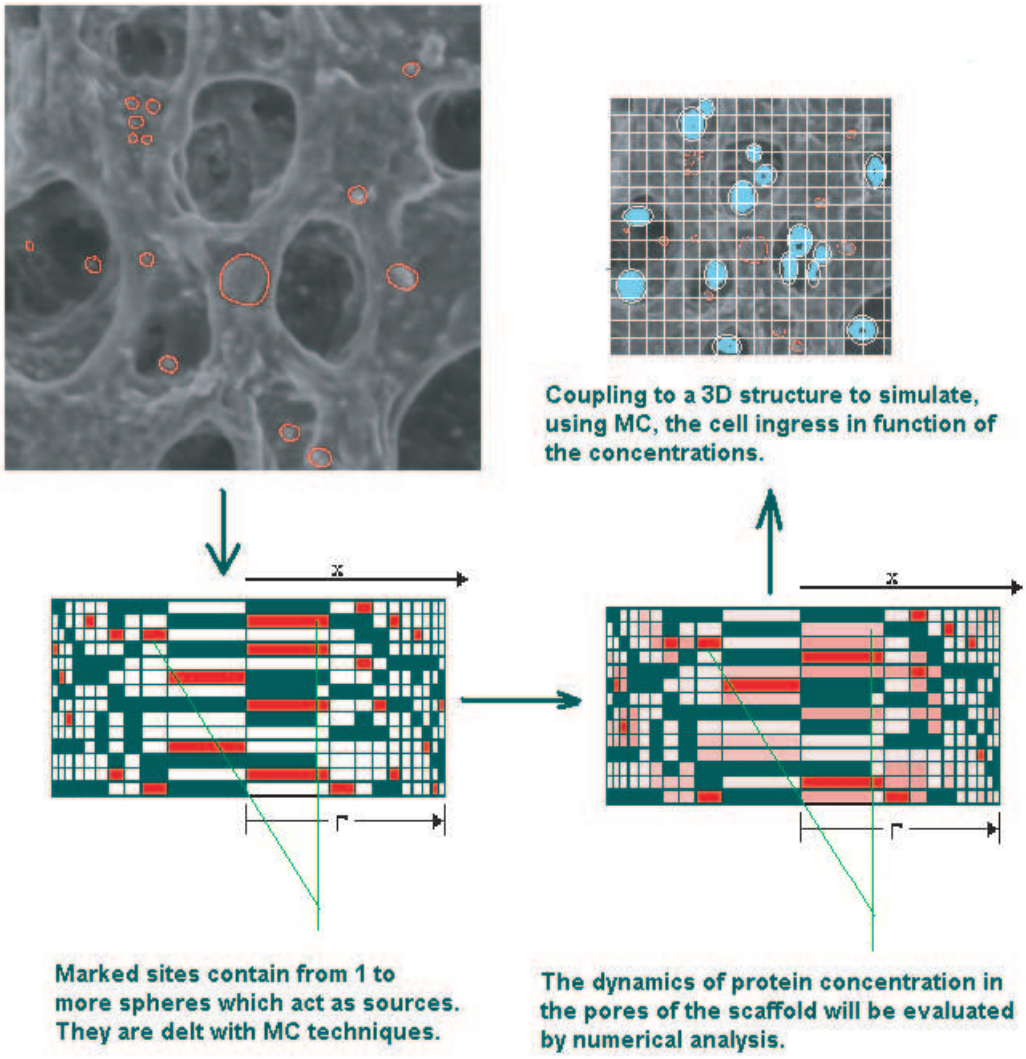

Figure 7.2: Illustration of the modelling approach chosen for the optimisation of therapeutical implants.

erable fluctuations of drug concentration in the blood. Therefore, the drugs can only be administered over a limited dosage and time period. Nanoparticles of biodegradable polymers and other bioadhesive materials might be an ideal alternative carrier, Feng (2006). The nanospheres are often coated with other type of polymers in order to obtain desired special release effects, Hawley et al. (1997); Illum et al. (2001); Stolnik et al. (1994). For example, nanospheres are utilised to produce excellent targeting of drugs and diagnostic agents to regional lymph nodes, Hawley et al. (1997). Depending on their surface characteristics, the distribution of the nanospheres can be significantly modified and the lymph node localisation dramatically enhanced by coating their surfaces with PLA:PEG co-polymers or by producing co-precipitate nanospheres of PLGA and PLA:PEG. PEG-coated magnetite nanospheres with different surface characteristics can also be utilised to target a diagnostic agent to regional lymph nodes, Illum et al. (2001).

Thus, further developments of the models A-C, simulating dissolution for nanospheres, might consider:

1. Possible interactions between pharmaceutical agents and the polymer composing the nanosphere.

2. Studying the effect on release profiles of coating spheres with different polymer types .

3. Investigation of nanospheres composed of a mixture of two or more types of polymers

4. Completing the work on models for spheres composed of surface-eroding polymer. To date this model has been qualitatively validated only as a part of the present work, due to lack of quantitative validation with experimental data. The qualitative model has to be calibrated against experimental data and quantitative agreement of at least the same quality as in Chapter 5 is desirable.

7.3.4 Inverse simulations

The work performed in Chapter 6 explores the use of Inverse Monte Carlo techniques in the field of Drug Delivery to elucidate unknown parameters and optimise the design of particulate drug delivery systems. Inverse simulations were performed and tested only on simulated data, which sought to postulate researchable parameter values for the size distribution and particle densities for particulates. The present model did not incorporate into the model any details related to the USP dissolution environment (such as: paddle rotation speed, dimensions of the vessel, dissolution medium viscosity etc). It would be interesting, however, to test the inverse MC technique on real data, and especially to calibrate this model for the particular environment of the USP apparatus in order to better understand the dissolution process in conjunction with its flow/mixing patterns.

The data available can be enriched by digital camera images of changes in the USP over the time period of the dissolution test. As *in vitro* experimental data, recorded on a digital camera, are noisy from an image analysis point of view, they must be processed to remove the visual noise due to movement of the compact in the apparatus. The data thus obtained would form a convenient time series for the dissolution and could be used for refinement of the inverse MC model.

The investigation of particulate systems can tie in with a study on disintegrating compacts. In this case the solid compact disintegrates, breaking into smaller particles or granules which then move around and dissolve within the test device. Again, the ability of the model to simulate changes in compact properties can be investigated.

These developments will bring about an increased understanding of how different formulation types behave in the USP paddle dissolution apparatus. This will also aid in understanding the sources of variability in the device that may lead to variable dissolution results in practice, helping choosing appropriate test conditions for *in vitro* dissolution studies which may be then successfully correlated with corresponding *in vivo* results for the development of *in vivo* - *in vitro* correlations (IVIVC's).

7.4 Concluding remarks

In conclusion this thesis reports a major step forward in investigating and quantifying a range of aspects of the drug dissolution problem, viewed as random phenomenon. The work opens up perspectives for future research on drug and treatment mechanisms, further applications of these investigations and future collaborations, targeting the drug dissolution field in general, and nanotechnology used for pharmaceutical reasons in particular.

Bibliography

A. Voutilainen, V. K. and Kaipio, J. (2001), 'Statistical inversion of aerosol size measurement data', *Inverse Problems in Engineering* **9**, 67–94.

Almeida, L., Simoes, S., Brito, P., Portugal, A. and Figueiredo, M. (1997), 'Modeling dissolution of sparingly soluble multisized powders', *Journal of Pharmaceutical Sciences* **86**(6), 726–732.

Antal, I., Zelkö, R., Röczey, N., Plachy, J. and Rácz, I. (1997), 'Dissolution and diffuse reflectance characteristics of coated theophylline particles', *International Journal of Pharmaceutics* **155**, 83–89.

Balant, L. P. and Gex-Fabry, M. (2000), 'Modelling during drug development', *European Journal of Pharmaceutics and Biopharmaceutics* **50**, 13–26.

Barat, A., Ruskin, H. J. and Crane, M. (2005), Modelling the in vitro Dissolution of Soluble Binary Drug Delivery Systems using Direct Monte Carlo techniques , *in* 'Open International Conference on Modeling and Simulation'.

Barat, A., Ruskin, H. J. and Crane, M. (2006a), 'Probabilistic models for drug dissolution. Part 1. Review of Monte Carlo and stochastic cellular automata approaches', *Simulation Modelling Practice and Theory* **14**, 843–856.

Barat, A., Ruskin, H. J. and Crane, M. (2006b), 'Probabilistic methods for drug dissolution. Part 2. Modelling a soluble binary drug delivery system dissolving in vitro', *Simulation Modelling Practice and Theory* **14**, 857–873.

Batycky, R. P., Hanes, J., Langer, R. and Edwards, D. A. (1997), 'A theoretical model of erosion and macromolecular drug release from biodegrading microspheres ', *Journal of Pharmaceutical Sciences* (12), 1464–1477.

Baxter, J. L., Kukura, J. and Muzzio, F. J. (2005), 'Hydrodynamics-induced variability in the usp apparatus ii dissolution test', *International Journal of Pharmaceutics* **292**(1-2), 17–28.

Binder, K. (1986), *Monte Carlo Methods in Statistical Physics*, 2nd edn, Springer Verlag.

Caraballo, I. (2004), 'Ultrasound-assisted compression. A new perspective for the preparation of controlled release systems', *Leader for Chemist* . http://www.cesil.com/leaderforchemist/chemist.htm.

Charlton, D., Peterson, M., Spiller, K., Lowman, A., Torzilli, P. and Maher, S. (2006), Mechanical Characterization of a Novel Scaffold for the Repair of Articular Cartilage . Kindly provided by the authors.

Chen, X., Chen, W., Hical, A. H., Shen, B.-C. and Fan, L. T. (1998), 'Stochastic modeling of controlled-drug release', *Biochemical Engineering Journal* **2**, 161–177.

Chen, Y., McCall, T., Baichwal, A. and Meyer, M. (1999), 'The application of an artificial neural network and pharmacokinetic simulations in the design of controlled-release dosage forms', *Journal of Controlled Release* **59**, 33–41.

Chopard, B. and Droz, M. (1998), *Cellular Automata Modeling of Physical Systems*, Cambridge University Press.

Costa, P. and Lobo, J. M. S. (2001), 'Modeling and comparison of dissolution profiles', *European Journal of Pharmaceutical Sciences* **13**, 123–133.

Coulter, B. (2006), 'Multisizer 3 coulter counter.the highest resolution for sizing and

counting particles', Online available at: http://www.beckmancoulter.com. Access date: 14/11/2006.

Crane, M., Crane, L., Healy, A.-M., Corrigan, O. I., Gallagher, K. M. and McCarthy, L. (2004b), 'A Pohlhausen solution for the Mass Flux From a Multi-layered Compact in the USP Drug Dissolution Apparatus', *Simulation Modelling Practice and Theory (SIMPAT)* **12/6**, 397–411.

Crane, M., Hurley, N. J., Crane, L., Healy, A.-M., Corrigan, O. I., Gallagher, K. M. and McCarthy, L. G. (2004a), 'Simulation of the USP drug delivery problem using CFD: experimental, numerical and mathematical aspects', *Simulation Modelling Practice and Theory (SIMPAT)* **12/2**, 147–158.

Crank, J. (1975), *The Mathematics of Diffusion*, Clarendon Press, Oxford.

Davies, M. E. (1998), 'Nonlinear noise reduction through Monte Carlo sampling', *Chaos* **8**(4), 775–781.

EurPh (2006), 'European Pharmacopoeia', Online homepage available from: http://www.pheur.org. Access date: 14/11/2006.

Feng, S. (2006), 'Chemotherapeutic Engineering: Polymeric Nanoparticles for Clinical Administration of Anticancer Drugs '. Access date: 14/11/2006.

Feng, S. and Chien, S. (2003), 'Chemotherapeutic engineering: application and further development of chemical engineering principles for chemotherapy of cancer and other diseases', *Chemical Engineering Science* **58**, 4087– 4114.

Feng, Y. (1997), Computer Modelling of Complex Systems with Applications in Physical and Related Areas, PhD thesis, Dublin City University.

Galeska, I., Kim, T.-K., Patil, S. D., Bhardwaj, U., Chatopadhyay, D., Papadimitrakopoulos, F. and Burgess, D. J. (n.d.), 'Controlled Release of Dexamethasone

from PLGA Microspheres Embedded Within Polyacid-Containing PVA Hydrogels', *The AAPS Journal* **7**(1).

Goodhill, J. (1997), 'Diffusion in axon guidance', *European Journal of Neuroscience* **9**, 1414–1421.

Göpferich, A. (1995), 'Modeling of polymer erosion in three dimensions: rotationally symmetric devices', *AIChE Journal* **41**(10).

Göpferich, A. (1996), 'Mechanisms of polymer degradation and erosion ', *Biomaterials* **17**, 243–249.

Göpferich, A. (1997*a*), 'Bioerodible implants with programmable drug release', *Journal of Controlled Release* **44**, 271–281.

Göpferich, A. (1997*b*), 'Erosion of composite polymer matrices', *Biomaterials* **18**, 397–403.

Göpferich, A. and Langer, R. (1995), 'Modeling monomer release from bioerodible polymers', *Journal of Controlled Release* **33**, 55–69.

Grassi, M., Colombo, I. and Lapasin, R. (2000), 'Drug release from an ensemble of swellable crosslinked polymer particles', *Journal of Controlled Release* **68**, 97–113.

Gropp, W., Lusk, E. and Skjellum, A. (1999), *Using MPI. Portable Parallel Programming with the Message-Passing Interface*, 2nd edn, The MIT Press, Cambridge, Mass.

Hawley, A. E., Illum, L. and Davis, S. S. (1997), 'Preparation of biodegradable, surface engineered PLGA nanospheres with enhanced lymphatic drainage and lymph node uptake', *Pharmaceutical Research* **14**(5), 657–661.

Healy, A.-M. (1995), Investigations of the dissolution mechanisms of acidic drug-excipient compacts, PhD thesis, University of Dublin, Trinity College.

Healy, A.-M. and Corrigan, O. I. (1992), 'Predicting the dissolution rate of ibuprofen-acidic excipient compressed mixtures in reactive media', *International Journal of Pharmaceutics* **84**, 167–173.

Healy, A.-M. and Corrigan, O. I. (1996), 'The influence of excipient particle size, solubility and acid strength on the dissolution of an acidic drug from two-component compacts', *International Journal of Pharmaceutics* **143**, 211–221.

Healy, A.-M., McCarthy, L. G., Gallagher, K. M. and Corrigan, O. I. (2002), 'Sensitivity of dissolution rate to location in the paddle dissolution apparatus', *Journal of Pharmacy and Pharmacology* **54**(3), 441–444.

Higdon, D., Lee, H. and Bi, Z. (2002), 'A Bayesian approach to characterizing Uncertainty in inverse problems using coarse and fine scale information', *IEEE transactions on signal processing* **50**(2), 389–399.

Higuchi, W. and Hiestand, E. (1963), 'Dissolution rates of finely divided drug powders', *Journal of Pharmaceutical Sciences* **52**(1), 67–71.

Huelsenbeck, J. P., Ronquist, F. and Hall, B. (2001), *Mrbayes: A program for the Bayesian inference of phylogeny.* Online homepage available from: http://mrbayes.csit.fsu.edu/, Access date: 01/12/2006.

ICHEC (2006), 'Irish Center for High-End Computing', Online available at: http://www.ichec.ie. Access date: 14/11/2006.

Illum, L., Church, A., Butterworth, M., Arien, A., Whetstone, J. and Davis, S. (2001), 'Development of systems for targeting the regional lymph nodes for diagnostic imaging: in vivo behaviour of colloidal PEG-coated magnetite nanospheres in the rat following interstitial administration', *Pharmaceutical Research* **18**(5), 640–645.

Kalampokis, A., Argyrakis, P. and Macheras, P. (1999), 'Heterogeneous tube model for the study of small intestinal transit flow', *Pharmaceutical Research* **16**(1).

Kang, F. and Singh, J. (2001), 'Effect of additives on the release of a model protein from PLGA microspheres ', *AAPS PharmSciTech* **2**(4), article 30.

Kilic, A. C., Capan, Y., Vural, I., Gursoy, R. N., Dalkara, T., Cuine, A. and Hincal, A. A. (2005), 'Preparation and characterization of PLGA nanospheres for the targeted delivery of NR2B-specific antisense oligonucleotides to the NMDA receptors in the brain ', *Journal of Microencapsulation* **22**(6), 633–641.

Kisler, J. M., Stevens, G. W. and O'Connor, A. J. (2001), 'Adsorption of proteins on mesoporous molecular sieves', *Materials Physics and Mechanics* **4**, 89–93.

Kosmidis, K. and Argyrakis, P. (2000), 'Fractal kinetics in drug release from finite fractal matrices', *Journal of Chemical Physics* **119**(12).

Kosmidis, K., Argyrakis, P. and Macheras, P. (2003a), 'A reappraisal of drug release laws using Monte Carlo simulations: the prevalence of the Weibull function', *Pharmaceutical Research* **20**.

Kosmidis, K., Rinaki, E., Argyrakis, P. and Macheras, P. (2003b), 'Analysis of case ii drug transport with radial and axial release from cylinders', *International Journal of Pharmaceutics* **254**.

Lam, X., Duenas, E., Daugherty, A., Levin, N. and Cleland, J. (2000), 'Sustained release of recombinant human insulin-like growth factor-I for treatment of diabetes ', *Journal of Controlled Release* **67**, 281–292.

Landau, D. P. and Binder, K. (2000), *Monte Carlo Simulations in Statistical Physics*, Cambridge University Press.

Lee, S.-J. E. and Chakraborty, A. K. (2002), 'Sequence dependence of polymer

dynamics in quenched disordered media: Weak attraction facilitates transport', *Journal of Chemical Physics* **117**(23).

Leuenberger, H., Rohera, B. and Haas, C. (1987), 'Percolation theory - a novel approach to solid dosage form design', *International Journal of Pharmaceutics* **38**, 109–115.

Lichtenegger, K. (2006), 'Stochastic Cellular Automata Models in Desease Spreading and Ecology', Masters Thesis. The Faculty of Science, Karl-Franzens Universitat Graz. Online homepage available from: http://physik.uni-graz.at/ kll/cthesis.pdf. Access date: 14/11/2006.

McCarthy, L., Kosiol, C., Healy, A.-M., Bradley, G., Sexton, J. and Corrigan, O. (2003), 'Simulating the hydrodynamic conditions in the United States Pharmacopeia paddle dissolution apparatus', *AAPS PharmSciTech* **4**(2), 109–115.

McMahon, N., Crane, M., Ruskin, H. and Crane, L. (2003), 'The Mechanics of Drug Dissolution', *Proceedings in Applied Mathematics and Mechanics (PAMM)* **3**, 392–393.

Merkle, H., Gander, B., Meinel, L. and Walter, E. (2002), Novel Opportunities of Microparticulates for the Delivery of Therapeutics and Vaccines , Technical report.

Meyer, R. and Christensen, N. (2000*a*), 'Bayesian Reconstruction of Chaotic Dynamical Systems', *Physical Review E* **62**, 3535–3542.

Meyer, R. and Christensen, N. (2000*b*), 'State-Space Modeling of Non-Linear Fisheries Biomass Dynamics Using the Gibbs Sampler', *Applied Statistics* **49**, 327–342.

Meyer, R. and Millar, R. (1999b), 'Bugs in bayesian stock assessments', *Can. J. Fish. Aquat. Sci* **56**, 1078–1086.

Meyer, R. and Millar, R. B. (1999a), 'Bayesian Stock Assessment using a State-Space

Implementation of the Delay Difference Model', *Canadian Journal of Fisheries and Aquatic Sciences* **56**, 37–52.

Mosegaard, K. and Sambridge, M. (2002), 'Monte Carlo analysis of inverse problems', *Inverse Problems* **18**, R29–R54.

Nagel, K. and Schreckenberg, M. (1992), ' A cellular automaton model for freeway traffic', *Journal de physique. I* **2**(12), 2221–2229.

Narasimhan, B. (2001), 'Mathematical models describing polymer dissolution: consequences for drug delivery', *Advanced Drug Delivery Reviews* **48**, 195–210.

Nicholson, C. and Sychova, E. (1998), 'Extracellular space structure revealed by diffusion analysis', *Trends in Neurosciences* **21**(5), 207–215.

Noyes, A. S. and Whitney, W. R. (1897), 'The rate of solution of solid substances in their own solutions', *Journal of the American Chemical Society* **19**, 930–934.

OpenGL (2006), 'OpenGL: The Industry's Foundation for High Performance Graphics', Online available at: http://www.opengl.org. Access date: 14/11/2006.

Prandtl, L. and Tietjens, O. (1957), *Applied Hydro- and Aeromechanics*, Dover Publications New York Paperback. Chapter IV.

Ramachandran, G. and Kandlikar, M. (1996), 'Bayesian analysis for inversion of aerosol size distribution data', *Journal of Aerosol Science* **27**(7), 1099–1112.

Ramtoola, Z. and Corrigan, O. I. (1987), 'Dissolution characteristics of benzoic acid and salicylic acid mixtures in reactive media', *Drug Development and Industrial Pharmacy* **13**, 9–11.

Rohde, K. (2005), 'Cellular automata and ecology', *Oikos* **110**(1), 203–207.

Rost, M. and Quist, P.-O. (2003), 'Dissolution of usp prednisone calibrator tablets effects of stirring conditions and particle size distribution', *Journal of Pharmaceutical and Biomedical Analysis* **31**(1), 1129–1143.

Sandor, M., Enscore, D., Weston, P. and Mathiowitz, E. (2001), 'Effect of protein molecular weight on release from micron-sized PLGA microspheres', *Journal of Controlled Release* **76**, 297–311.

Santra, S. B., Sapoval, B., Barboux, P. and Devreux, F. (1998), 'Pseudo-equilibrum between a random system and a solution: a Monte-Carlo study of glass dissolution in water', *C. R. Acad. Sci. Paris* **326**, 129–134.

Schlichting, H. (1979), *Boundary-Layer Theory*, 7th edn, McGraw-Hill, New York; London [etc.]. Chap. XII.

Siepmann, J. (2001), 'Mathematical modeling of controlled drug delivery', *Advanced Drug Delivery Reviews* **48**, 137–138. Preface.

Siepmann, J., Faisant, N. and Benoit, J.-P. (2002), ' A new mathematical model quantifying drug release from bioerodible microparticles using Monte Carlo simulations ', *Pharmaceutical Research* **19**(12), 1885–1893.

Siepmann, J. and Göpferich, A. (2001), 'Mathematical modeling of bioerodible, polymeric drug delivery systems', *Advanced Drug Delivery Reviews* **48**, 229–247.

Siepmann, J., Kranz, H., Peppas, N. and Bodmeier, R. (2000), 'Calculation of the required size and shape of hydroxypropyl methylcellulose matrices to achieve desired drug release profiles', *International Journal of Pharmaceutics* **201**, 151–164.

Siepmann, J. and Peppas, N. A. (2001), 'Modeling of drug release from delivery systems based on hydroxypropyl methylcellulose (HPMC)', *Advanced Drug Delivery Reviews* **48**, 139–157.

Simoes, S., de Almeida, L. and Figueiredo, M. (1996*a*), 'Testing the applicability of classical diffusional models to polydisperse systems', *International Journal of Pharmaceutics* **139**(1), 169–176.

Simoes, S., de Almeida, L. P. and Figueiredo, M. (1996*b*), 'Testing the applicability of classical diffusional models to polydisperse systems', *International Journal of Pharmaceutics* **139**, 169–176.

Sirisuth, N. and Eddington, N. D. (2002), 'In-vitro-in-vivo correlation definitions and regulatory guidance', *International Journal of Generic Drugs* **1**(11).

Small, D. (2006), 'Statistics Notes: Bayesian Statistics Continued', Online homepage available from: http://www-stat.wharton.upenn.edu/ dsmall/stat512-s05/notes28.doc. Access date: 4/12/2006.

SMC (2006), 'Sequential Monte Carlo', Online homepage available from: http://www-sigproc.eng.cam.ac.uk/smc/index.html. Access date: 14/11/2006.

Srinivasan, R. (1997), 'Application of the Monte Carlo method to the dissolution of a polycrystalline solid', *Materials Letters* **31**, 5–9.

Stauffer, D. and Aharony, A. (1992), *Cluster numbers, in Introduction to Percolation Theory*, 2nd edn, Taylor & Francis, London and Philadelphia.

Stolnik, S., Dunn, S., Garnett, M., Davies, M., Coombes, A., Taylor, D., Irving, M., Purkiss, S., Tadros, T. and Davis, S. (1994), 'Surface modification of poly(lactide-co-glycolide) nanospheres by biodegradable poly(lactide)-poly(ethylene glycol) copolymers', *Pharmaceutical Research* **11**(12), 1800–1808.

Sun, Y., Peng, Y., Chen, Y. and Shukla, A. J. (2003), 'Application of artificial neural networks in the design of controlled release drug delivery systems', *Advanced Drug Delivery Reviews* **55**, 1201–1215. Preface.

Sycara, K. (2006), 'Multi-Agent Systems', Online homepage available from: http://aaai.org/AITopics/html/multi.html. Access date: 14/11/2006.

Takahara, Takayama, K. and Nagai, T. (1997), 'Multi-objective simultaneous op-

timization technique based on an artificial neural network in sustained release formulations', *Journal of Controlled Release* **49**, 11–20.

Takayama, K., Takahara, J., Fujikawa, M., Ichikawa, H. and Nagai, T. (1999), 'Formula optimization based on artificial neural networks in transdermal drug delivery', *Journal of Controlled Release* **62**, 161–170.

Tracy, M., Ward, K., Firouzabadian, L., Wang, Y., Dong, N., Qian, R. and Zhang, Y. (2001), 'Factors affecting the degradation rate of poly(lactide-co-glycolide) microspheres in vivo and in vitro ', *Biomaterials* **20**(11), 1057–1062.

ul Ain, Q., Sharma, S. and Khuller, G. K. (2003), 'Chemotherapeutic Potential of Orally Administered Poly(Lactide-Co-Glycolide) Microparticles Containing Isoniazid, Rifampin, and Pyrazinamide against Experimental Tuberculosis ', *Antimicrobial Agents and Chemotherapy* **47**(9), 3005–3007.

Ungaro, F., Biondi, M., Indolfi, L., Rosa, G. D., Rotonda, M. I. L., Quaglia, F. and Netti, P. (2004), 'Bioactivated Polymer Scaffolds for Tissue Engineering ', *V Biomaterials* .

USP (2006), 'United States Pharmacopoeia', Online homepage available from: http://www.usp.org/frameset.htm. Access date: 14/11/2006.

Vaithiyalingam and Khan, M. (2002), 'Optimization and characterization of controlled release multi-particulate beads formulated with a customized cellulose acetate butyrate dispersion', *International Journal of Pharmaceutics* **234**, 179–193.

Vlugt-Wensink, K. D., Vlugt, T. J., Jiskoot, W., Crommelin, D. J., Verrijk, R. and Hennink, W. E. (2006), 'Modeling the release of proteins from degrading crosslinked dextran microspheres using kinetic Monte Carlo simulations', *Journal of Controlled Release* pp. 117–127.

Vogelson, C. (2001), 'Advances in drug delivery systems ', *Modern Drug Discovery from Concept to Developmant* **1**, 49–52.

von Neumann, J. (1966), *Theory of Self-Reproducing Automata*, University of Illinois Press.

Voutilainen, A. and Kaipio, J. (2005), 'Sequential monte carlo estimation of aerosol size distributions', *Computational Statistics and Data Analysis* **48**(4), 887–908.

wikipedia (2006), Online homepage available from: http://wikipedia.org. Access date: 14/11/2006.

Williford, R. E., Baer, D. R., Amonette, J. E. and Lea, A. S. (2004), 'Dissolution and growth of (1 0 1 4) calcite in flowing water: estimation of back reaction rates via kinetic Monte Carlo Simulations', *Journal of Crystal Growth* **262**, 503–518.

Wolfram, S. (2002), *A New Kind of Science* , Wolfram Media, Inc.

Zhang, M., Yang, Z., Chow, L.-L. and Wang, C.-H. (2003), 'Simulation of drug release from biodegradable polymeric microspheres with bulk and surface erosions ', *Journal of Pharmaceutical Sciences* **92**(10), 2040–2056.

Zhang, S. and Liu, J. (2005), *Massively Multi-Agent Systems I* , Springer Berlin / Heidelberg, chapter A Massively Multi-agent System for Discovering HIV-Immune Interaction Dynamics, pp. 161–173.

Zhao, A. and Rodgers, V. (2006), 'Using TEM to couple transient protein distribution and release for PLGA microparticles for potential use as vaccine delivery vehicles ', *Journal of Controlled Release* **113**(12), 15–22.

Zuse, K. (1970), *Calculating Space*, Cambridge, Mass. MIT Technical Translation.

Zygourakis, K. and Markenscoff, P. A. (1996), 'Computer-aided design of bioerodible devices with optimal release characteristics: a cellular automata approach', *Biomaterials* **17**, 125–135.

Appendix 1

Main features and implementation aspects

Several main principles and programming methods have been used to write the code to implement the model. Modelling is based on the UML scheme represented in Figure 3. Classes are used to represent every element in the virtual world, hence the full power of object-oriented programming can be brought to bear on the problem. A graphical interface is available for following the phenomena which occur during simulation.

Description of the main classes

- The class `lattice`.

This is the main class of the program because it initiates the whole set of objects and causes them to evolve, by update orders. In practice, this class contains a matrix of pointers to objects of class `place`. On initiation, this matrix is populated. Each element then corresponds to an object of class `border` (objects filling the border of the virtual world) or `common` (objects filling the ordinary inner places of the virtual world). The main construction of the lattice takes place using a classical constructor method using default parameters, the method `adapt()` allows the user parameters to be considered and the method `fill()` populates the matrix with the elements inherited from `place` (`common` and `border`). The creation of the objects of class `obstacle` (which model the PLGA bulk) on the sites is implemented by the method `fill_obstacle`. This method results in a random population of obstacles in certain predefined zones of the object `lattice` (contained within a sphere). Once the lattice is constructed, it needs to be updated: all sites belonging to it are accessed in turn in order to determine whether their elements need to be updated. This is implemented by the `update()` method which screens the lattice (visiting each site), for possible objects to update. Finally the class contains different

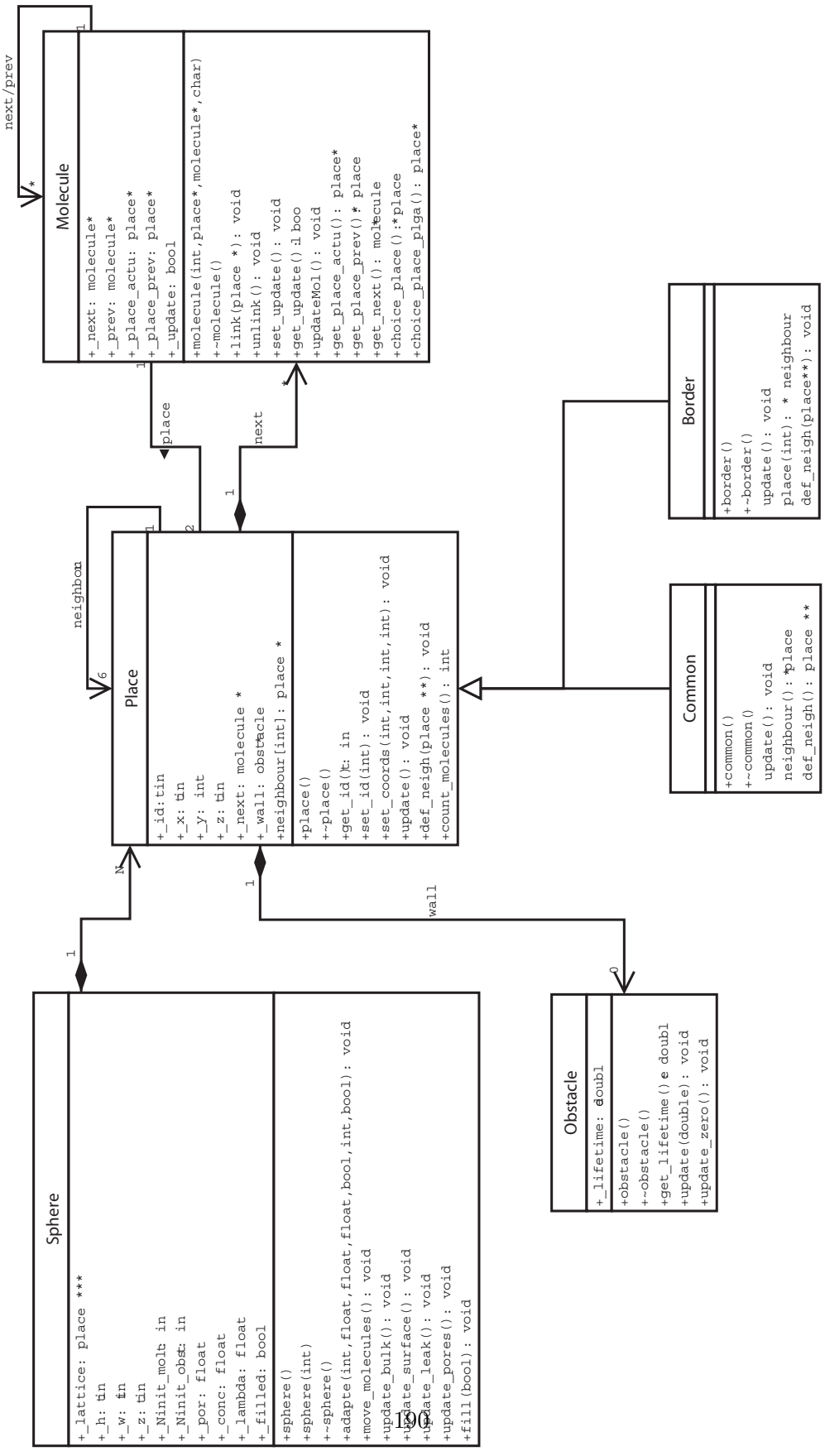

Figure 3: UML scheme of the simulation. Only the most important elements are shown.

methods permitting the passing of necessary information to other code making calls to this class. In this way, the program `main()` can ask the lattice for information on its composition. Also, the objects present on the lattice can access information which is needed (e.g. List of neighbouring sites for an inner site of the lattice).

- The class `molecule`.

This class contains the essentials of the dynamics of the program. An object of the class `molecule` represents a computational entity which models a large protein or small group of molecules, according to how the program is being used. The concept linked list data structure [2] has been used in this class. The molecules from one site of the lattice are linked in such a way that each molecule knows its nearest neighbours. This data structure permits an easier and more rapid update than in Chapter 3 [3], by processing recursively different treatments. The design of the movement and action of an entity is implemented through the following:

- The classic constructor method, which permits the construction of n molecules on a given site, in the linked list mentioned earlier. `Choice_place()` is one of the main methods of implemented: it permits the molecules to chose the site to move to (according to a procedure of highest score in the case the molecule can move to more than one site).

- `unlink()` and `link()` manage the linked lists of molecules. When a molecule is moving, it executes its `unlink()` method which permits it to leave its current chain. Then it calls the method `link()` which links it to the chain of the arrival site. The choice is to link the molecule between the site and the

[2] In computer science, a linked list is one of the fundamental data structures used in computer programming. It consists of a sequence of nodes, each containing arbitrary data fields and one or two references ("links") pointing to the next and/or previous objects (nodes). A linked list is a self-referential datatype because it contains a pointer or link to another data of thesame type. Linked list permit insertion or removal of nodes at any point in the list, but do not allow random access wikipedia (2006).

[3] The technique of programming the particles as a linked list has been compared to the methods used for the particles in the previous chapter. The linked list performed better in the case where a site is populated with a small number of particles.

first molecule (to avoid going through the whole list before linking to the last molecule).

- `update()` is the function called by the lattice during global update. It is a recursive function which permits the sphere to update not only the given molecule, but also all the molecules linked to this first molecule. Globally, the update function calls all the functions described earlier to permit the update of the molecule and thus its movement.

- `set_update()` is a switchstate function, which is used to toggle the update state of each molecule from 0 to 1 each time the molecule performs a movement on the lattice.

Chronology of an iteration

In order to check if programmed entities were performing correctly, a graphical interface has been designed and it can be used, in particular to visualise the initial morphologies of the spheres, as well as the way in which molecules behave after each simulation update. The graphical interface has been programmed using OPENGL.[4].

The implementation of updates benefited the most from the use of OPENGL. The use of the non-graphical mode (from command-line) permits to perform a given number of iterations, without graphically illustrating the state of the sphere, for the sake of rapidity of computation. This permits to verify the state of the erosion of the sphere and its porosity pattern after n iterations.

The iterations of the program are globally controlled by the method `glutMainLoop()` if a graphical interface is being used and the method `update()` in versions which do not use the graphical illustrations. At each time step, the `update()` function of the lattice is called. The method makes a call to the

[4]OPENGL OpenGL (2006) is a powerful graphical library, permitting both the creation of graphical primitives and implementation of 3D-engine functions. A 3D-engine can be defined as a set of structures, functions and algorithms used to visualize, after many calculations and transformations, 3D objects on a 2D screen.

`update()` method of the lattice, which, as noted, updates each of the objects present on the matrix. Then, if applicable, the update of the graphical interface OpenGL is performed. In the `update()` method of the lattice, each site is queried on the existence of a molecule or of an obstacle. If an object exists, it is updated by making a call to its update function, (through the encapsulation principle). After being updated, the molecules are restored tp their state of "non-updated". As the update is made in a site by site fashion, the update state must be controlled during an iteration to avoid multiple updates of a molecule. The restore is also recursive, as the lattice has direct access only to the first molecule of a site. The update of the graphics is implemented by the function `draw_lattice()` which implements, when called, a screening of the lattice to test the existence of different types of objects on each site, and to represent a graphical element relevant to the presence of a given type of objects.

Appendix 2

Glossary of terms

Biocompatibility - the quality of not having toxic or injurious effects on biological systems, the ability of a material to perform with an appropriate host response in a specific application.

Biodegradable - capable of decaying through the action of living organisms.

Blocked and unblocked end groups - hydrocarbon end groups and free acid end groups respectively.

Desorb - departure from the surface to which (a substance) is adsorbed. (adsorb - to gather (a gas, liquid, or dissolved substance) on a surface in a condensed layer).

Diglycerides and Tryglycerides - Glycerides are esters formed from glycerol and fatty acids. Glycerides have three hydroxyl functional groups which can be esterified with one, two or three fatty acids to form monoglycerides (Figure 4) diglycerides and triglycerides.Vegetable oils and animal fats contain mostly triglycerides, but are broken down by natural enzymes (lipases) into mono- and diglycerides and free fatty acids.

Method of microencapsulation - there are several methods of encapsulation available. Among them solvent evaporation extraction methods are the most widely employed in the case of therapeutic peptides and proteins. The polymer is dissolved in an appropriate organic solvent immiscible with water (e.g. methylene chloride, ethyl acetate) and the solution dispersed in an aqueous continuous phase containing a stabilizer. Other methods also exist, like cryogenic and non-aqueous microencapsulation methods, particularly suitable to maintain protein integrity during encapsulation and achieve high protein encapsulation efficiencies, (Ungaro et al., 2004).

- *Solid in oil in water (s/o/w)* - encapsulation technique where hydrophilic drugs are incorporated as solid micronised pardticles (e.g. freeze-dried proteins) suspended in an organic phase.

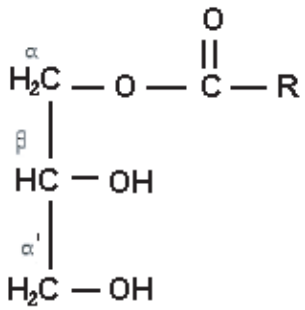

Figure 4: Monoglyceride formula

- *Water in oil in water (w/o/w)* - encapsulation technique where hydrophilic drugs are emulsified in the organic phase as a water solution - that is the double or multiple emulsion technique.

Poly(glycolic)acid (PGA) and poly(lactic acid) (PLA) - aliphatic polyesters of poly(a-hydroxy acids). These polymers and their associated copolymers are perhaps the most common biodegradable synthetic polymers known and have been used in drug delivery, bone osteosynthesis and tissue engineering of skin.

Poly(lactic-co-glicolide acid) (PLGA) - a Food and Drug Administration (FDA) approved copolymer which is used in a range of therapeutic devices, owing to its biodegradability and biocompatibility. PLGA is synthesized by means co-polymerization of two different monomers, the cyclic dimers (1,4-dioxane-2,5-diones) of glycolic acid and lactic acid.

Polyvinyl acetate (PVA) - a rubbery synthetic polymer. It is prepared by polymerization of vinyl acetate, Figure 5.

a)

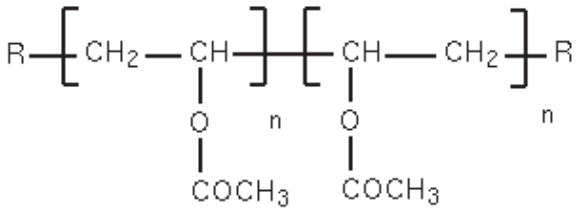

Figure 5: Polyvinyl acetate formula

Appendix 3

Notations and abbreviations used in the Chapter

This appendix gives a complete list of the notations and the abbreviations used throughout Chapter 6.

General

- t - the time variable.
- j - the index of the time variable at which time is discretised. $j = 1, ..., m$.
- y_t - the experimental data (measurement) observed at time t. In this study y_t stands for the *measured* weight of the particles in the solution at time t.
- w_j - weight of the agglomeration of solid matter (undissolved particles) in solution at time j, calculated using a deterministic model.
- $N_{tot,j}$ - total number of particles at time j.
- μ_j and σ_j - mean and standard deviation respectively of the size distribution at time j.
- $\overrightarrow{\theta_j}$ - vector of all physical state parameters which are considered unobserved and are to be reconstructed. Example: $\overrightarrow{\theta_j} = (N_{tot,j}, \mu_j, \sigma_j)$.
- x - diameter of a particle.
- $i = 1...n$ - Index representing size classes.
- $x_i = \frac{x_{max,i} - x_{min,i}}{2}$, average value of the diameters of particles in size class i.
- N_i - number of particles in class i.
- $\frac{N_i}{N_{tot}}$ - proportion of particles in this size range i.

For Bayesian observational and time-evolution models

- $F()$ - model relating observed data to unobserved parameters. In this case $F()$ is a functional relationship between observed experimental data and state parameters at time t.

- u_t - zero - mean Gaussian noise component, possibly related to: i) spatially heterogeneous hydrodynamic conditions, ii) measurement error, iii) model related error.

- $y_t = F(\overrightarrow{\theta}_t, \psi) + u_t$ - *observation model* - in other words a probabilistic way to relate the observed data and the unobservable parameters by incorporating a certain level of noise.

- ψ - some extra noise parameters. Its meaning is that there might be other factors than $\overrightarrow{\theta}_t$, conditioning the observation of y_t.

- $G()$ - *time-evolution mode*l - in other words a deterministic way to relate the state parameters $\overrightarrow{\theta_t}$ at time t to state parameters $\overrightarrow{\theta}_{t+1}$ at time $t+1$.

- $\overrightarrow{v}_t$ - stochastic term, accounting for additive dynamical noise factors, which can be related to either of: i) the speed of evolution of the states of the system ii) the time-dependent flow conditions iii) the accuracy of the time-evolution model $G()$.

- $\overrightarrow{\theta}_{t+1} = G(\overrightarrow{\theta_t}) + \overrightarrow{v}_t$ - *time evolution model* - Markov chain - stochastically relates the evolution of the state parameters based on the previous state.

- Bayesian paradigm: $P_{post}(\overrightarrow{\theta}|\overrightarrow{y}) = \frac{L(\overrightarrow{y}|\overrightarrow{\theta})P(\overrightarrow{\theta})}{P(\overrightarrow{y})}$.

- $P_{post}(\overrightarrow{\theta_j}|y_j)$ - updated probability of the unobserved parameters of interest, $\overrightarrow{\theta}_j$, given that y_j is observed.

- $L(\overrightarrow{y}|\overrightarrow{\theta})$ - likelihood of the model, or the probability of obtaining the data $\overrightarrow{y}$ given the set of parameters $\overrightarrow{\theta}$ and the function $F()$. In the particu-

lar case of this study it has been chosen that: $L(\overrightarrow{y}|\overrightarrow{\theta}) = P(\overrightarrow{y}|\overrightarrow{\theta}) = \frac{1}{\sigma_{y_j}} exp(-\frac{1}{2\sigma_{y_j}}(y_j - F(\overrightarrow{\theta_j})^2)$.

- $P(\overrightarrow{\theta})$ - probability of sampling this particular set of parameters - usually based on *prior* knowledge about the studied case.
- $P(\overrightarrow{y})$ - probability of observing/measuring this particular data set.
- σ_{y_j} - variance of the random variable u_t, which represents the noise in the observation model.
- Transition kernel - distribution of $\overrightarrow{\theta}_{j+1}$ given $\overrightarrow{\theta}_j$. In this particular study it has been chosen as: $P(\overrightarrow{\theta}_{j+1}|\overrightarrow{\theta}_j) = N(G(\overrightarrow{\theta}_j), \Gamma_j)$.
- Γ_{j+1}- matrix having on its diagonal the variances of the prior distributions (prior to comparing them to the observations) of the unobserved parameters $\overrightarrow{\theta}_{j+1}$.
- γ_{j+1} - standard deviation of the prior distributions of the unobserved parameters (the values from the diagonal of the matrix Γ_{j+1}).
- $\hat{\theta_j}$ - minimum variance Bayes estimate or the minimum a posteriori estimate.
- $s_{\hat{\overrightarrow{\theta_j}}}$ - standard deviation of the expected value.

For the deterministic time-evolution model for a particulate drug delivery system

- x_{crit} - critical diameter: different models $G()$ are applied for particles larger or smaller than this critical value for the particle diameter.
- C - concentration of solute in the solvent.
- $\frac{dC}{dt}$ - time rate of variation of concentration of solute.

- C_S - saturation concentration.
- D - diffusion coefficient, independent of the concentration.
- α - a shape factor related to the general shape of the particle.
- h - thickness of the diffusion layer outside the solid surface (the concentration boundary layer).

Notations involved in generating data with direct simulations

- μ_0 - mean of the initial distribution
- σ_0 - standard deviation of the initial distribution.
- N_{tot_0} - total number of particles from the initial distribution.
- Δx - length of the spatial intervals for discretisation of the distributions.
- Δt_{direct} - length of the time intervals for the time discretisation in generating data.
- $\Delta t_{sampling}$ - sampling time intervals when generating direct data.
- t_{tot} - total time for a direct or an inverse simulation.
- cv - coefficient of variation.

For inverse simulations

- p - sample size.
- k - index of a member from the sample.
- $\Delta t_{inverse}$ - length of the time intervals for the time discretisation in inverse simulations.

- $(N_{tot_j}^k, \mu_j^k, \sigma_j^k, \alpha_j^k)$, $k = 1, ..., p$ - example of one member of the sample population from the inverse simulation.

- ω_j^k ($omega$) - importance weight of a member of a sample. Evaluated on the basis of the likelihood.

- $\{\overrightarrow{\theta}_j^{(k)}, k = 1, ..., p\}$ sample from the $p(\overrightarrow{\theta_j}|y_{1:j})$.

- $(\overrightarrow{\widetilde{\theta}}_{j+1}^{(k)})$ - sample from the prior prediction density at the next time step $(p(\overrightarrow{\theta}_{j+1}|y_{1:j}))$.

- Transition kernel - $P(\overrightarrow{\theta}_{j+1}|\overrightarrow{\theta}_j) = N(G(\overrightarrow{\theta}_j), \Gamma_j) = N(\hat{\theta}_{j+1}, \Gamma_{j+1})$.

- γ_{j+1} - standard deviation of the prior distributions of the unobserved parameters (the values from the diagonal of the matrix Γ_{j+1}: $\gamma_{Ntot_{j+1}}$, $\gamma_{\mu_{j+1}}$, $\gamma_{\sigma_{j+1}}$,$\gamma_{\alpha_{j+1}}$).

- $\hat{\theta}_{j+1}$- vector of means of the marginal prior distributions.

- min and max - lower and upper boundaries of the intervals for sampling θ_{j+1}.

- $(\overrightarrow{\theta_a}, \overrightarrow{\theta_b})$ - a $100(1-\beta)\%$ credibility interval.

- β - a small number, usually chosen such that there is at least a 95% probability $100(1-\beta)\%$ that the estimated parameter is found.

- $M_{x\,runs}$ and $sd_{x\,runs}$ - average and standard deviation of the reconstructed parameters obtained at different runs of the simulation.

- t_{tot} - total time for a direct or an inverse simulation.

Appendix 4

Published Papers

1. Barat, A., Ruskin, H. J., Crane, M. (2005), "Modelling the in vitro Dissolution of Soluble Binary Drug Delivery Systems using Direct Monte Carlo techniques", *Proceedings of 1st Open International Conference on Modeling and Simulation June 12-15th, 2005 - ISIMA, Blaise Pascal University, Clermont-Ferrand, France.*

2. Barat, A., Ruskin, H. J., Crane, M. (2006), "Probabilistic Models for Drug Dissolution. Part 1. Review of Monte Carlo and Cellular Automata Approaches", *Simulation Modelling Practice and Theory (SIMPAT)* **14**, 843-856.

3. Barat, A., Ruskin, H. J., Crane, M. (2006), " Probabilistic Models for Drug Dissolution. Part 2. Modelling a Soluble Binary Drug Delivery System Dissolving *in vitro*", *Simulation Modelling Practice and Theory (SIMPAT)* **14**, 857-873.